

POLITECNICO DI TORINO

Corso di Laurea in Ingegneria Aerospaziale

Tesi di Laurea Magistrale



**Lunar gravity assisted escape trajectories
towards Near Earth Asteroids**

Relatore:
Prof. Lorenzo Casalino

Candidato:
Andrea Novelli

Marzo 2018

Contents

1	Introduction	15
1.1	What is a gravity assist?	17
1.2	Lunar Gravity Assisted missions	19
1.2.1	STEREO - Solar Terrestrial Relations Observatory	21
1.2.2	Nozomi	23
1.2.3	ISEE 3 - International Sun-Earth Explorer 3	24
1.3	NEAs as potential mission targets	25
1.3.1	A classification of NEAs	25
1.3.2	Feasible targets	28
2	Frames of reference	33
2.1	Useful frames of reference	33
2.1.1	Heliocentric Aries Ecliptic Coordinate System	34
2.1.2	Geocentric Equatorial Inertial Coordinate System	35
2.1.3	Geocentric Equatorial Rotating Coordinate System	36
2.1.4	Geocentric Lunar Coordinate System	37
2.1.5	Zenith-East-North Coordinate System	38
2.1.6	Perifocal Coordinate System	39
2.2	Transformation matrices	40
2.2.1	Transformation from T_{HAE} to T_{GEI}	42
2.2.2	Transformation from T_{GEI} to T_{GL}	44
2.2.3	Transformation from T to T_{ZEN}	46
2.2.4	Transformation from T_P to T_{GEI}	48
3	Mathematical model	51
3.1	Kepler's laws of planetary motion	51
3.1.1	The Law of Ellipses	52
3.1.2	The Law of Equal Areas	53
3.1.3	The Law of Harmonies	53
3.2	The n-body problem	55
3.3	The 2-body problem	58
3.3.1	Constants of motion	59
3.4	The trajectory equation	61

3.4.1	The conic sections	62
3.5	Keplerian orbits and orbital elements	66
3.5.1	Elliptical orbit	66
3.5.2	Circular orbit	66
3.5.3	Parabolic orbit	67
3.5.4	Hyperbolic orbit	68
3.5.5	Orbital parameters	70
3.5.6	Determination of position and velocity vectors from the orbital parameters	72
3.6	Trajectory analysis	73
3.6.1	The Patched Conic Approximation	73
3.6.2	Sphere of influence	74
3.7	Gravity Assist	76
3.7.1	Mathematical model of the Gravity Assist maneuver	77
3.7.2	Pump and crank angles	79
3.7.3	Turn angle	80
3.8	Canonical Units	82
3.8.1	Standard Metric Units	82
3.8.2	Solar Canonical Units	83
3.8.3	Terrestrial Canonical Units	84
4	Analysis	87
4.1	Mission scenarios	87
4.2	Resolution method	90
4.3	Evaluation of the escape leg L-E	90
4.3.1	Escape leg scenarios	91
4.3.2	Determination of the orbital parameters	93
4.4	Evaluation of the intermediate leg L-L	94
4.4.1	Resonant transfers	95
4.4.2	Non resonant coplanar prograde transfers	95
4.4.3	Non resonant coplanar retrograde transfers	97
4.4.4	Non resonant non coplanar transfers	99
4.5	Evaluation of the departure leg P-L	100
4.6	Mass evaluation	101
4.6.1	Mass at escape	101
4.6.2	Mass at destination	103
5	Results	105
5.1	In plane escape trajectories with small V_{esc}	106
5.1.1	Single fly-by scenario	106
5.1.2	Multiple fly-by scenario	110
5.1.3	Resonant fly-by scenario	116
5.1.4	Considerations	122

5.2	Out of plane escape trajectories with small V_{esc}	123
5.2.1	ARRM Example - Analytical approach	125
5.2.2	ARRM Example - Precomputed trajectories approach	127
5.3	In plane escape trajectories with large V_{esc}	129
5.3.1	Single fly-by scenario	130
5.3.2	Multiple fly-by scenario	134
5.3.3	Resonant fly-by scenario	139
5.3.4	Considerations	144
5.4	Conclusions	146

List of Figures

1.1	Example of a direct escape trajectory	16
1.2	Example of a lunar assisted escape trajectory	16
1.3	Spacecraft's fly-by speed components relative to Jupiter	17
1.4	Spacecraft's fly-by speed components relative to the Sun	18
1.5	AsiaSat 3 rescue trajectory	19
1.6	STEREO's mission profiles	21
1.7	Evolution of the trajectories of the STEREO missions	22
1.8	Mission profile of the Nozomi probe	23
1.9	Mission profile of the ISEE 3 probe	24
1.10	Near Earth Asteroids discovered during the period 1980-2017	26
1.11	Orbit of an asteroid belonging to the Amors family	26
1.12	Orbit of an asteroid belonging to the Apollos family	27
1.13	Orbit of an asteroid belonging to the Atens family	27
1.14	Orbit of an asteroid belonging to the Atiras family	27
2.1	Heliocentric Aries Ecliptic coordinate system	34
2.2	Geocentric Equatorial Inertial coordinate system	35
2.3	Geocentric Equatorial Rotating coordinate system	36
2.4	Geocentric Lunar coordinate system	37
2.5	Zenith East North coordinate system	38
2.6	Perifocal coordinate system	39
2.7	Reference frames with common origin	40
2.8	Mutual orientation of HAE and GEI coordinate systems	42
2.9	Mutual orientation of GEI and GL coordinate systems	44
2.10	Zenith East North coordinate system	46
2.11	Mutual orientation of T_P and T_{GEI} frames of reference	48
3.1	Example of elliptical orbit around the Sun	52
3.2	Graphic representation of Kepler's second law	53
3.3	Overview of the n-body problem	55
3.4	Overview of the 2-body problem	58
3.5	Simplified representation of an elliptical orbit	62
3.6	The conic sections	65

3.7	Geometry of an hyperbola	69
3.8	Perifocal and inertial coordinate systems	70
3.9	Earth-Mars trajectory with the patched conics approximation	74
3.10	Geometry of a gravity assist	76
3.11	Trajectories before (O^-) and after (O^+) the gravity assist	78
3.12	Pump and crank angles	79
3.13	Turn angle and ΔV	82
4.1	Example of a PLE scenario	89
4.2	Example of a PLLE scenario	89
4.3	Example of a resonant PLLE scenario	90
4.4	Different types of escape hyperbolas	92
4.5	Geometry of coplanar prograde transfers	96
4.6	Geometry of coplanar retrograde transfers	98
4.7	Geometry of non coplanar transfers	99
5.1	Escape mass as a function of the escape data, single fly-by	106
5.2	XY, YZ, XZ views of the single fly-by scenario	109
5.3	Overview of the single fly-by scenario	109
5.4	Escape mass as a function of the escape data, multiple fly-by	110
5.5	XY, YZ, XZ views of the multiple fly-by scenario, case 1	112
5.6	Overview of the multiple fly-by scenario, case 1	113
5.7	XY, YZ, XZ views of the multiple fly-by scenario, case 2	114
5.8	Overview of the multiple fly-by scenario, case 2	115
5.9	Escape mass as a function of the escape data, resonant 11 fly-by	116
5.10	Escape mass as a function of the escape data, resonant 32 fly-by	116
5.11	XY, YZ, XZ views of the resonant fly-by scenario, case 1	119
5.12	Overview of the resonant fly-by scenario, case 1	119
5.13	XY, YZ, XZ views of the resonant fly-by scenario, case 2	121
5.14	Overview of the resonant fly-by scenario, case 2	121
5.15	Families of pre-computed Moon to Moon trajectories	124
5.16	Achievable C3 as a function of the escape declination	125
5.17	Overview of the trajectory from the analytical approach	126
5.18	Overview of the trajectory from the precomputed approach	128
5.19	Escape mass as a function of k, single fly-by scenario	130
5.20	Turn angles as a function of k, single fly-by scenario	132
5.21	Trajectory architecture for k=1, single fly-by scenario	132
5.22	Trajectory architecture for k=1.3, single fly-by scenario	133
5.23	Escape mass as a function of k, multiple fly-by scenario	134
5.24	Turn angles as a function of k, multiple fly-by scenario	135
5.25	Trajectory architecture for k=1.2, multiple fly-by scenario	137
5.26	Trajectory architecture for k=1.3, multiple fly-by scenario	137
5.27	Lateral views for k=1.2 (left) and k=1.3 (right)	138

5.28	Escape mass as a function of k , resonant fly-by scenario 11	139
5.29	Turn angles as a function of k , resonant fly-by scenario 11	141
5.30	Escape mass as a function of k , resonant fly-by scenario 32	142
5.31	Turn angles as a function of k , resonant fly-by scenario 32	143
5.32	Comparison of the different scenarios' performances	144

List of Tables

1.1	Population of the principal families of NEAs	28
3.1	Overview of the Solar System’s planets orbital properties	54
3.2	Perturbative accelerations acting on an Earth-orbiting spacecraft	57
4.1	Overview of the feasible escape hyperbolas	93
4.2	Non resonant coplanar prograde intermediate transfers	97
4.3	Non resonant coplanar retrograde intermediate transfers	99
4.4	Non resonant non coplanar intermediate transfers	100
5.1	Overview of the single fly-by scenario inputs	107
5.2	Escape and destination mass for the single fly-by scenario	107
5.3	Orbital parameters for the single fly-by scenario	107
5.4	Useful parameters for the single fly-by scenario	108
5.5	Overview of the multiple fly-by scenario inputs	111
5.6	Escape and destination mass for the multiple fly-by scenario	111
5.7	Orbital parameters for the multiple fly-by scenario, case 1	111
5.8	Useful parameters for the multiple fly-by scenario, case 1	112
5.9	Orbital parameters for the multiple fly-by scenario, case 2	113
5.10	Useful parameters for the multiple fly-by scenario, case 2	114
5.11	Overview of the resonant fly-by scenario inputs	117
5.12	Escape and destination mass for the resonant fly-by scenario	117
5.13	Orbital parameters for the resonant fly-by scenario, case 1	117
5.14	Useful parameters for the resonant fly-by scenario, case 1	118
5.15	Orbital parameters for the resonant fly-by scenario, case 2	120
5.16	Useful parameters for the resonant fly-by scenario, case 2	120
5.17	Overview of the in plane scenarios performances	122
5.18	Analytical approach - summary	126
5.19	Analytical approach - fly-bys	126
5.20	Solar perturbed approach - summary	127
5.21	Solar perturbed approach - flybys	127
5.22	Escape mass as a function of k, single fly-by scenario	130
5.23	Turn angles as a function of k, single fly-by scenario	131

5.24	Escape mass as a function of k , multiple fly-by scenario	134
5.25	Turn angles as a function of k , multiple fly-by scenario	135
5.26	Escape mass as a function of k , resonant fly-by scenario 11	139
5.27	Turn angles as a function of k , resonant fly-by scenario 11	140
5.28	Escape mass as a function of k , resonant fly-by scenario 32	141
5.29	Turn angles as a function of k , resonant fly-by scenario 32	142

Abstract

In this study I will analyze how one or more gravity assists from the Moon can be exploited to escape the Earth's sphere of gravitational influence, thus saving fuel and increasing the payload mass.

The ultimate goal could be sending the spacecraft to a Near Earth Asteroid, or NEA, with the intent of study its composition and, eventually, take some samples back to Earth.

After a brief introduction, in which the fly-by maneuver will be presented and the missions that used one or more Lunar Gravity Assists, or LGAs, will be recalled, the mathematical model and the possible mission scenarios will be presented.

Following, the methods for the calculation of the escape trajectories will be proposed.

The results of the analysis will be reported, with particular attention on how the launch date, within a 28-day window, which coincides with the Moon's revolution period, can affect the value of the payload mass that can reach the asteroid.

In the final chapter, the possible future developments of this work will be presented.

Chapter 1

Introduction

Since the 17th of December 1903, date in which the first motorized human-made object performed a controlled flight, mankind pursued the desire of explore the skies, at first, with the ultimate goal of reach space, send a man into its deepness and, eventually, set foot on another celestial body.

With the Kitty Hawk, Wilbur and Orville Wright set the fundamentals of the aviation age and only half a century later, RKA (the URSS Space Agency) managed to put the *Sputnik I* into a geocentric orbit: the so-called space age had just began.

As we all know, that particular event marked the start of the space race, with USA and URSS as direct opponents. The Russians focused their attention on scientific missions, while the Americans carried out a series of missions (primarily *Gemini*, *Mercury* and *Apollo*) which culminated in the *Apollo 11*, that allowed Neil Armstrong and Buzz Aldrin to descend on the surface of the Moon.

Even if, after the *Apollo* missions, the human activity in space have been reduced only to the Low Earth Orbit, or LEO, the exploration of the Solar System continued, for example with the *Voyager I* and *II* probes.

But if we want a spacecraft to travel around the Solar System, it is first necessary to escape the Earth's gravitational influence; by convention, this is defined as a sphere with a 1 million kilometers radius. To pursue this, it is possible to follow two different ways:

1. **Direct Escape**, in which the spacecraft starts from a low earth parking orbit and, via a $\Delta V \geq 3$ km/s, puts itself on a hyperbolic trajectory that allows it to escape Earth's gravitational attraction.
2. **Lunar Gravity Assisted Escape**, based on exploiting one or more fly-bys of the Moon. Every fly-by event works as a slingshot for the spacecraft and changes its orbital parameters, with the possibility of acquire enough speed to escape the Earth's gravity.

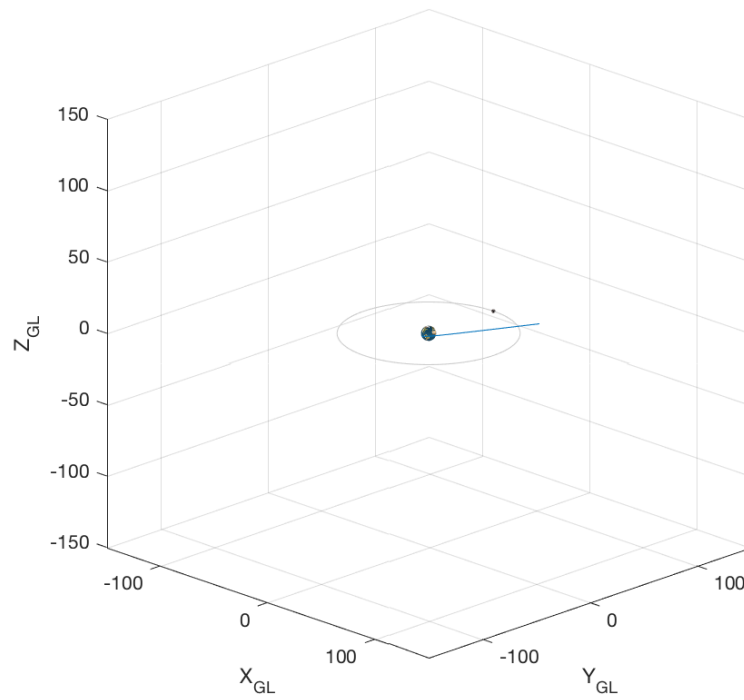


Figure 1.1: **Example of a direct escape trajectory**

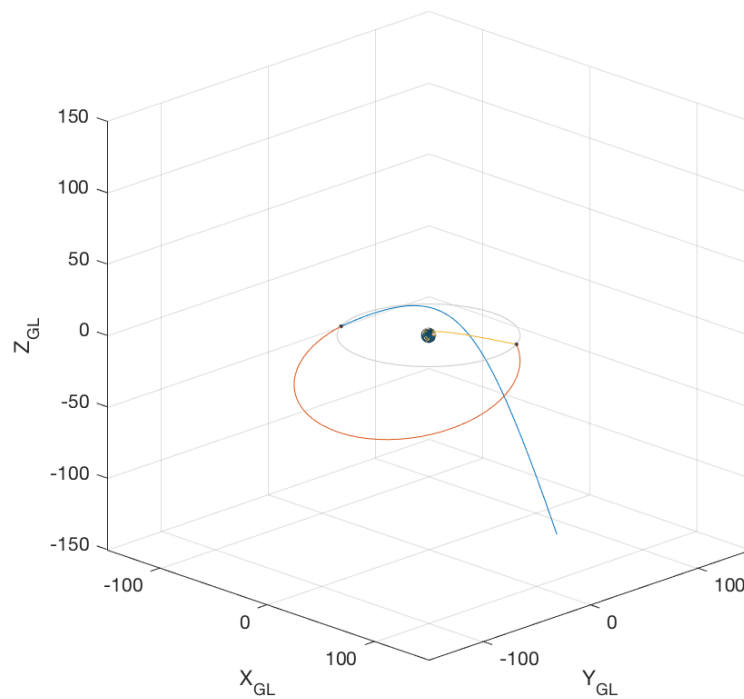


Figure 1.2: **Example of a lunar assisted escape trajectory**

1.1 What is a gravity assist?

By doing some elementary calculations, it is possible to assert that the Sun holds the 99.85% of the entire Solar System mass. But if we focus on the angular momentum, which is the cross product of a celestial body's position vector (relative to the Sun) and its momentum

$$\vec{H} = \vec{r} \times m\vec{v}$$

we can state that the 96.6% of it belongs to the planets, with an astounding 60% attributed to Jupiter.

The gravity-assist is a maneuver proposed in the early 1960s by Michael Minovitch, a JPL employee, that consists of a close pass next to a celestial body (a satellite, in this specific work), during which an exchange in angular momentum between the spacecraft and the body itself occurs. It is generally used in heliocentric orbits, to help a spacecraft reach the outer Solar System, much farther than its launch vehicle could have done.

Two different cases are possible:

1. **Approach from behind**, in which the spacecraft chases the body and is accelerated respect to the central body.
2. **Approach from ahead**, in which the spacecraft is chased by the body, thus resulting in a deceleration respect to the central body.

We will now analyze a typical *approach from behind scenario*: a Jupiter fly-by, often used to boost the probes to the outer Solar System.

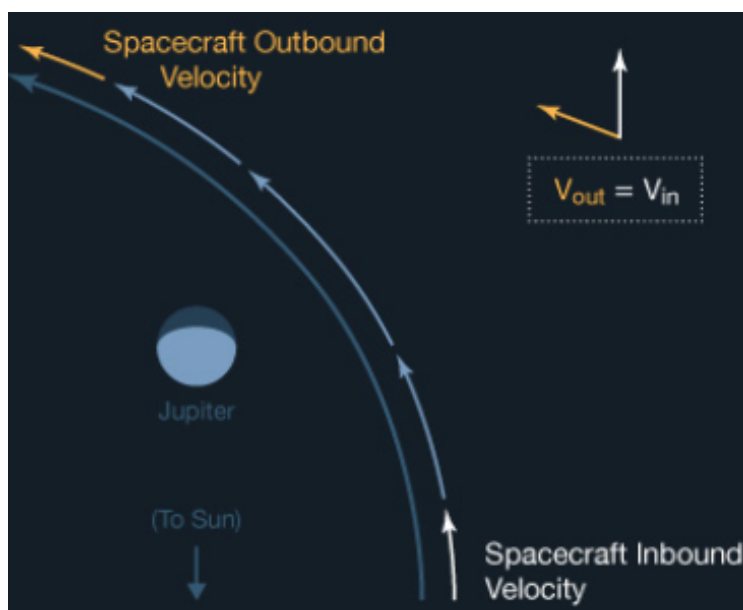


Figure 1.3: Spacecraft's fly-by speed components relative to Jupiter

As can be seen in Figure 1.3, the Jupiter-relative speed component of the probe increases during the inbound leg, reaches its maximum value at the point of closest approach and then decreases on the outbound leg, thus remaining constant through the fly-by event. The only thing that changed is the direction of the speed vector.

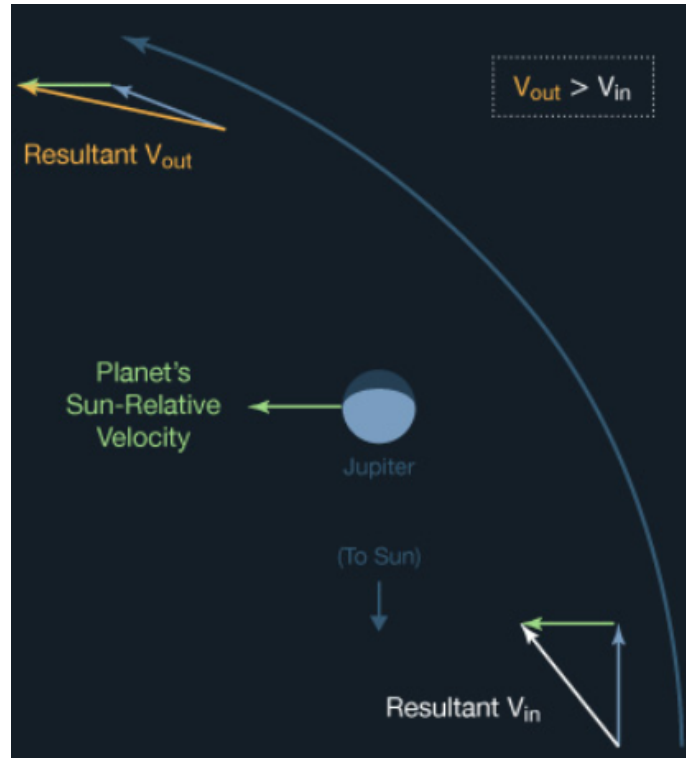


Figure 1.4: **Spacecraft's fly-by speed components relative to the Sun**

If we focus now on the speed components respect to the Sun, as can be seen in Figure 1.4, we can state that the orbital energy exchange allows the probe to leave Jupiter's gravitational influence with some additional angular momentum, while the planet's loss is too small to be measured. The result of the fly-by event is that the Jupiter's Sun-relative orbital speed is added to the spacecraft's one.

Gravity assists can also be used to slow down a spacecraft, following a so-called *approach from ahead scenario*, in which the probe reduces its orbital speed by donating some of its orbital energy to the planet.

For example, the Galileo probe used an Io's gravity-assist to slow down and ease the orbit insertion around Jupiter, thus saving around 100 kg of propellant.

Nevertheless, a Jupiter's fly-by is often used to lower the spacecraft's perihelion as part of an Oberth maneuver, the one that allows to escape the Sun's gravitational influence.

1.2 Lunar Gravity Assisted missions

On the 3rd of January 1959 the Russian probe *Luna 1*, following a fly-by of the Moon at an altitude of 5995 km, inserted itself on a hyperbolic trajectory that, 34 hours later, led it out of Earth's sphere of gravitational influence, thus making it the first man-made object to reach a heliocentric orbit.

Launched the day before from the Baikonur Cosmodrome in Kazakhstan, the goal of the mission was to impact on the surface of the Moon, but an incorrect timing in the upper stage burn occurred and the spacecraft, instead of crashing, transited a few thousand kilometers from the surface. This unintentional close encounter, as previously explained, produced an exchange of angular momentum between the Moon and the probe that resulted in a boost for the latter.

Apart from this episode, LGAs have intentionally been exploited in a few missions either to save valuable fuel, a topic that will be analyzed in the following subsections, or to rescue a stranded spacecraft, as happened with the *AsiaSat 3* satellite.

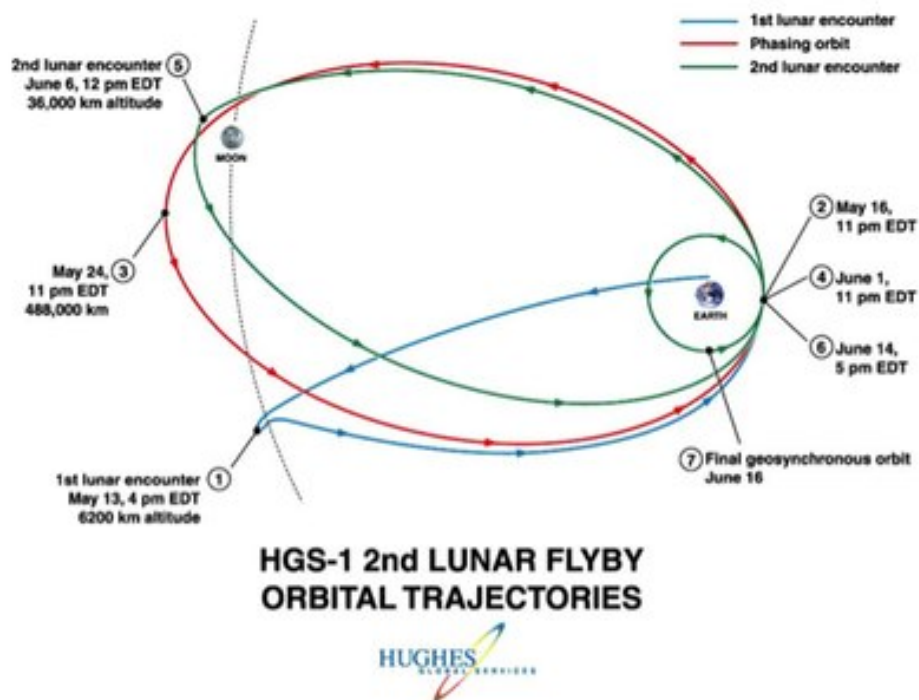


Figure 1.5: AsiaSat 3 rescue trajectory

AsiaSat 3 was launched on the 24th of December 1997 by means of a Proton-K vehicle from the Baikonur Cosmodrome in Kazakhstan and was intended to assume a Geostationary Earth Orbit. Unfortunately, due to a malfunction, the fourth stage failed to perform

the plane change, leaving the spacecraft on a 51° inclined and elliptical orbit. All of the satellite's systems were however fully functional, but it was impossible for it to reach its operating orbit because of the little amount of fuel it carried.

After the failure event, Hughes Global Services took control of the spacecraft and suggested a recovery trajectory that involved one or more fly-bys of the Moon.

The apogee of the satellite was initially raised so that it could encounter the Moon, event that took place on the 13th of May 1998 at an altitude of 6200 km and that put it on another geocentric orbit that reencountered the Moon on the 6th of June at a distance of 34300 km. The two fly-bys succeeded in both raising the perigee to the geosynchronous value and lowering the inclination from 51° to only 8° . AsiaSat 3 therefore ended in a geosynchronous orbit, instead of a geostationary one.

In Figure 1.5 it is illustrated the recovery trajectory performed by the satellite.

Also, an interesting application of LGAs that is strictly connected with the AsiaSat 3 issue has recently been presented: fly-bys of the Moon could be used as an alternative to the Geostationary Transfer Orbit, or GTO, which is pretty expensive, especially if the launch site isn't located on the Equator. In particular, the ΔV required by the classical GTO for the circularization and the plane change is higher than the escape one. So, a highly eccentric orbit with an apogee nearby the Moon could be used, in order to exploit the Moon's gravity both for apogee raising and for the change in inclination.

1.2.1 STEREO - Solar Terrestrial Relations Observatory

This mission consisted of two nearly identical probes:

- *Stereo-A*, which stands for ahead, put onto a heliocentric orbit that precedes Earth,
- *Stereo-B*, which stands for behind, that orbits around the Sun following Earth on its path.

A single Delta-II vehicle was used on the 26th of October 2006 to launch both the spacecrafts, whose primary goal was to provide stereoscopic imaging of the Sun and its phenomena, e.g. coronal mass ejections.

After a coast phase in LEO, the orbit's energy was increased by means of the second and third stage engines, that provided the necessary ΔV to achieve a highly elliptical orbit whose apogee reached the Moon's orbit. This high energy phasing orbit was covered for four times before the probes encountered the Moon on the 15th of December 2006. At this point, as illustrated in Figure 1.6 due to the fact that their orbits around Earth were slightly different, their paths separated.

Stereo-A was ejected from the Earth's sphere of gravitational influence and reached an heliocentric orbit with a 347 days period.

Stereo-B followed another geocentric orbit that reencountered the Moon on the 21st of January 2007 and, by means of this second fly-by event, abandoned Earth's gravity in the opposite direction to that of *Stereo-A*. Its revolution around the Sun takes 387 days to be completed.

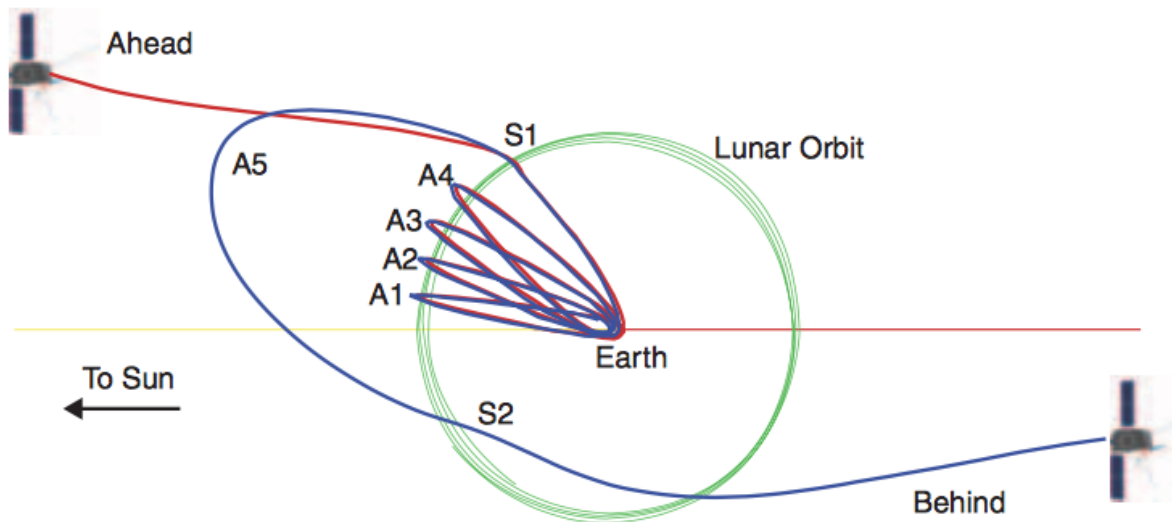


Figure 1.6: STEREO's mission profiles

As a result of their orbits, the STEREO-A/Sun/Earth angle increases of $22^\circ/\text{year}$, while the STEREO-B/Sun/Earth angle has a $-22^\circ/\text{year}$ rate of change, as stated in Figure 1.7.

With the current drift rates, Ahead's closest approach to Earth will happen on the 20th of August 2023 at a distance of 8.2 million kilometers, while Behind's will be on the 14th of July 10.0 million kilometers away from our planet.

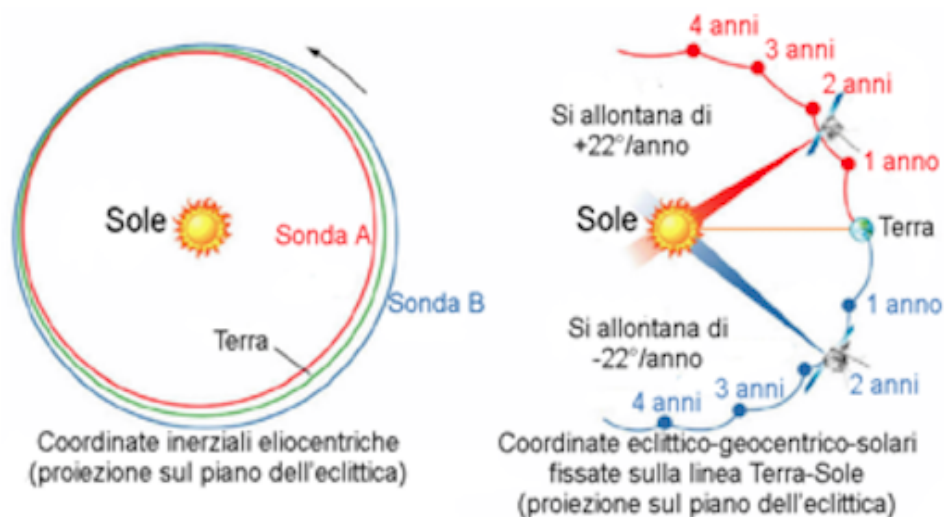


Figure 1.7: Evolution of the trajectories of the STEREO missions

As regards the future of the mission, Behind probe's fuel can still provide a $\Delta V \approx 60 \text{ m/s}$. By using half of that, the drift rate could be increased to $-22.5^\circ/\text{year}$ so that the probe, after a third LGA in 2023, could be positioned in a HALO orbit around the Lagrange point L2 of the Earth-Moon system.

1.2.2 Nozomi

The *Nozomi* probe, Japanese word meaning "Hope", was launched from Kagoshima Space Center on the 4th of July 1998 with the intent of reach Mars and study its upper atmosphere, in particular its interaction with the solar wind, as well as provide photographs of the red planet's surface.

It reached a parking orbit around Earth, with a perigee of 340 km and an apogee of 400000 km aboard a Mu-5, a solid-fuel rocket specifically designed to launch scientific satellites.

The spacecraft then experienced two LGAs on the 24th of September 1998 and on the 18th of December 1998, the latter of which sent it towards an Earth swing-by that, coupled with a seven-minute burn, should have put Nozomi on an escape trajectory towards Mars, to be reached in October 1999. But a valve malfunction caused a loss of fuel, hence a lower acceleration, that resulted in a different than predicted heliocentric trajectory.

The mission needed to be reprogrammed and the new plan left the probe around the Sun for four more years, during which it flew by Earth two times, in December 2002 and in June 2003, with the goal of reach Mars in December 2003. Unfortunately, weeks before the first fly-by, an electrical malfunction occurred, compromising the ability to perform the orbit insertion around Mars. On the 3rd of December 2003 the mission was officially ended and the probe is currently onto a 2-year orbit around the Sun.

A graphic overview of the mission is reported in Figure 1.9, where the dates in brackets were programmed but never happened due to the failure.

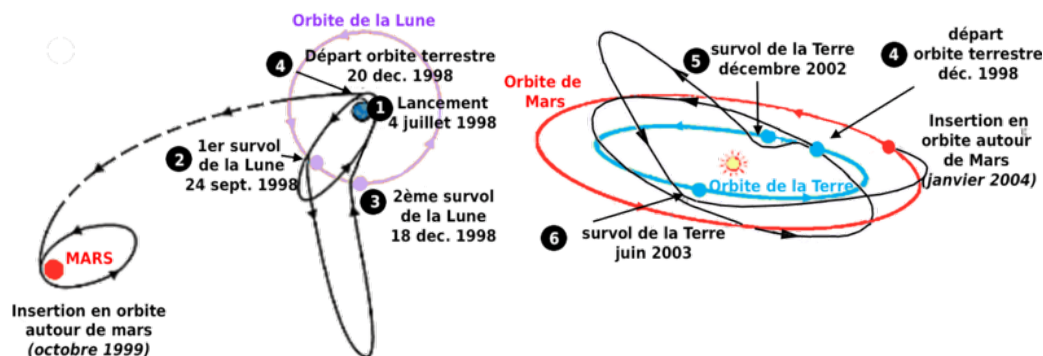


Figure 1.8: Mission profile of the Nozomi probe

1.2.3 ISEE 3 - International Sun-Earth Explorer 3

Launched from Cape Canaveral on the 12th of August 1978 aboard a Delta 2000 vehicle, its main objective was to study the interaction between the solar wind and the Earth's magnetic field.

On the 20th of November 1978 it was placed onto a HALO orbit around the Lagrange point L1 of the Sun-Earth system, about 1.5 million kilometers from our planet, thus becoming the first spacecraft to assume such a pathway. Because of the uncertainties that the insertion and maintenance of such an orbit involved, the probe carried a large supply of fuel, that eventually made possible the extension of the mission.

On the 10th of June 1982, in fact, after three and a half years, ISEE-3 left the halo orbit and began a transfer orbit that, after five LGAs (the last of which on the 22nd of December 1983) and a few slight maneuvers, allowed it escape the Earth-Moon system towards a heliocentric orbit. Such 355-days orbit, with a perihelion of 0.93 AU and an aphelion of 1.03 AU, took it nearby the Giacobini-Zimmer comet in 1985, so that the probe was renamed as *International Cometary Explorer* or *ICE*.

On the 5th of May 1997 NASA ended the mission, with the possibility of reboot it to observe other comets.

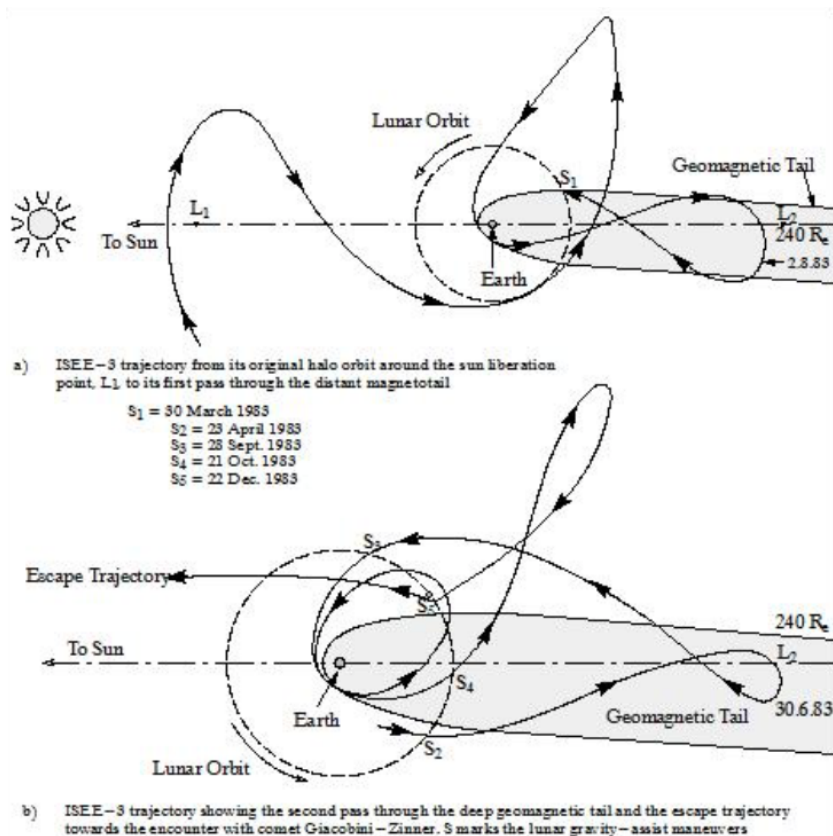


Figure 1.9: Mission profile of the ISEE 3 probe

1.3 NEAs as potential mission targets

The most trustworthy hypothesis about asteroids states that they are the leftover material from the formation of the Solar System's inner planets: Mercury, Venus, Earth and Mars, occurred roughly 4.6 billion years ago.

Recent spectroscopic studies, during which the reflected light from the asteroids has been analyzed with the goal of finding out what they might contain, stated that these particular celestial bodies almost certainly contain large amount of resources, such as: iron, nichel, magnesium, perhaps gold, platinum and even water.

John S. Lewis, in his book *Mining the Sky*, said that a 1 kilometer in diameter asteroid, weighing approximately 2 billion tons, could hold 30 million tons of nichel, 1.5 million tons of cobalt and 7500 tons of platinum that, alone, is worth more than 150 billion dollars. Also, astronomers assumed that in the entire Solar System, there are roughly 1 million asteroids like that.

In relation to a possible, future unmanned mining mission, an escape trajectory assisted by the Moon could increase the payload, thus permitting the return of more resources to Earth. Furthermore, LGAs could be used during the reentry to perform a capture maneuver around Earth, eventuality that would allow to save some additional propellant. In relation to this, the search for a target asteroid should focus on the so-called Near Earth Asteroids, or NEAs.

1.3.1 A classification of NEAs

Near Earth Asteroids are a particular family of Solar System bodies characterized by an orbit that brings them nearby Earth, so that their orbital parameters are not so different from the Earth's ones. More specifically, an asteroid can be defined as a NEA if its point of closest approach to the Sun, i.e. its perihelion, is less than 1.3 AU.

Our interest for these bodies considerably increased in the 1980s, when astronomers realized how dangerous they could become for our planet.

As Figure 1.10 illustrates, in the last 35 years the number of Near Earth Asteroids annually discovered exponentially increased, particularly as for the smallest ones (with a diameter less than or equal to 140 m). In this regard, the vast majority of the trackings have been achieved with the help of the following projects: *LINEAR* (*Lincoln Near Earth Asteroid Research*), *NEAT* (*Near Earth Asteroid Tracking*), *Spacewatch*, *LONEOS* (*Lowell Observatory Near Earth Object Search*), *Catalina Sky Survey* and *Pan-STARRS* (*Panoramic Survey Telescope and Rapid Response System*).

To date, October 2017, more than 16700 NEAs with a diameter of more than 1 meter (dimension under which are classified as meteoroids) have been discovered and it is believed that more than 95% of those with a diameter of more than 1 km have been tracked. Our attention is primarily focused on these last, because of the global consequences that the eventuality of an impact could produce.

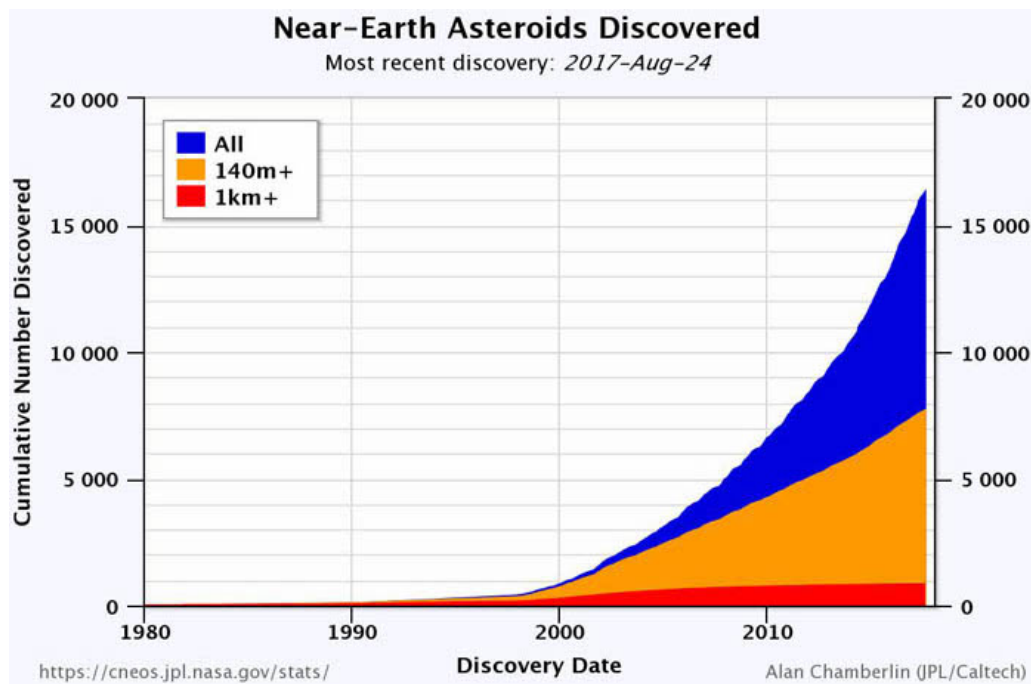


Figure 1.10: Near Earth Asteroids discovered during the period 1980-2017

By taking into account the values of their orbital parameters, primarily semimajor axis a , aphelion r_p and perihelion r_a , Near Earth Asteroids are categorized into four principal groups:

- **Amors**, whose orbits are exterior to Earth's orbit, but interior to Mars', characterized by a greater than 1 AU and r_p between 1.017 and 1.3 AU.

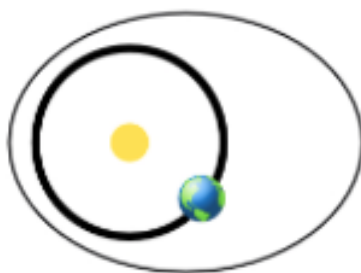


Figure 1.11: Orbit of an asteroid belonging to the Amors family

- **Apollos**, whose orbits are Earth crossing, characterized by a greater than 1 AU and r_p smaller than 1.017.



Figure 1.12: Orbit of an asteroid belonging to the Apollos family

- **Atens**, whose orbits are Earth crossing, characterized by a smaller than 1 AU and r_a greater than 0.983.

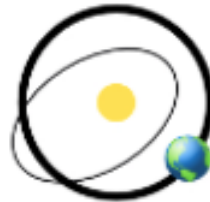


Figure 1.13: Orbit of an asteroid belonging to the Atens family

- **Atiras**, whose orbits are entirely contained within Earth's orbit, so that a is smaller than 1 AU and r_a is smaller than 0.983 AU.

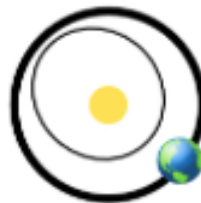


Figure 1.14: Orbit of an asteroid belonging to the Atiras family

As can be seen in Table 1.1, in which the population of every group has been set out, the vast majority of NEAs belongs to the Amors and Apollos families.

Family	Population and percentage
Amors	6400 or 38.2%
Apollos	9083 or 54.3%
Atens	1230 or 7.3%
Atiras	16 or 0.095%

Table 1.1: **Population of the principal families of NEAs**

As of 3 October 2017, 884 NEAs larger than 1 km have been discovered and 157 of them are classified as Potentially Hazardous Asteroids, or PHAs, for our planet. This particular family contains all the asteroids characterized by a Minimum Orbit Intersection Distance, or MOID, of 0.05 AU or less and an Absolute Magnitude of 22.0 or brighter, because of the fact that a bigger magnitude is an indicator of larger size.

Due to planetary perturbations, Near Earth Asteroids often face either an ejection from the Solar System or a collision with a planet or the Sun itself, so that their permanence in heliocentric orbit is reduced to a few million years: a really short amount of time if compared to the age of the Solar System. This means that new asteroids must continuously be moved into the neighborhood of Earth, to explain their presence.

A largely accepted hypothesis states that asteroids from the main belt, that extends between Mars and Jupiter, interact in gravitational resonance with Jupiter and move into the inner Solar System, thus becoming NEAs.

1.3.2 Feasible targets

Up to now, four principal candidates have been identified as possible mission targets, but their number is predicted to grow by one or two units per year by means of further observations.

The process of inclusion of a a NEA into the just mentioned list starts by exploiting telescopes on Earth and in space to observe new objects and track their approximate orbits. Once observed, orbital data are sent to the International Astronomical Union Minor Planet Center to be analyzed and, principally, to verify if that particular object has already been classified or not. If not, further observations are programmed in the next couple of days in order to precisely determine its orbit.

Obviously, these preliminar studies are not sufficient: detailed analysis have to be performed with the objective of calculate axis and speed of rotation, spectral class, shape, dimensions, surface properties and possibly the composition of the body.

With the asteroid moving millions of kilometers distant from Earth, all of these studies are anything but easy and, to achieve this, astronomers generally rely on the interplanetary radar. The two, most important, radar astronomy facilities of current use in the world are the Arecibo Planetary Radar (with a 350 meters in diameter antenna) and the Goldstone Solar System Radar (with some 70 meters in diameter antennas): they send

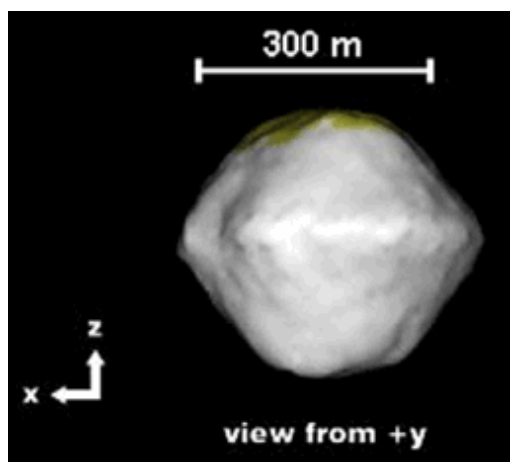
a beam of microwaves in the direction of the body of interest and then they study the reflected electromagnetic signal. If the asteroid is not in the field of view of the interplanetary radar, the Spitzer Space Telescope, that observes in the infrared, can also be used. Close passes nearby Earth represent another tool in the hands of the astronomers: these events, in fact, are often exploited to refine the information they already possess.

A list of the more interesting asteroids is now presented, with particular attention to their dimensions, orbital parameters and composition.

2008 EV₅

It is classified also as PHA and it is current belief that it originally made part of a much larger body orbiting in the main belt, probably about 100 km in diameter, that broke apart and whose fragments formed a large number of minor asteroids.

Asteroids like 2008 EV₅ are the most common in the Solar System; classified as C-type, meaning carbonaceous, they are characterized by a very low reflection of sunlight (generally from 3 to 9 percent) which makes them very dark and so pretty hard to detect. Another reason to explore this particular body is that this family of asteroids usually harbor significant amount of water, in the form of hydrated minerals, that can be split into hydrogen and oxygen to feed the rocket engines.

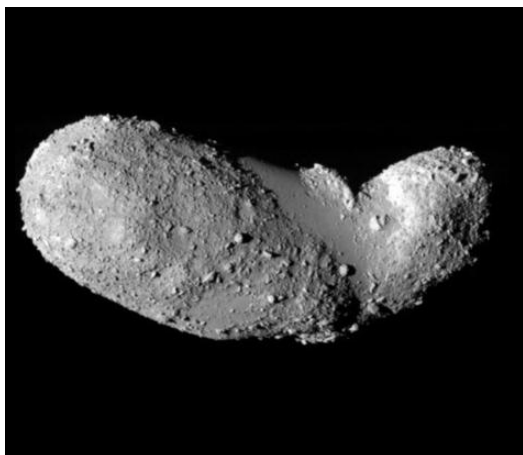


Complete Name	341843 2008 EV ₅
Discovery Date	4 March 2008
Family	Atens
Shape	Oblate Spheroid
Aphelion	1.0384 AU
Perihelion	0.8782 AU
Semimajor Axis	0.9583 AU
Orbital Period	342.7 d
Diameter	400 m
Earth MOID	0.01381 AU

Itokawa

This asteroid, also classified as PHA, was the first target of a sample mission return and the first one ever photographed and visited by a spacecraft, the Japanese probe *Hayabusa*. The most trustworthy hypothesis about its formation states that it originally was a binary system that eventually merged. Recent studies about its low density, which is about 2.5 g/cm³, suggest that, instead of a monolith, it could be just a series of fragments that covered over time.

Itokawa is an S-type asteroid, that means that its composition is mainly siliceous.



Complete Name	25143 Itokawa
Discovery Date	26 September 1998
Family	Apollos
Shape	Irregular
Aphelion	1.6951 AU
Perihelion	0.9531 AU
Semimajor Axis	1.3241 AU
Orbital Period	557 d
Size	535 x 294 x 205 m
Earth MOID	0.0129 AU

Bennu

Bennu is a carbonaceous B-type, a subcategory of C-type, asteroid. By means of the Palermo Technical Impact Hazard Scale, it obtained a cumulative score of -1.71, the third highest rating ever, with a chance in 2700 of impacting Earth between 2175 and 2196. Because of this, to better understand its composition and the possible evolutions of its orbit, it was selected as target for NASA's mission *OSIRIS-REx*.

The probe departed from Earth in September 2016, is expected to reach the asteroid in August 2018 and return to Earth with the collected samples in September 2023.

This body was originally part of a much bigger one, with a diameter of approximately 100 km, that formed roughly 4.5 billion years ago during the birth of the Solar System itself.



Complete Name	101955 Bennu
Discovery Date	11 September 1999
Family	Apollos
Shape	Spheroid
Aphelion	1.3559 AU
Perihelion	0.8969 AU
Semimajor Axis	1.1264 AU
Orbital Period	436.6 d
Diameter	500 m
Earth MOID	0.0032 AU

Ryugu

The Japanese mission *Hayabusa 2*, that departed from Earth in December 2014, is heading towards this asteroid and it is expected to rendezvous with it in July 2018. The mission profile is pretty similar to the *OSIRIS-REx* one: after a year and a half of survey, the probe will depart from Ryugu in December 2019 to return to Earth by December

2020.

Ryugu presents the typical features of both C-type (carbonaceous) and G-type (a sub-category of C-type) asteroids, thus making it a quite interesting target for an exploration mission.

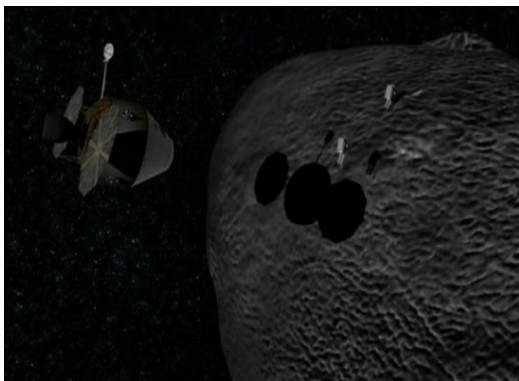


Complete Name	162173 Ryugu
Discovery Date	10 May 1999
Family	Apollos
Shape	Spheroid
Aphelion	1.4158 AU
Perihelion	0.9633 AU
Semimajor Axis	1.1895 AU
Orbital Period	473.9 d
Diameter	980 m
Earth MOID	0.00032 AU

2000SG344

This Aten asteroid, with a diameter of 37 meters, is estimated to have a mass of $7.1 \cdot 10^7$ kg. Despite its low dimensions, it maintained the highest probability of hitting Earth in the next 100 years until December 2004, when it was overtaken by 99942 Apophis.

Due to its orbit, that justified its classification as a PHA, NASA is taking it into account as a feasible target for manned Orion's Exploration Mission 2, scheduled for the early 2020s.



Complete Name	2000SG344
Discovery Date	29 September 2000
Family	Atens
Shape	Spheroid
Aphelion	1.0429 AU
Perihelion	0.9121 AU
Semimajor Axis	0.9775 AU
Orbital Period	353.0 d
Diameter	37 m
Earth MOID	0.0009 AU

Chapter 2

Frames of reference

A frame of reference is defined, in physics, as a system of coordinates with respect to which a particular phenomenon can be observed and measured.

2.1 Useful frames of reference

The frames of reference that the optimization of an escape trajectory departing from Earth and involving the Moon requires are principally six:

- the Heliocentric Aries Ecliptic (HAE) Coordinate System;
- the Geocentric Equatorial Inertial (GEI) Coordinate System;
- the Geocentric Equatorial Rotating (GR) Coordinate System;
- the Geocentric Lunar (GL) Coordinate System;
- the Zenith-East-North (ZEN) Coordinate System;
- the Perifocal (P) Coordinate System.

In the following pages, each of these six frames of reference will be discussed and the transformation matrices between those coordinates systems will be derived. In particular, for every coordinate system the position of the origin, the orientation of the fundamental plane X - Y and the direction of the Z -axis will be described.

2.1.1 Heliocentric Aries Ecliptic Coordinate System

This frame of reference is particularly useful to represent position and trajectories of bodies within the Solar System, due to the small inclination that the vast majority of the celestial bodies (except for Mercury) possesses with respect to the ecliptic plane, i.e. the plane identified by Earth's orbit around the Sun.

As reported in Figure 2.1, its origin is set in the center of the Sun and, for simplicity, it will be referred to as $T_{HAE}(X_{HAE}, Y_{HAE}, Z_{HAE})$, where the subscript HAE stands for *Heliocentric Aries Ecliptical*.

Its axes' directions are defined as follows:

- X_{HAE} towards the First Point of Aries, defined as the intersection between the Earth's equatorial plane and the ecliptic plane. In other words, X_{HAE} coincides with the Sun-Earth direction when Earth passes through the vernal equinox;
- Z_{HAE} perpendicular to the plane of Earth's orbit around the Sun, assuming positive the North direction;
- Y_{HAE} lies on the ecliptic plane and completes the right-handed frame.

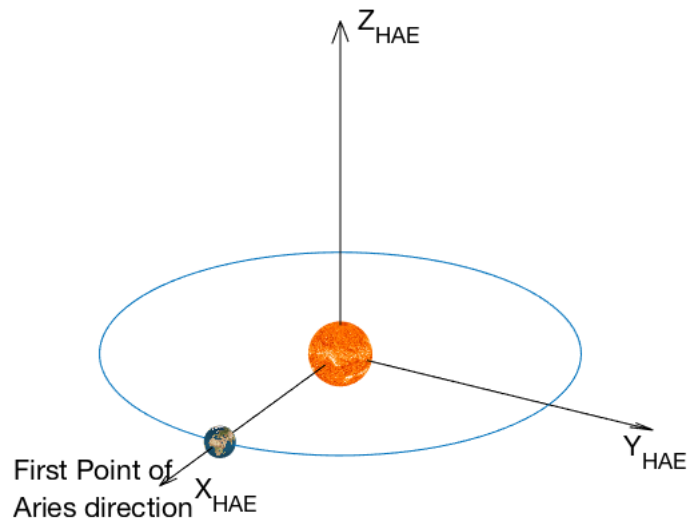


Figure 2.1: **Heliocentric Aries Ecliptic coordinate system**

This system is, at first approximation, stationary with respect to the fixed stars. However, perturbing forces acting on Earth cause the celestial equator to slowly move with a period of approximately 26000 years, an effect that takes the name of precession. Due to this phenomenon, X_{HAE} direction is not fixed in time, thus making the HAE Coordinate System not a perfectly inertial frame of reference.

When major precision is required, an epoch, which is the specification of the equinox at a particular date, needs to be specified; the most commonly used for what regards spacecrafts' orbits is the epoch known as $J2000.0$.

2.1.2 Geocentric Equatorial Inertial Coordinate System

When the locations of Earth-orbiting spacecrafts must be specified, it is convenient to rely on this particular frame of reference because, with respect to it, it is possible to define any Keplerian orbit.

Throughout this work, it will be referred to as $T_{GEI}(X_{GEI}, Y_{GEI}, Z_{GEI})$, where the subscript GEI stands for *Geocentric Equatorial Inertial*.

The center of Earth is the system's origin and the three axes are oriented as follows:

- X_{GEI} towards the First Point of Aries, which is the intersection point between Earth's equatorial plane and the plane defined by its orbit around the Sun;
- Z_{GEI} parallel to Earth's rotation axis, i.e. perpendicular to the equatorial plane, directed to the North Pole;
- Y_{GEI} lies on the equatorial plane and completes the right-handed frame.

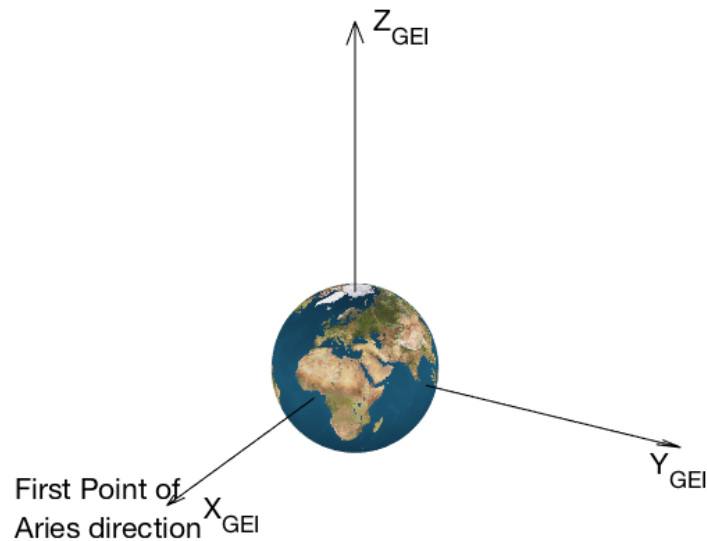


Figure 2.2: **Geocentric Equatorial Inertial coordinate system**

As can be seen in Figure 2.2, this frame of reference is pretty similar to the Heliocentric Aries Ecliptic system and it is also subject to the precession phenomenon, so that, in order for it to be considered an inertial frame, an epoch must be specified.

Due to the fact that its X -axis points towards an approximately fixed point in space, T_{GEI} cannot be considered stationary with respect to the planet.

2.1.3 Geocentric Equatorial Rotating Coordinate System

This coordinate system is nearly identical to the previous one, except for the fact that it follows Earth's rotation, thus appearing stationary with respect to the planet itself. It will be referred to as $T_{GER}(X_{GER}, Y_{GER}, Z_{GER})$, where the GER subscript stands for *Geocentric Equatorial Rotating* and its origin is still set in the center of the Earth. The three axes are oriented as follows:

- X_{GER} towards the intersection between the equator and the Greenwich meridian, i.e. the origin of latitude and longitude;
- Z_{GER} perpendicular to the equatorial plane, directed towards the North pole;
- Y_{GER} completes the frame, making it right-handed.

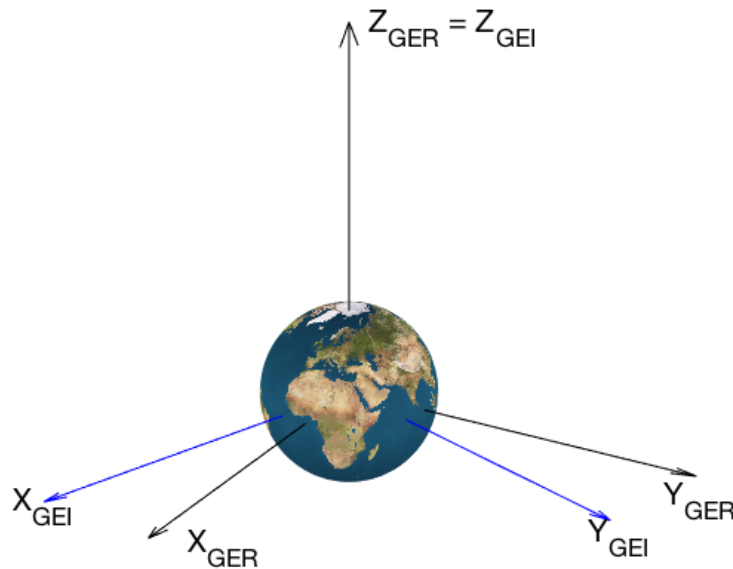


Figure 2.3: **Geocentric Equatorial Rotating coordinate system**

Figure 2.3 states that the Z -axes of GEI and GER frames coincide, but T_{GER} rotates with respect to T_{GEI} , around its polar axis, with an angular velocity that is Earth's angular velocity:

$$\omega_E = 7.2921 \cdot 10^{-5} \text{ rad/s}$$

2.1.5 Zenith-East-North Coordinate System

This particular frame of reference is an auxiliary system that can be defined in any generic right-handed frame $T(X, Y, Z)$, useful to define a body's position and speed components on a particular point P of its orbit.

It will be referred to as $T_{ZEN}(X_{ZEN}, Y_{ZEN}, Z_{ZEN})$ and the orientation of its axes depends on the position P .

Assuming that the origin of T_{ZEN} and T coincide, the three axes are defined as follows:

- X_{ZEN} connects the origin with the point P ;
- Z_{ZEN} points to the North direction;
- Y_{ZEN} orthogonal to X_{ZEN} and directed towards East with respect to it, thus completing the right-handed frame.

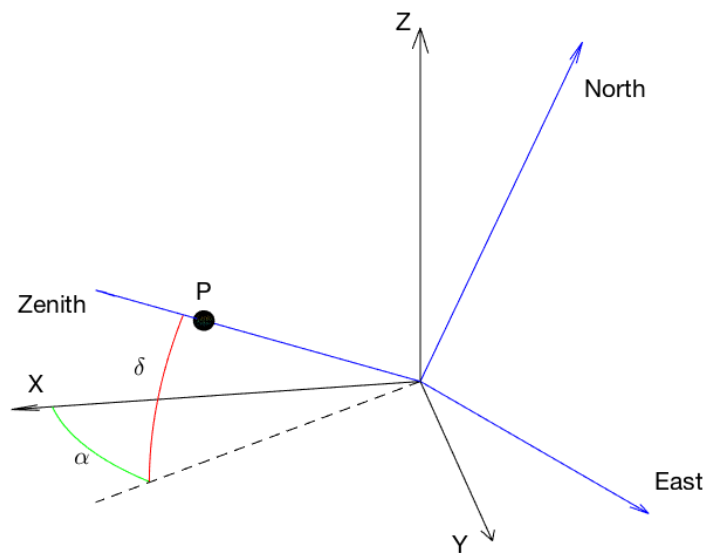


Figure 2.5: Zenith East North coordinate system

2.1.6 Perifocal Coordinate System

This is one of the most convenient reference frames when the motion of a satellite needs to be described. Its fundamental plane coincides with the orbital plane and its origin is set in the body around which the spacecraft moves.

It will be referred to as $T_P(X_P, Y_P, Z_P)$ and its axes are defined as follows:

- X_P is directed towards the orbit's periapsis;
- Y_P is rotated of an angle of 90° in the direction of the spacecraft's motion and lies on the orbital plane;
- Z_P is parallel to the angular momentum vector and completes the frame, making it right-handed.

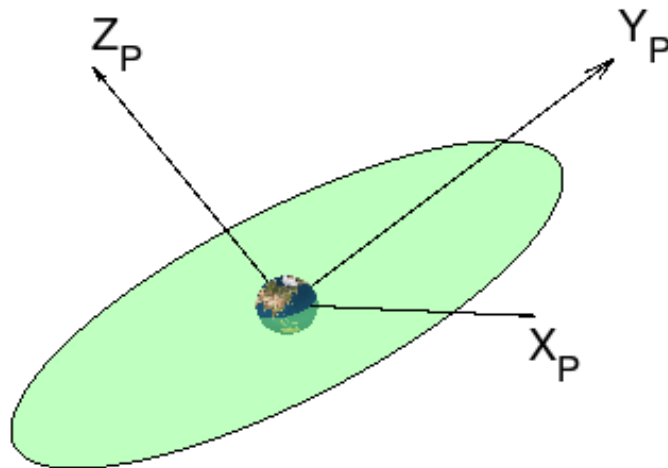


Figure 2.6: Perifocal coordinate system

2.2 Transformation matrices

Throughout this work, it will be useful being able to switch from one coordinate system to another, because of the fact that some inputs are given in a heliocentric frame of reference, while the output should be analyzed from a geocentric point of view.

Let now introduce a generic vector, defined in the generic coordinate system $t(x, y, z)$

$$\vec{a}_t = \begin{bmatrix} a_x \\ a_y \\ a_z \end{bmatrix}$$

Our goal is now derive the matrix operations necessary to obtain the components of \vec{a} in another frame of reference, say $T(X, Y, Z)$, whose origin coincides with t 's

$$\vec{a}_T = \begin{bmatrix} a_X \\ a_Y \\ a_Z \end{bmatrix}$$

In order to achieve this, we need to know the mutual orientation of the two frames.

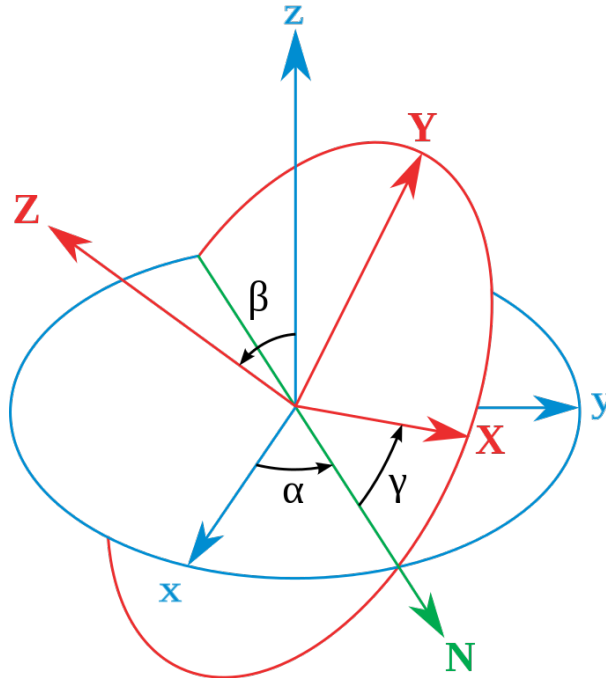


Figure 2.7: Reference frames with common origin

At first, a rotation of an angle equal to α around the z -axis is required, so that the x -axis aligns itself with the line of nodes, identified by the N direction. The first elementary rotation matrix will be:

$$\mathbb{R}_z(\alpha) = \begin{bmatrix} \cos \alpha & \sin \alpha & 0 \\ -\sin \alpha & \cos \alpha & 0 \\ 0 & 0 & 1 \end{bmatrix}$$

Note that the angle α is assumed positive if, in order to make x coincident to X , the rotation to perform is clockwise (following the righ-hand rule).

The second step involves a rotation around the N direction, that now coincides with the x -axis, of an angle equal to β . Following this operation, z -axis is now parallel to Z -axis. The second elementary rotation matrix can be evaluated as:

$$\mathbb{R}_x(\beta) = \begin{bmatrix} 1 & 0 & 0 \\ 0 & \cos \beta & \sin \beta \\ 0 & -\sin \beta & \cos \beta \end{bmatrix}$$

The last rotation required is around z -axis of an angle equal to γ , in order to make the two systems perfectly coincident.

$$\mathbb{R}_z(\gamma) = \begin{bmatrix} \cos \gamma & 0 & -\sin \gamma \\ 0 & 1 & 0 \\ \sin \gamma & 0 & \cos \gamma \end{bmatrix}$$

The complete transformation between t and T can now be written as follows:

$$\vec{a}_T = [\mathbb{R}_z(\alpha) \cdot \mathbb{R}_x(\beta) \cdot \mathbb{R}_z(\gamma)] \vec{a}_t$$

so that

$$\begin{bmatrix} a_X \\ a_Y \\ a_Z \end{bmatrix} = \begin{bmatrix} \cos \alpha & \sin \alpha & 0 \\ -\sin \alpha & \cos \alpha & 0 \\ 0 & 0 & 1 \end{bmatrix} \begin{bmatrix} 1 & 0 & 0 \\ 0 & \cos \beta & \sin \beta \\ 0 & -\sin \beta & \cos \beta \end{bmatrix} \begin{bmatrix} \cos \gamma & 0 & -\sin \gamma \\ 0 & 1 & 0 \\ \sin \gamma & 0 & \cos \gamma \end{bmatrix} \begin{bmatrix} a_x \\ a_y \\ a_z \end{bmatrix}$$

Where a transformation matrix has been introduced

$$\mathbb{T}_{t \rightarrow T} = [\mathbb{R}_z(\alpha) \cdot \mathbb{R}_x(\beta) \cdot \mathbb{R}_z(\gamma)]$$

2.2.1 Transformation from T_{HAE} to T_{GEI}

The goal is to express the components of a generic vector, originally known only in the Heliocentric Aries Ecliptic system, also with respect to the Geocentric Equatorial Inertial frame.

First of all, the mutual orientation of the two coordinate system must be specified. In particular, as can be seen in Figure 2.8:

- the origin of T_{HAE} is set in the center of Earth, while T_{GEI} 's lies in the center of the Sun, this means that the Sun-Earth position vector must be introduced in order to perform a translational transformation;
- Z_{GEI} -axis is inclined, relative to Z_{HAE} , of an angle $i_E = 23^\circ 27'$ defined as the inclination of Earth's equator with respect to the ecliptic plane.

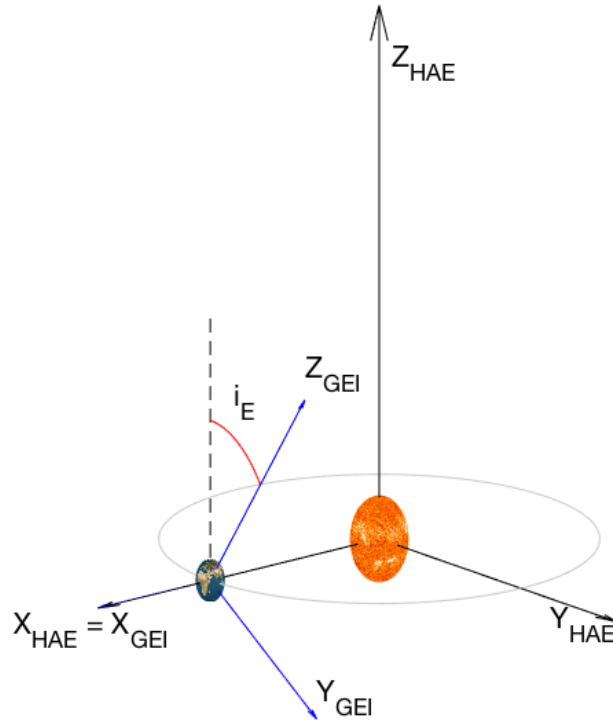


Figure 2.8: Mutual orientation of HAE and GEI coordinate systems

Our interest is only focused on the orientation of the vector and not on its point of application, fact that implies that the two frames of reference can be assumed to possess the same origin. This means that the translational transformation is not required anymore. The components of the generic vector in the two coordinate system are defined as follows:

$$\vec{a}_{HAE} = \begin{bmatrix} a_x \\ a_y \\ a_z \end{bmatrix}_{HAE}$$

$$\vec{a}_{GEI} = \begin{bmatrix} a_x \\ a_y \\ a_z \end{bmatrix}_{GEI}$$

And the transformation implies a simple, counterclockwise, rotation equal to i_E around X_{HAE} , so that:

$$\mathbb{T}_{HAE \rightarrow GEI} = \mathbb{R}_x(-i_E) = \begin{bmatrix} 1 & 0 & 0 \\ 0 & \cos i_E & -\sin i_E \\ 0 & \sin i_E & \cos i_E \end{bmatrix}$$

The components of \vec{a} can be expressed in the Geocentric Equatorial Inertial frame by means of this relation:

$$\vec{a}_{GEI} = \mathbb{T}_{HAE \rightarrow GEI} \cdot \vec{a}_{HAE}$$

In matrix notation:

$$\begin{bmatrix} a_x \\ a_y \\ a_z \end{bmatrix}_{GEI} = \begin{bmatrix} 1 & 0 & 0 \\ 0 & \cos i_E & -\sin i_E \\ 0 & \sin i_E & \cos i_E \end{bmatrix} \begin{bmatrix} a_x \\ a_y \\ a_z \end{bmatrix}_{HAE}$$

The inverse transformation can easily be computed as follows:

$$\vec{a}_{HAE} = \mathbb{T}_{HAE \rightarrow GEI}^{-1} \cdot \vec{a}_{GEI}$$

In matrix notation:

$$\begin{bmatrix} a_x \\ a_y \\ a_z \end{bmatrix}_{HAE} = \begin{bmatrix} 1 & 0 & 0 \\ 0 & \cos i_E & \sin i_E \\ 0 & -\sin i_E & \cos i_E \end{bmatrix} \begin{bmatrix} a_x \\ a_y \\ a_z \end{bmatrix}_{GEI}$$

Where :

$$\mathbb{T}_{HAE \rightarrow GEI}^{-1} = \mathbb{T}_{GEI \rightarrow HAE}$$

Furthermore, since rotation matrices are orthogonal, their transpose is identical to their inverse, so that:

$$\mathbb{T}_{HAE \rightarrow GEI}^{-1} = \mathbb{T}_{HAE \rightarrow GEI}^T$$

2.2.2 Transformation from T_{GEI} to T_{GL}

The two frames of interest share the same origin point, i.e. the center of the Earth, but their axes are tilted with respect to each other. In particular, in order to express the components of a T_{GEI} -defined vector also in the T_{GL} frame, two consecutive rotations are required:

- First of all, a rotation of T_{GEI} about Z_{GEI} of an angle Ω_M , that is the right ascension of the ascending node (RAAN) of the Moon's orbit with respect to X_{GEI} -axis. This transformation allows X_{GEI} to coincide with X_{GL} , so that we obtain an intermediate frame;
- The second rotation will be around X_{GEI} of an angle $i_M = 5.145^\circ$, that is the inclination of the Moon's orbit with respect to the ecliptic plane, so that the two frames eventually coincide.

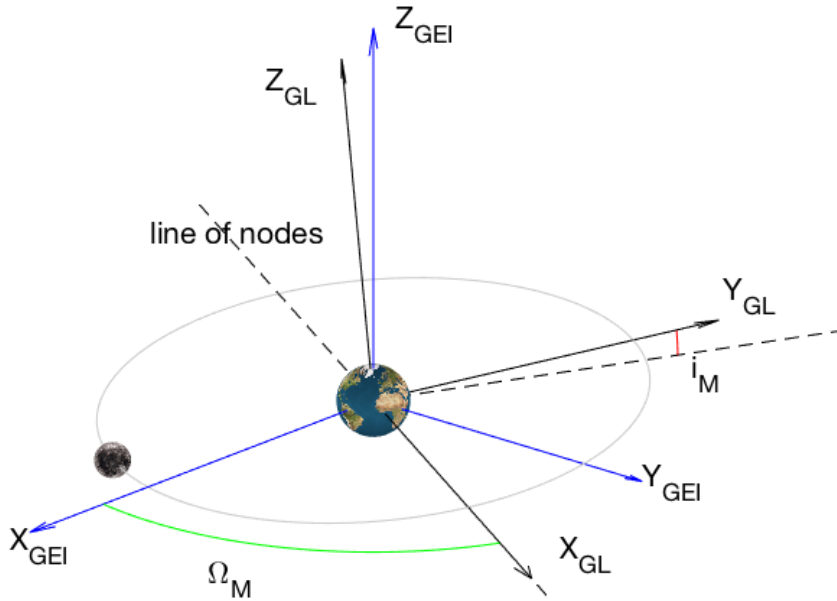


Figure 2.9: Mutual orientation of GEI and GL coordinate systems

The transformation matrix will be computed as a combination of two elementary rotation matrices:

$$T_{GEI \rightarrow GL} = \mathbb{R}_x(i_M)\mathbb{R}_z(\Omega_M)$$

Where the two elementary rotation matrices are:

$$\mathbb{R}_x(i_M) = \begin{bmatrix} 1 & 0 & 0 \\ 0 & \cos i_M & \sin i_M \\ 0 & -\sin i_M & \cos i_M \end{bmatrix} \quad \text{and} \quad \mathbb{R}_z(\Omega_M) = \begin{bmatrix} \cos \Omega_M & \sin \Omega_M & 0 \\ -\sin \Omega_M & \cos \Omega_M & 0 \\ 0 & 0 & 1 \end{bmatrix}$$

The transformation can be written as:

$$\vec{a}_{GL} = \mathbb{T}_{GEI \rightarrow GL} \cdot \vec{a}_{GEI}$$

That, in matrix notation, states:

$$\begin{bmatrix} a_x \\ a_y \\ a_z \end{bmatrix}_{GL} = \begin{bmatrix} \cos \Omega_M & \sin \Omega_M & 0 \\ -\cos i_M \sin \Omega_M & \cos i_M \cos \Omega_M & \sin i_M \\ \sin i_M \sin \Omega_M & -\sin i_M \cos \Omega_M & \cos i_M \end{bmatrix} \begin{bmatrix} a_x \\ a_y \\ a_z \end{bmatrix}_{GEI}$$

The inverse transformation, from T_{GL} to T_{GEI} can be easily derived:

$$\vec{a}_{GEI} = \mathbb{T}_{GL \rightarrow GEI} \cdot \vec{a}_{GL}$$

Where, as explained in the previous subsection:

$$\mathbb{T}_{GL \rightarrow GEI} = \mathbb{T}_{GEI \rightarrow GL}^{-1} = \mathbb{T}_{GEI \rightarrow GL}^T$$

The matrix notation can be computed as follows:

$$\begin{bmatrix} a_x \\ a_y \\ a_z \end{bmatrix}_{GEI} = \begin{bmatrix} \cos \Omega_M & -\cos i_M \sin \Omega_M & \sin i_M \sin \Omega_M \\ \sin \Omega_M & \cos i_M \cos \Omega_M & -\sin i_M \cos \Omega_M \\ 0 & \sin i_M & \cos i_M \end{bmatrix} \begin{bmatrix} a_x \\ a_y \\ a_z \end{bmatrix}_{GL}$$

2.2.3 Transformation from T to T_{ZEN}

As previously stated, the Zenith-East-North frame of reference can be defined within another right-handed coordinate system, say $T(X, Y, Z)$. The characteristic angles that establish the orientation of T with respect to T_{ZEN} are α and δ .

Let's now compute the transformation between those two frames:

- First of all, a rotation of T around its Z -axis of an angle equal to α has to be performed, so that an intermediate frame in which the two Y -axes coincide is created;
- Then, a rotation around Y -axis of an angle $-\delta$ is required

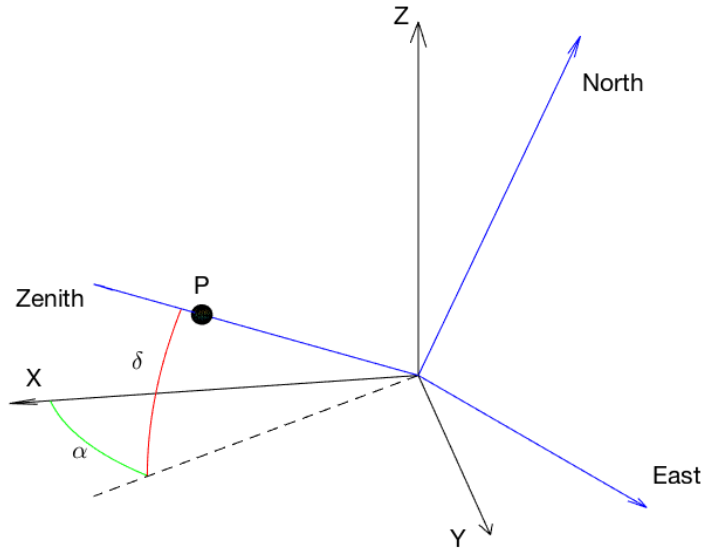


Figure 2.10: **Zenith East North coordinate system**

The transformation matrix can therefore be computed as follows:

$$\mathbb{T}_{T \rightarrow ZEN} = \mathbb{R}_y(-\delta)\mathbb{R}_z(\alpha)$$

Where the two elementary rotation matrices are:

$$\mathbb{R}_y(-\delta) = \begin{bmatrix} \cos \delta & 0 & \sin \delta \\ 0 & 1 & 0 \\ -\sin \delta & 0 & \cos \delta \end{bmatrix} \quad \text{and} \quad \mathbb{R}_z(\alpha) = \begin{bmatrix} \cos \alpha & \sin \alpha & 0 \\ -\sin \alpha & \cos \alpha & 0 \\ 0 & 0 & 1 \end{bmatrix}$$

So that the transformation relation states:

$$\vec{a}_{ZEN} = \mathbb{T}_{T \rightarrow ZEN} \cdot \vec{a}_T$$

Written in matrix notation:

$$\begin{bmatrix} a_{Zenith} \\ a_{East} \\ a_{North} \end{bmatrix} = \begin{bmatrix} \cos \delta \cos \alpha & \cos \delta \sin \alpha & \sin \delta \\ -\sin \alpha & \cos \alpha & 0 \\ -\sin \delta \cos \alpha & -\sin \delta \sin \alpha & \cos \delta \end{bmatrix} \begin{bmatrix} a_x \\ a_y \\ a_z \end{bmatrix}$$

The inverse transformation, from T_{ZEN} to T can be easily derived:

$$\vec{a}_T = \mathbb{T}_{ZEN \rightarrow T} \cdot \vec{a}_{ZEN}$$

Where, as explained in the previous subsections:

$$\mathbb{T}_{ZEN \rightarrow T} = \mathbb{T}_{T \rightarrow ZEN}^{-1} = \mathbb{T}_{T \rightarrow ZEN}^T$$

The matrix notation can be computed as follows:

$$\begin{bmatrix} a_x \\ a_y \\ a_z \end{bmatrix} = \begin{bmatrix} \cos \delta \cos \alpha & -\sin \alpha & -\sin \delta \cos \alpha \\ \cos \delta \sin \alpha & \cos \alpha & -\sin \delta \sin \alpha \\ \sin \delta & 0 & \cos \delta \end{bmatrix} \begin{bmatrix} a_{Zenith} \\ a_{East} \\ a_{North} \end{bmatrix}$$

2.2.4 Transformation from T_P to T_{GEI}

In order to let T_{GEI} and T_P coincide, it is necessary to derive a rotation matrix that can be calculated from three elementary rotation matrices. As can be seen in Figure 2.11, in which the fundamental plane is the red one and the orbital plane is the green one, the two systems' mutual orientation can be expressed as follows:

- T_{GEI} first needs to be rotated about its Z -axis of an angle Ω , in order to obtain an intermediate frame T' ;
- Then, a rotation of this intermediate frame around its X' -axis of an angle i has to be performed, so that a second intermediate system T'' -axis is obtained;
- Finally, T'' can be rotated about its Z'' -axis of an angle ω , so that the two frames coincide.

The angles Ω , ω and i are three orbital parameters, whose meaning will be object of further deepening in the following chapter.

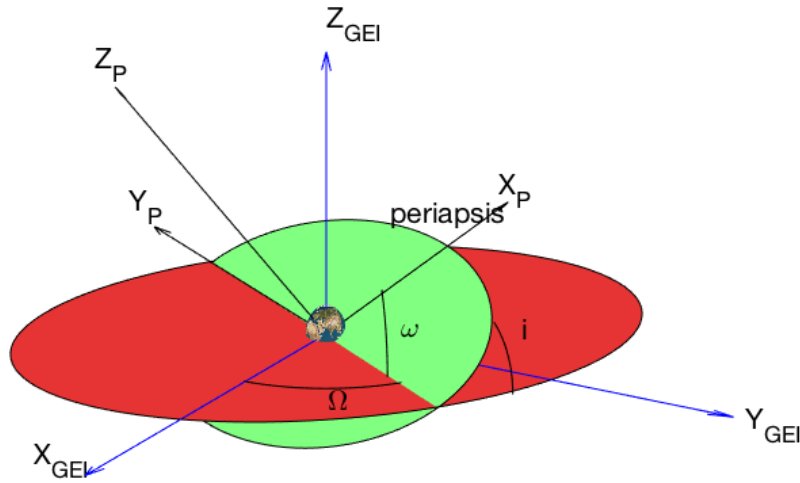


Figure 2.11: Mutual orientation of T_P and T_{GEI} frames of reference

The transformation matrix can be calculated as the product of three different elementary rotation matrices:

$$\mathbb{T}_{P \rightarrow GEI} = \mathbb{R}_z(\omega) \mathbb{R}_x(i) \mathbb{R}_z(\Omega)$$

So that the transformation can be expressed as follows:

$$\vec{a}_{GEI} = \mathbb{T}_{P \rightarrow GEI} \cdot \vec{a}_P$$

Where:

$$\mathbb{T}_{P \rightarrow GEI} = \begin{bmatrix} \cos \Omega \cos \omega - \sin \Omega \sin \omega \cos i & \sin \Omega \cos \omega + \cos \Omega \sin \omega \cos i & \sin \omega \sin i \\ -\cos \Omega \sin \omega - \sin \Omega \cos \omega \cos i & -\sin \Omega \sin \omega + \cos \Omega \cos \omega \cos i & \cos \omega \sin i \\ \sin \Omega \sin i & -\cos \Omega \sin i & \cos i \end{bmatrix}$$

The inverse transformation can easily be derived:

$$\vec{a}_P = \mathbb{T}_{GEI \rightarrow P} \cdot \vec{a}_{GEI}$$

Where:

$$\mathbb{T}_{GEI \rightarrow P} = \begin{bmatrix} \cos \Omega \cos \omega - \sin \Omega \sin \omega \cos i & -\cos \Omega \sin \omega - \sin \Omega \cos \omega \cos i & \sin \Omega \sin i \\ \sin \Omega \cos \omega + \cos \Omega \sin \omega \cos i & -\sin \Omega \sin \omega + \cos \Omega \cos \omega \cos i & \cos \Omega \sin i \\ \sin \omega \sin i & -\cos \omega \sin i & \cos i \end{bmatrix}$$

Chapter 3

Mathematical model

This chapter is intended to present the most important mathematical relations on which the motion of planets and, in general, the celestial bodies, is founded.

The first and second sections are focused on recalling the three laws of Kepler and defining the n-body problem. Then, some simplifications will be introduced in order to reduce it to the classical 2-body problem.

In the following sections, after introducing the conic sections, the four types of Keplerian orbits and the orbital elements will be derived and described.

Other sections will be dedicated to the Patched Conic Approximation, to the Gravity Assist model and to the Canonical Units adopted throughout the work.

3.1 Kepler's laws of planetary motion

During the second half of the XVIth century, the Danish astronomer Tycho Brahe performed hundreds of observations regarding the position of stars and planets, keeping accurate records of his studies. When Tycho died, in 1601, one of his students came into possession of his record books and started to summarize them, looking for some common features in the motion of the celestial bodies; his name was Johannes von Kepler.

During the following years, basing himself on the Copernican model of the Solar System and using his mentor's data, Kepler managed to formulate the first and second law of planetary motion, published in 1609.

After that, ten years of additional work were necessary for him to achieve the third law.

At that time, motion was considered an intrinsic characteristic of objects, so that every scientist confined himself to its description, rather than investigating its cause. Kepler suggested that the Sun could exert a force upon the planets, but never specified which kind of force was that. However, his studies prepared the ground for Newton's work, that eventually came up with a solution regarding the occurrence of what he called the gravitational attraction.

3.1.1 The Law of Ellipses

"The orbit of every planet is an ellipse with the Sun at one of the two foci"

The consultation of Tycho's papers, together with his studies, persuaded Kepler to abandon the theory of circular orbits, pretty common at that time due to the perfection of the shape, to focus on the possibility that the planets could follow an ellipse around the Sun.

An ellipse is a particular curve characterized by the fact that the sum of the distances between every point on the curve and two other points, classified as foci of the ellipse, is a constant. The closer the foci, the more the ellipse resembles a circle.

Due to the definition of ellipse, the distance between the planet and the Sun varies along the orbit, so that two peculiar orbital points can be introduced:

- **Aphelion**, defined as the point in the orbit of a celestial body where it is farthest from the Sun;
- **Perihelion**, which is the nearest point to the Sun of a body's orbit.

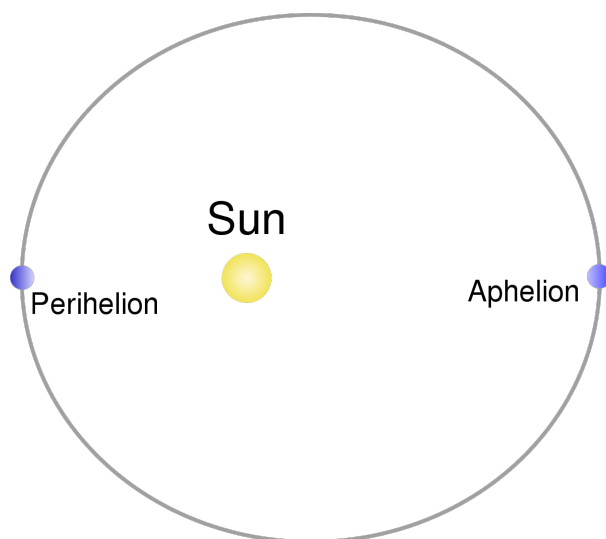


Figure 3.1: **Example of elliptical orbit around the Sun**

3.1.2 The Law of Equal Areas

"A line joining a planet and the Sun sweeps out equal areas in equal intervals of time"

This sentence states that the orbital velocity of the planet along its orbit is not a constant, but varies over time. In particular, the orbital speed reaches its maximum value when the planet crosses the perihelion, and its minimum at the aphelion.

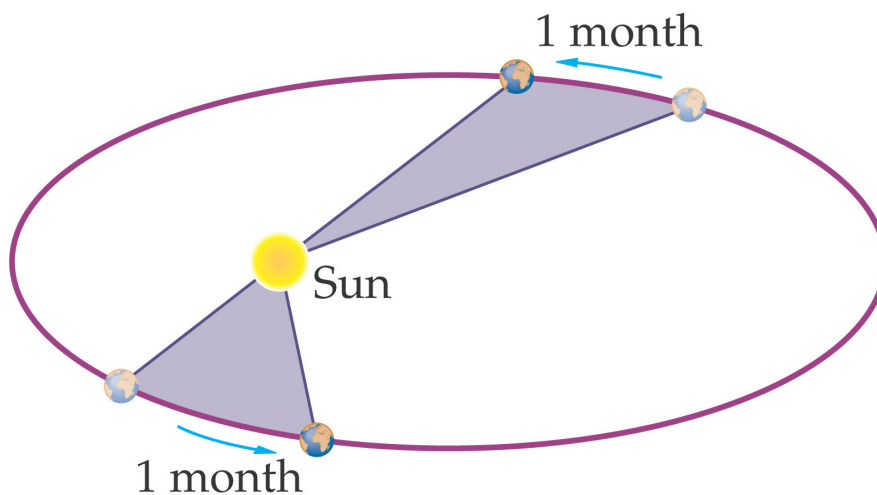


Figure 3.2: Graphic representation of Kepler's second law

As illustrated in Figure 3.2, the position of the planet along the orbit influences its orbital velocity and so the arcs of orbit swept in the same amount of time. This leads to the fact that the two purple areas can be considered equal.

3.1.3 The Law of Harmonies

"The square of the orbital period of a planet is directly proportional to the cube of the semi-major axis of its orbit"

Unlike the first and the second law, that describe the properties of a planet's motion around the Sun, the third law provides a relationship between the orbital periods of the planets and their distance from the Sun. The same rule is also valid if referred to the satellites orbiting around the single planets.

An overview of the orbital properties of the most important celestial bodies of the Solar System is presented in Table 3.1. As can be seen, their semi-major axis and their orbital period are related by almost the same ratio.

Planet	Orbital period T [yr]	Average distance R [AU]	T^2R^{-3}
Mercury	0.241	0.39	0.98
Venus	0.615	0.72	1.01
Earth	1.00	1.00	1.00
Mars	1.88	1.52	1.01
Jupiter	11.8	5.20	0.99
Saturn	29.5	9.54	1.00
Uranus	84.0	19.18	1.00
Neptune	165	30.06	1.00

Table 3.1: Overview of the Solar System's planets orbital properties

These laws are to be considered exact only if the following hypothesis are satisfied:

- the planet's mass is considered negligible with respect to the star's mass;
- the gravitational influences of other planets on a planet's motion, that cause slight perturbations of its orbit, are neglected.

After the publication of Kepler's work, the issue regarding what caused the planets to orbit the Sun was to be unknown for decades to come.

In 1665, the University of Cambridge was forced to close for a period of two years due to an outbreak of the plague. During this pause from the studies, one of its students, whose name was Isaac Newton, conceived the law of gravitation, the laws of motion and the fundamental concepts of differential calculus.

However, due to some discrepancies explaining the Moon's motion around Earth, Newton decided to wait another 20 years before publishing *The Mathematical Principles of Natural Philosophy*, or, more simply, *Principia*, in 1687.

The two major achievements contained in that work were the Law of Universal Gravitation and the Second Law of Motion.

Law of Universal Gravitation

This relation states that two bodies attract to each other with a force that is proportional to the product of their masses and inversely proportional to the square of their distance, so that, in vector notation:

$$\vec{F}_g = -G \frac{Mm}{r^2}$$

Where we introduced the gravitational constant $G = 6.67408 \cdot 10^{-11} \frac{m^3}{kg \cdot s^2}$

Second Law of Motion

According to this law, the rate of change of a body's momentum is proportional to the force impressed and is in the same direction as that force. Mathematically, it can be expressed as follows:

$$\sum F = m\ddot{r}$$

3.2 The n-body problem

In physics, the *n-body problem* deals with the prediction of the individual motion of a group of celestial objects that interact with each other gravitationally.

For the sake of simplicity, the planets are assumed to be:

- perfectly spherical, due to the fact that the gravitational potential of a sphere is equal to that of a point in which the sphere's mass is condensed;
- homogeneous, which implies that the mass density is not a function of the position inside the body.

Our attention will be focused on the motion of the i -th body, influenced by the gravitational attraction of the remaining $n-1$ bodies: $m_1, \dots, m_{i-1}, m_{i+1}, \dots, m_{n-1}, m_n$.

In order to achieve this, we need to introduce a generic, inertial reference frame $T(X, Y, Z)$ with regard to which the position vectors of the n bodies are known and can be expressed as $\vec{r}_1, \vec{r}_2, \dots, \vec{r}_n$.

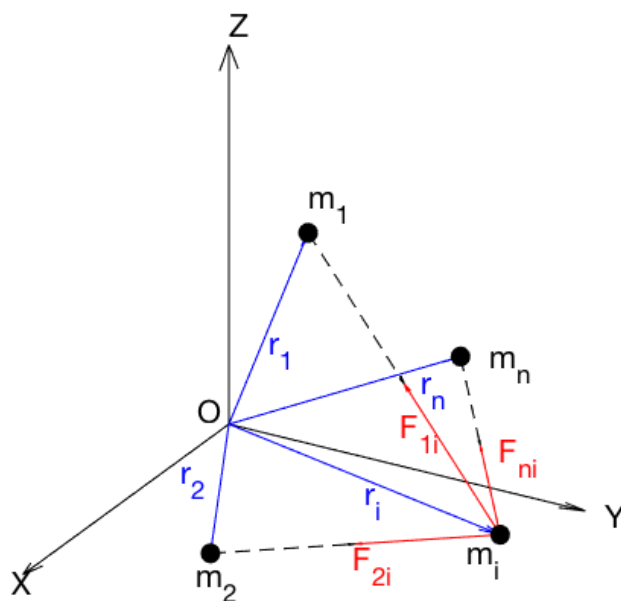


Figure 3.3: Overview of the n-body problem

By applying the law of universal gravitation, the force exerted on m_i by m_n can be evaluated as follows:

$$\vec{F}_{ji} = -G \frac{m_i m_j}{r_{ij}^3} \vec{r}_{ij} \quad (3.1)$$

And the relative position vector between m_i and m_j can be written as:

$$\vec{r}_{ij} = \vec{r}_i - \vec{r}_j = \vec{r}_{ij}$$

The sum vector, that takes into account the presence of the n-1 bodies, will be:

$$\vec{F}_i = \sum_{j=1, j \neq i}^n \vec{F}_{ij} = -Gm_i \sum_{j=1, j \neq i}^n \frac{m_j}{r_{ij}^3} \vec{r}_{ij} \quad (3.2)$$

That, under the assumption of bodies having constant mass, eventually allows to obtain the expression for the acceleration vector of the i^{th} body relative to the coordinate system T :

$$\vec{r}_i = -G \sum_{j=1, j \neq i}^n \frac{m_j}{r_{ij}^3} \vec{r}_{ij} \quad (3.3)$$

Due to the fact that Newton's second law states that the application of a force always results in a variation of the body's momentum:

$$\vec{F}_i = \frac{d}{dt}(m_i \vec{V}_i) = m_i \ddot{\vec{r}}_i \quad (3.4)$$

Equation 3.3 is a second order, nonlinear, vector, differential equation and, in absence of strong simplification hypothesis, an analytical solution is impossible to find.

Let now assume m_1 as Earth, m_2 as an Earth-orbiting spacecraft and m_3, \dots, m_n as the other Solar System's celestial bodies; if we rewrite Equation 3.3 for 1 and 2, we obtain:

$$\vec{r}_1 = -G \sum_{j=2}^n \frac{m_j}{r_{1j}^3} \vec{r}_{1j} \quad (3.5)$$

$$\vec{r}_2 = -G \sum_{j=1, j \neq 2}^n \frac{m_j}{r_{2j}^3} \vec{r}_{2j} \quad (3.6)$$

But our interest is focused on the motion of m_2 relative to m_1 , so it is convenient to subtract Equation 3.6 from Equation 3.5. The following relations are valid:

$$\vec{r}_{12} = \vec{r}_2 - \vec{r}_1$$

and

$$\ddot{\vec{r}}_{12} = \ddot{\vec{r}}_2 - \ddot{\vec{r}}_1$$

That leads to:

$$\ddot{\vec{r}}_{12} = -G \sum_{j=1, j \neq 2}^n \frac{m_j}{r_{2j}^3} \vec{r}_{2j} + G \sum_{j=2}^n \frac{m_j}{r_{1j}^3} \vec{r}_{1j} \quad (3.7)$$

This one, rearranged, can be written as:

$$\vec{r}_{12} = -G \frac{m_1 + m_2}{r_{12}^3} \vec{r}_{12} - G \sum_{j=3}^n m_j \left(\frac{\vec{r}_{j2}}{r_{j2}^3} - \frac{\vec{r}_{j1}}{r_{j1}^3} \right) \quad (3.8)$$

The first term of Equation 3.8 represents the gravitational influence of Earth on the spacecraft, while its second term is related to the other celestial bodies' interaction with m_2 . If we assume that the influence of m_3, \dots, m_n is much smaller than that of m_1 with respect to m_2 , we can assume the summation term as a perturbation.

To better understand the order of magnitude of the main gravitational attraction between Earth and the spacecraft and to compare it with the perturbative terms, let us consider a spacecraft orbiting Earth at a distance of 200 NM from the surface, equivalent to 370 km, which is approximately the International Space Station orbit altitude.

In the following table, the relative accelerations between the spacecraft and the other celestial bodies will be expressed in terms of a fraction of g , defined as the standard value of gravitational acceleration at sea level.

Celestial body	Acceleration [g]
Earth	0.89
Sun	$6 \cdot 10^{-4}$
Mercury	$2.6 \cdot 10^{-10}$
Venus	$1.9 \cdot 10^{-8}$
Mars	$7.1 \cdot 10^{-10}$
Jupiter	$3.2 \cdot 10^{-8}$
Saturn	$2.3 \cdot 10^{-9}$
Uranus	$8 \cdot 10^{-11}$
Neptune	$3.6 \cdot 10^{-11}$
Pluto	10^{-12}
Moon	$3.3 \cdot 10^{-6}$

Table 3.2: **Perturbative accelerations acting on an Earth-orbiting spacecraft**

For further comparison, the perturbative acceleration due to the non perfectly spherical shape of Earth, that takes the name of oblateness, accounts for approximately $10^{-3}g$, so that this effect is far more important than all the other bodies' presence.

3.3 The 2-body problem

In the current section, a particular case of the n-body problem will be discussed. Our goal remains to derive a general expression for the relative motion of two bodies, but in this case there will be no perturbing bodies around the main ones.

In order to achieve this, we need to make two assumptions regarding our model:

- the bodies are considered to be spherically symmetric, thus enabling us to consider them as punctiform masses;
- the system is only subject to the gravitational attraction between the two bodies, because the other internal or external forces are considered null.

The geometry of the problem is schematized in Figure 3.4: with regard to the inertial reference frame $T(X, Y, Z)$, the position vectors \vec{r}_m and \vec{r}_M of the two masses m and M have been defined.

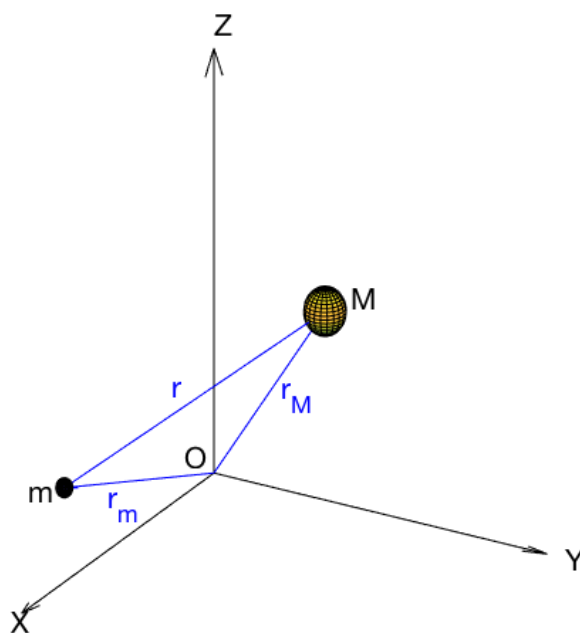


Figure 3.4: Overview of the 2-body problem

It is now possible to apply Newton's laws to obtain the acceleration to which the smaller body is subject:

$$\vec{\ddot{r}} = -G \frac{M + m}{r^3} \vec{r} \quad (3.9)$$

This is a second order vector differential equation equivalent to Equation 3.8 under the assumption that the perturbative term is equal to zero.

But in this study, the smaller body's mass can be considered negligible with respect to the larger one, so that the following relation can be assumed valid:

$$G(M + m) \approx GM = \mu$$

Where μ is defined as the *gravitational parameter*, that has different values for each major attracting body. The equation of motion relative to a two-body system can easily be derived:

$$\vec{r} = -\frac{\mu}{r^3}\vec{r} \quad (3.10)$$

This second order vector differential equation can be integrated and the analytical solution for the 2-body problem can be found.

The results obtained from this relation are correct only if the two assumptions made at the beginning of this section are valid and if $M \gg m$; if not so, μ needs to be replaced by the correct value of the expression $G(M + m)$.

3.3.1 Constants of motion

When a body is only subject to the influence of a gravitational field, the sum of its potential and kinetic energy, which is the system's mechanical energy, will remain unchanged over time and the only feasible energy exchange is between these two forms. This implies that the gravitational field is conservative.

Furthermore, in order to obtain a variation of the system's angular momentum, a tangential component of force is needed, but the gravitational force is always directed in the radial direction, towards the center of the larger mass. This implies that also the angular momentum must remain constant over time.

Let now prove these two statements.

Conservation of mechanical energy

Let now recall Equation 3.10 and dot multiply it by \vec{r} , thus obtaining:

$$\vec{r} \cdot \vec{r} + \vec{r} \cdot \frac{\mu}{r^3}\vec{r} = 0 \quad (3.11)$$

If we substitute $\vec{v} = \dot{\vec{r}}$ and $\vec{v} = \dot{\vec{r}}$ and $r \cdot \dot{\vec{r}} = r\dot{r}$ we can write:

$$v\dot{v} + \frac{\mu}{r^3}r\dot{r} = 0 \quad (3.12)$$

And by using the following relations:

$$\frac{d}{dt}\left(\frac{v^2}{2}\right) = v\dot{v}$$

$$\frac{d}{dt}\left(-\frac{\mu}{r}\right) = \frac{\mu}{r^2}\dot{r}$$

We can reach the final relation:

$$\frac{d}{dt} \left(\frac{v^2}{2} - \frac{\mu}{r} \right) = 0$$

That implies:

$$\mathcal{E} = \frac{v^2}{2} - \frac{\mu}{r} = \text{constant} \quad (3.13)$$

Where \mathcal{E} is the system's specific mechanical energy, that is the sum of the kinetic energy per unit of mass $\frac{v^2}{2}$ and the potential energy per unit of mass $\frac{\mu}{r}$. As a result of what we have just said, \mathcal{E} remains constant along the body's orbit, without decreasing or increasing by means of its motion.

Conservation of angular momentum

If instead we cross multiply Equation 3.10 by \vec{r} , what we obtain is:

$$\vec{r} \times \vec{\dot{r}} + \vec{r} \times \frac{\mu}{r^3} \vec{r} = 0 \quad (3.14)$$

But the cross product of a vector by himself leads to a null result, because of the fact that they are parallel to each other. This means that the second term vanishes, so that:

$$\vec{r} \times \vec{\dot{r}} = 0$$

Noticing that:

$$\frac{d}{dt} (\vec{r} \times \dot{r}) = \vec{\dot{r}} \times \vec{r} + \vec{r} \times \vec{\dot{r}}$$

The equation written above becomes:

$$\frac{d}{dt} (\vec{r} \times \vec{\dot{r}}) = 0$$

or

$$\frac{d}{dt} (\vec{r} \times \vec{v}) = 0$$

This means that the quantity between brackets must be another constant of motion, that takes the name of *specific angular momentum*:

$$\vec{h} = \vec{r} \times \vec{v} \quad (3.15)$$

An important note regarding h is that it is, by definition, the cross product of r by v and, due to the fact that it is constant, these two vectors must remain in the same plane. Therefore, the body's motion is necessarily confined to a plane that is fixed in space and takes the name of *orbital plane*.

3.4 The trajectory equation

Equation 3.10 is a pretty simple relation, especially if compared to its importance, that concerns the relative motion for the two-body problem. Despite its simplicity, a complete solution is quite hard to obtain, that is why we will concentrate on finding a partial one in order to distinguish the possible shapes and sizes of the orbits. Recalling Equation 3.10:

$$\ddot{\vec{r}} = -\frac{\mu}{r^3}\vec{r}$$

If we cross multiply it by \vec{h} , we obtain a relation that can be integrated:

$$\ddot{\vec{r}} \times \vec{h} = \frac{\mu}{r^3}(\vec{h} \times \vec{r}) \quad (3.16)$$

Whose first member is equal to:

$$\frac{d}{dt}(\dot{\vec{r}} \times \vec{h})$$

And the second one can be traced back to:

$$\frac{\mu}{r^3}(\vec{h} \times \vec{r}) = \frac{\mu}{r^3}(\vec{r} \times \vec{v}) \times \vec{r} = \frac{\mu}{r^3}[\vec{v}(\vec{r} \cdot \vec{r}) - \vec{r}(\vec{r} \cdot \vec{v})] = \frac{\mu}{r}\vec{v} - \frac{\mu\dot{r}}{r^2}\vec{r}$$

So that Equation 3.16 can be rewritten as follows:

$$\frac{d}{dt}(\dot{\vec{r}} \times \vec{h}) = \mu \frac{d}{dt}\left(\frac{\vec{r}}{r}\right) \quad (3.17)$$

Both members can now be integrated:

$$\dot{\vec{r}} \times \vec{h} = \mu \frac{\vec{r}}{r} + \vec{B} \quad (3.18)$$

Where \vec{B} is defined as the *vector constant of integration*. We can obtain a scalar equation by simply dot multiplying the last relation by \vec{r} :

$$\vec{r} \cdot \dot{\vec{r}} \times \vec{h} = \vec{r} \cdot \mu \frac{\vec{r}}{r} + \vec{r} \cdot \vec{B} \quad (3.19)$$

And because $\vec{a} \cdot \vec{b} \times \vec{c} = \vec{a} \times \vec{b} \cdot \vec{c}$ and $\vec{a} \cdot \vec{a} = a^2$, it follows that:

$$h^2 = \mu r + rB \cos \nu \quad (3.20)$$

Where ν is the angle between the radius vector \vec{r} and the constant vector \vec{B} . By specifying r we eventually obtain:

$$r = \frac{h^2/\mu}{1 + (B/\mu) \cos \nu} \quad (3.21)$$

This is the *trajectory equation* expressed in polar coordinates and, in order to determine what kind of curve it represents, the general equation of a conic section needs to be recalled:

$$r = \frac{p}{1 + e \cos \nu} \quad (3.22)$$

That is mathematically equivalent to the trajectory equation. Three quantities need to be specified: p is a geometrical constant of the conic that takes the name of *semilatus rectum*, e is the *eccentricity*, a property that determines which type of conic we are taking into account and ν is the *true anomaly*, that indicates the point along the trajectory occupied by the smaller body, while the larger one is located in one of the two foci. An overview is reported in Figure 3.5, in which the two crosses represent the ellipse's foci.

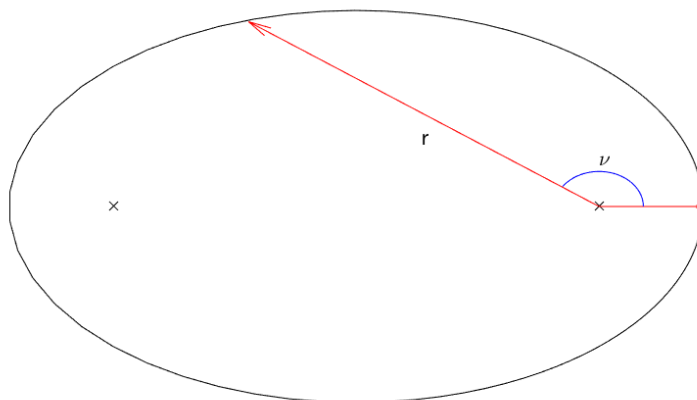


Figure 3.5: **Simplified representation of an elliptical orbit**

3.4.1 The conic sections

These particular curves derive by the intersection of a plane and a right circular cone. If the plane cuts entirely an half cone, the resulting curve will be an *ellipse*, while a *circle* is generated if the plane is parallel to the cone's base; the *parabola* is the result of an inclination of the plane equal to that of the cone's surface and the *hyperbola* is given when the plane cuts both of the half cones.

For the circle, the two foci are considered coincident, so that their half-distance $c = 0$, for the ellipse $c > 0$, for the parabola $c \rightarrow \infty$ and for the hyperbola $c < 0$.

It follows that, for any conic, the *eccentricity* can be defined as:

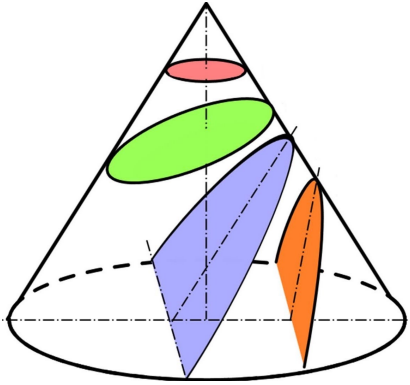
$$e = \frac{c}{a} \quad (3.23)$$

And the *semilatus rectum*:

$$p = a(1 + e^2) \quad (3.24)$$

Or

$$p = \frac{h^2}{\mu} \quad (3.25)$$



Curve	Eccentricity	Semi-major axis
Circle	$e = 0$	$a = \text{radius}$
Ellipse	$0 < e < 1$	$a > 0$
Parabola	$e = 1$	$a \rightarrow \infty$
Hyperbola	$e > 1$	$a < 0$

It is useful now to recall the definitions of periapsis and apoapsis, in order to further investigate their meaning: the *periapsis* r_p is defined as the point of minimum distance from the larger body and the *apoapsis* r_a as the farthest. While, for an elliptical orbit these two points are separated and easy to recognize, for a circular path they cannot be determined. It is possible to relate these two properties to the *true anomaly* ν by means of the following relations:

$$r_p = a(1 - e) = \frac{p}{1 + e \cos 0^\circ} \quad (3.26)$$

$$r_a = a(1 + e) = \frac{p}{1 + e \cos 180^\circ} \quad (3.27)$$

When deriving the trajectory equation, we introduced the *constant vector of integration* \vec{B} , pointing towards the periapsis, and by comparing this relation with the general equation of a conic section, it is easy to conclude that $B = \mu e$. If we recall Equation 3.18:

$$\vec{r} \times \vec{h} = \mu \frac{\vec{r}}{r} + \vec{B}$$

And we solve it for \vec{B} , what we obtain is:

$$\vec{B} = \vec{v} \times \vec{h} - \mu \frac{\vec{r}}{r} \quad (3.28)$$

Hence:

$$\vec{e} = \frac{\vec{v} \times \vec{h}}{\mu} - \frac{\vec{r}}{r} \quad (3.29)$$

If we now substitute \vec{h} with $\vec{r} \times \vec{v}$:

$$\mu \vec{e} = \vec{v} \times (\vec{r} \times \vec{v}) - \mu \frac{\vec{r}}{r} \quad (3.30)$$

That, if the triple product is solved and v^2 is substituted to $\vec{v} \cdot \vec{v}$, states:

$$\vec{e} = \frac{1}{\mu} \left[\left(v^2 - \frac{\mu}{r} \right) \vec{r} - (\vec{r} \cdot \vec{v}) \vec{v} \right] \quad (3.31)$$

This is the *eccentricity vector*: directed towards the periapsis and whose modulus is equivalent to the orbit's eccentricity, that can assume any value from zero to infinity.

It is now useful to derive some expressions that allow to put into relation the energy of the orbit \mathcal{E} with the value of its semi-major axis a . In order to do that, it is necessary for us to recall the definition of energy:

$$\mathcal{E} = \frac{v^2}{2} - \frac{\mu}{r}$$

Furthermore, at the apoapsis and periapsis the position vector and the velocity vector are orthogonal and the flight path angle is null. This means that the angular momentum can be computed as follows:

$$h = r_p v_p = r_a v_a \quad (3.32)$$

So that, by substituting v^2 and focusing on the periapsis point, we obtain:

$$\mathcal{E} = \frac{h^2}{2r_p} - \frac{\mu}{r_p} \quad (3.33)$$

But, from Equation 3.26 and Equation 3.24, we already know that:

$$\begin{aligned} r_p &= a(1 - e) \\ p &= a(1 - e^2) \end{aligned}$$

So that we can derive the following expression for the angular momentum:

$$h^2 = \mu a(1 - e^2) \quad (3.34)$$

That can be substituted into the expression for \mathcal{E} :

$$\mathcal{E} = \frac{\mu a(1 - e^2)}{2a^2(1 - e^2)} - \frac{\mu}{a(1 - e)} \quad (3.35)$$

That reduces to:

$$\mathcal{E} = -\frac{\mu}{2a} \quad (3.36)$$

This relation, whose meaning is that the orbit's semi-major axis only depends on the spacecraft's specific mechanical energy, represented by the values of r and v in any point of the orbit, is valid for every conic orbit.

We already know that a is negative for circles and ellipses, null for parabolas and greater than zero for hyperbolas; this implies that the specific mechanical energy of a spacecraft is negative if it lies on a closed orbit, i.e. a circle or an ellipse, null for a parabola and possesses a positive value in case of an hyperbolic trajectory, so that its energy is sufficient to determine which type of orbit it is on.

It is now possible, by means of the relations just derived, to compute an expression for the eccentricity e , whose value determines the exact shape of a conic orbit. Solving Equation 3.24 for e lets us to obtain:

$$e = \sqrt{1 - \frac{p}{a}}$$

Recalling Equation 3.25 and Equation 3.36:

$$p = \frac{h^2}{\mu}$$

$$a = -\frac{\mu}{2\mathcal{E}}$$

So that, for a generic conic orbit, the eccentricity modulus can be calculated with the following expression:

$$e = \sqrt{1 + \frac{2\mathcal{E}h^2}{\mu^2}} \quad (3.37)$$

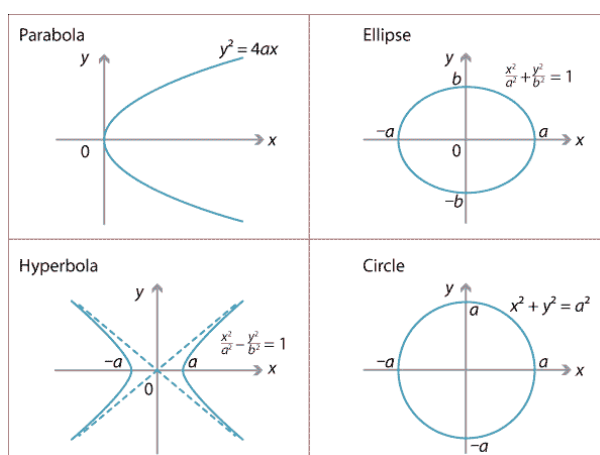


Figure 3.6: **The conic sections**

3.5 Keplerian orbits and orbital elements

What follows is an overview of the different types of orbits, in which the characteristics of every conic section, as well as the differences between them, will be recalled. This will allow us to introduce, at the end of this section, the six quantities that are known as *classical orbital parameters*.

3.5.1 Elliptical orbit

The figures drawn by the planets around the Sun are ellipses, and since the ellipse is a closed curve, this implies that all the Solar System's principal bodies travel on the same paths over and over again. At first, some simple, geometrical considerations need to be done.

For an ellipse, the apoapsis and periapsis distances are related to the value of the semi-major axis by the following law:

$$r_a + r_p = 2a \quad (3.38)$$

While the distance between the foci can be computed as:

$$r_a - r_p = 2c \quad (3.39)$$

And the eccentricity, according to its definition, can be written as:

$$e = \frac{c}{a} = \frac{r_a - r_p}{r_a + r_p} \quad (3.40)$$

As stated before, an ellipse is a closed curve, and the interval of time between two consecutive passes of the spacecraft upon the same location of the orbit can be computed. This takes the name of *orbital period* and only depends on the semi-major axis value:

$$T = 2\pi\sqrt{\frac{a^3}{\mu}} \quad (3.41)$$

Equation 3.41 can also be seen as a proof to Kepler's third law "*the square of the period is proportional to the cube of the mean distance*", due to the fact that the semi-major axis is the average between the apoapsis and periapsis distances.

3.5.2 Circular orbit

The circular orbit is just a particular eventuality of an elliptical path, in which the semi-major axis coincide with the radius, so that the apoapsis and periapsis are undefined. Regardless of this, the relations derived in the previous paragraph are still valid.

Adapting Equation 3.41 leads to:

$$T = 2\pi\sqrt{\frac{r^3}{\mu}} \quad (3.42)$$

In order for a spacecraft to maintain its circular path around a planet, it must possess a certain speed, which is called *circular velocity* v_c and whose value can be computed recalling the definition of specific mechanical energy:

$$\mathcal{E} = \frac{v^2}{2} - \frac{\mu}{r} = -\frac{\mu}{2a}$$

And, remembering that for a circular orbit $a = r$, it follows that:

$$\frac{v_c^2}{2} - \frac{\mu}{r} = -\frac{\mu}{2r}$$

That, solving for v_c , leads to:

$$v_c = \sqrt{\frac{\mu}{r}} \quad (3.43)$$

That implies that the greater the distance from the planet, the slower the spacecraft will move around it. Assuming Earth as the main body, for a spacecraft in LEO, $v_c \approx 7.5$ km/s, while the circular speed of the Moon on its orbit is roughly 1 km/s.

It is also possible to calculate the distance at which the circular speed of the spacecraft equals the circular speed on the surface, that is 1.67 km/s on the Equator for our planet. This peculiarity belongs to an altitude of 42168 km from the center of Earth, that correspond to 35790 km from its surface. The so-called *geosynchronous altitude* can be computed recalling Equation 3.42 and solving it for r :

$$r_{geos} = \sqrt[3]{\frac{\mu T_{rot}^2}{4\pi^2}}$$

That, by substituting $T_{rot} = 86164.09$ s and $\mu = 398600$ km³/s², leads to:

$$r_{geos} = 42168 \text{ km}$$

3.5.3 Parabolic orbit

The parabolic orbit is pretty rare in nature and it has been observed in the trajectories of some comets. It can be interpreted as the borderline case between open and closed paths, i.e. between hyperbolic trajectories and elliptical orbits.

Since for this kind of conic section the eccentricity is unitary, the periapsis distance can be easily computed as:

$$r_p = \frac{p}{2} \quad (3.44)$$

While the apoapsis cannot be determined, in fact, parabolas can be seen as infinitely long ellipses.

In connection with the parabolic orbits, it is useful to introduce the notion of *escape speed*, defined as that value of velocity that allows a body to reach an infinite distance from another, more massive, body, without falling back. This means that, as its distance from the main body increases, its speed decreases, thus approaching zero value when it is infinitely far away and the gravitational attraction can be considered null.

The escape speed can be computed using the mechanical energy definition, in particular by writing it for two different points along the parabolic escape trajectory:

$$\mathcal{E} = \frac{v_{esc}^2}{2} - \frac{\mu}{r} = \frac{v_{\infty}^2}{2} - \frac{\mu}{r_{\infty}}$$

But the third term can be completely neglected, because we suppose that $v_{\infty} \rightarrow 0$ and $r_{\infty} \rightarrow \infty$. It follows that:

$$\mathcal{E} = \frac{v_{esc}^2}{2} - \frac{\mu}{r} = 0$$

Hence, solving for v_{esc} :

$$v_{esc} = \sqrt{2\frac{\mu}{r}} = \sqrt{2}v_c \quad (3.45)$$

Which means that the velocity the spacecraft needs to reach to escape is $\sqrt{2}$ times the circular speed that competes to an orbit at the same altitude.

3.5.4 Hyperbolic orbit

This kind of path is typically assumed by the space probes during their interplanetary journey, this because it is necessary for them to escape the main body's gravitational attraction with some extra speed. This quantity takes the name of *hyperbolic excess velocity* v_{∞} and can be computed by recalling the definition of specific mechanical energy. In particular, its expression can be written for two points along the trajectory:

$$\mathcal{E} = \frac{v^2}{2} - \frac{\mu}{r} = \frac{v_{\infty}^2}{2} - \frac{\mu}{r_{\infty}}$$

Where $r_{\infty} \rightarrow \infty$, hence:

$$v_{\infty}^2 = v^2 - 2\frac{\mu}{r}$$

But, by means of Equation 3.45, the hyperbolic excess velocity becomes:

$$v_{\infty} = \sqrt{v^2 - v_{esc}^2} \quad (3.46)$$

As illustrated in Figure 3.7, the two branches of the hyperbola possess two asymptotes that intersect in the origin, and the *turn angle* δ between them can be seen as the deviation experienced by the probe by means of its encounter with the planet. This quantity is defined as follows:

$$\sin \frac{\delta}{2} = \frac{a}{c} = e^{-1} \quad (3.47)$$

This implies that the greater the eccentricity, the smaller the turning angle will be.

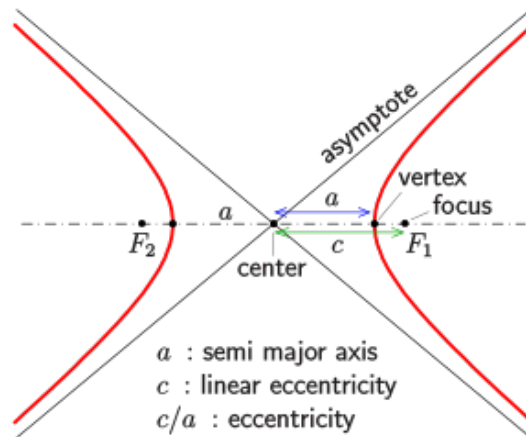


Figure 3.7: **Geometry of an hyperbola**

Another important parameter in the analysis of interplanetary flights is the square of v_∞ :

$$C_3 = v_\infty^2 \quad (3.48)$$

That, by recalling the definition of specific mechanical energy, leads to:

$$C_3 = 2\mathcal{E} \quad (3.49)$$

Where \mathcal{E} is the specific mechanical energy associated to the generic hyperbolic orbit.

3.5.5 Orbital parameters

The size, shape and orientation of an orbit can be univocally determined by means of five quantities, in combination with a sixth one that allows to pinpoint the position of the spacecraft on its path, that take the name of *classical orbital parameters*.

Assuming a generic inertial reference frame $T(X, Y, Z)$, the orbital parameters are:

1. the semi-major axis a , that defines the orbit's size and energy;
2. the eccentricity e , that defines the exact shape of the orbit
3. the inclination i , between the Z -axis and the direction of the angular momentum vector \vec{h} , that defines the orbit's inclination with respect to an arbitrary frame of reference;
4. the right ascension of the ascending node Ω , or *RAAN*, measured counterclockwise (as viewed from the North direction) between the X -axis and the point where the spacecraft crosses the fundamental plane with a northerly direction, i.e. the ascending node;
5. the argument of periapsis ω , measured in the spacecraft's orbital plane and in the direction of its motion, between the ascending node and the periapsis;
6. the true anomaly ν measured on the orbital plane between the periapsis and the position of the spacecraft along the orbit.

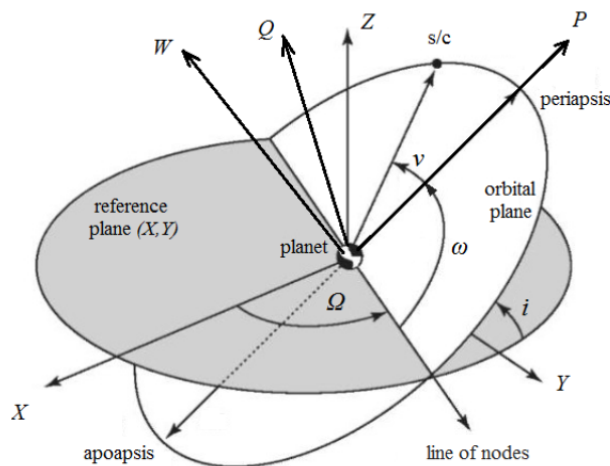


Figure 3.8: **Perifocal and inertial coordinate systems**

Obviously, the same quantities can be defined with respect to a heliocentric reference frame, in order to determine a planet's path around the Sun or a probe's interplanetary

trajectory.

Let now \hat{i} , \hat{j} and \hat{k} be the unit vectors of an inertial coordinate system, directed respectively in the direction of X , Y and Z -axes, as can be seen in Figure 3.8.

Since the inclination has been defined as the angle between the angular momentum vector \vec{h} and the Z -axis, this implies that i can be written as follows:

$$i = \arccos\left(\frac{\vec{h} \cdot \hat{k}}{h}\right) \quad (3.50)$$

Furthermore, in the case of a non-equatorial orbit, the orbital plane will intersect the reference plane $X - Y$ in two points that, depending on the direction of the spacecraft's motion, will be referred to as *ascending node* and *descending node*, or AN and DN . In particular, the ascending node will be the one for which the Z -component of velocity is greater than zero.

In relation to this, the *line of nodes* is defined as the one that joins AN with DN and its direction, \hat{N} , is the versor pointing from the origin towards the ascending node. By definition, \hat{N} is orthogonal with respect to both \vec{h} and \hat{k} , so that it can be computed as follows:

$$\hat{N} = \frac{\hat{k} \times \vec{h}}{\|\hat{k} \times \vec{h}\|} \quad (3.51)$$

We defined the right ascension of the ascending node as the angle between the X -axis and the line of nodes, so that it can be written as:

$$\begin{cases} \Omega = \arccos(\hat{i} \cdot \hat{N}) & \text{if } \hat{N} \cdot \hat{j} > 0 \\ \Omega = 2\pi - \arccos(\hat{i} \cdot \hat{N}) & \text{if } \hat{N} \cdot \hat{j} < 0 \end{cases} \quad (3.52)$$

For what concerns the argument of periapsis, instead, ω is the angle between the line of nodes and the position of periapsis. Therefore, its expression is:

$$\begin{cases} \omega = \arccos(\hat{e} \cdot \hat{N}) & \text{if } \vec{r} \cdot \vec{v} > 0 \\ \omega = 2\pi - \arccos(\hat{e} \cdot \hat{N}) & \text{if } \vec{r} \cdot \vec{v} < 0 \end{cases} \quad (3.53)$$

Where the eccentricity versor is computed as follows:

$$\hat{e} = \frac{\vec{e}}{e} \quad (3.54)$$

Similarly, the true anomaly can be expressed by means of the following relation:

$$\begin{cases} \nu = \arccos(\hat{e} \cdot \hat{r}) & \text{if } \vec{r} \cdot \vec{v} > 0 \\ \nu = 2\pi - \arccos(\hat{e} \cdot \hat{r}) & \text{if } \vec{r} \cdot \vec{v} < 0 \end{cases} \quad (3.55)$$

It is now useful to introduce a classification of the orbits based on their inclination value:

- a *direct orbit* is characterized by an inclination $0 < i < \pi/2$, so that the spacecraft's direction is the same in which the planets revolve around the Sun;
- a *retrograde orbit* is the opposite of a direct one, meaning that $\pi/2 < i < \pi$;
- a *polar orbit* is characterized by an $i = \pi/2$;
- an *equatorial orbit* can be identified when $i = 0$ or $i = \pi$.

3.5.6 Determination of position and velocity vectors from the orbital parameters

In the previous chapter, more precisely in *Section 1.1.6*, we introduced a frame of reference that is particularly useful when a spacecraft's motion through space has to be described: the *Perifocal coordinate system*.

In order to determine the future position of a satellite along its orbit, we should be able to derive its position and velocity vectors once the six orbital parameters are known.

The Perifocal frame of reference is particularly useful because of the simple expressions assumed by the two vectors of interest with respect to it. In fact, both of them possess only two non-zero components:

$$\vec{r}_P = \begin{bmatrix} r_\rho \\ r_\theta \\ 0 \end{bmatrix} = \begin{bmatrix} r \cos \nu \\ r \sin \nu \\ 0 \end{bmatrix} \quad (3.56)$$

And

$$\vec{v}_P = \begin{bmatrix} v_\rho \\ v_\theta \\ 0 \end{bmatrix} = \begin{bmatrix} \dot{r} \\ r\dot{\nu} \\ 0 \end{bmatrix} \quad (3.57)$$

That, by recalling Equation 3.22, leads to:

$$\vec{r}_P = \begin{bmatrix} \frac{p \cos \nu}{1+e \cos \nu} \\ \frac{p \sin \nu}{1+e \cos \nu} \\ 0 \end{bmatrix} \quad (3.58)$$

While, for what concerns the velocity vector, the following relation can be written:

$$\vec{v} = \vec{r}' = (\dot{r} \cos \nu - r\dot{\nu} \sin \nu)\vec{i} + (\dot{r} \sin \nu + r\dot{\nu} \cos \nu)\vec{j} \quad (3.59)$$

Now, noting that $h = r^2\dot{\nu}$ and $p = h^2/\mu$ and that by differentiating Equation 3.22 we obtain:

$$\dot{r} = \frac{\mu}{p}e \sin \nu \quad (3.60)$$

And

$$r\dot{\nu} = \frac{\mu}{p}(1 + e \cos \nu) \quad (3.61)$$

The velocity vector can be expressed as follows:

$$\vec{r}_P = \begin{bmatrix} \frac{\mu}{p} e \sin \nu \\ \frac{\mu}{p}(1 + e \cos \nu) \\ 0 \end{bmatrix} \quad (3.62)$$

That allows to compute the two vectors of interest, once the orbital parameters are defined.

3.6 Trajectory analysis

The computation of a precise trajectory for an interplanetary probe is an issue that must be solved by means of a numerical integration of the complete equations of motion, so that all the perturbative gravitational effects can be taken into account.

Typically, the trajectory analysis consists of different phases, during which the level of precision grows up but that can take years of work to be completed.

However, during the preliminary design of a mission, it can be useful to rely on simplified methodologies that, by means of analytical techniques, allow to perform an estimation of the necessary ΔV and of the other parameters involved. The best available method for such an analysis takes the name of *patched conic approximation*.

3.6.1 The Patched Conic Approximation

This technique is based on the assumption that the spacecraft is considered under the gravitational influence of one body at a time and, in order to do this, the mission is split into a number of different phases, or legs, so that its motion can always be considered Keplerian. Furthermore, it is necessary to introduce the concept of *sphere of influence*, defined as the region of space in which the probe experiences the attraction of a single celestial body. This item will be subject to further deepening in the following subsection.

During each of the mission phases, the spacecraft is assumed to move along a conic, i.e. a Keplerian orbit, deriving from its interaction with one, major, celestial body. The departure point of one leg coincides with the arrival point of the previous leg, and these junction points between two mission segments are often located on the surface of the body's sphere of influence.

For example, an interplanetary mission from Earth to Mars can be divided into three phases:

1. A geocentric phase, during which the spacecraft escapes from Earth's sphere of influence upon a hyperbolic trajectory;

2. A heliocentric phase, in which an Hohmann transfer towards Mars is exploited;
3. An areocentric phase, that begins when the spacecraft enters Mars' sphere of influence, where a capture maneuver is performed.

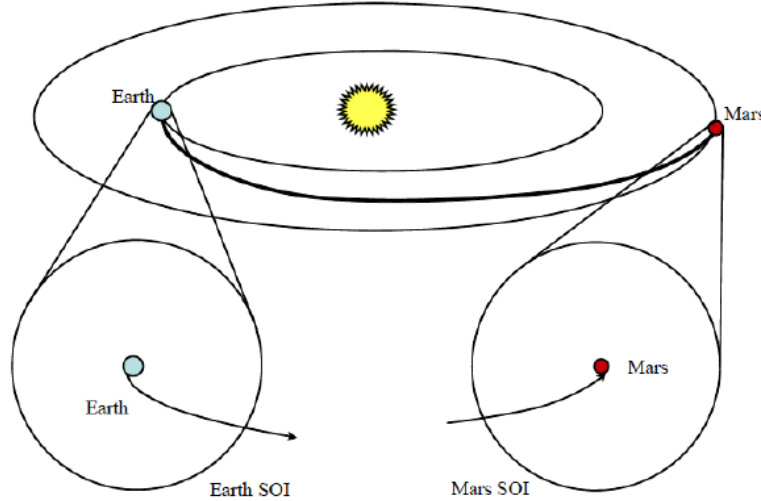


Figure 3.9: **Earth-Mars trajectory with the patched conics approximation**

The level of accuracy guaranteed by the use of this technique is quite high, especially if compared to the computational and economical cost required.

3.6.2 Sphere of influence

in the previous subsection we stated that the patched conic approximation relies on the concept of sphere of influence, that will be investigated through this paragraph.

It is obviously absurd to claim that a spacecraft needs to reach an infinite distance from a body in order to escape from its gravitational pull, so it is more useful to state that, beyond a certain distance, the attraction of that body can be neglected. This distance is defined as the radius of the sphere of influence and it is of major importance for the patched conic approximation, because it allows to compute the intersection points between two consecutive legs.

It is possible to calculate the radius of a body's sphere of influence by setting up an n-body problem in which $n=3$. In particular, there will be two main bodies m_1 and m_2 , with an additional mass represented by the spacecraft m_s . The acceleration experienced by the probe due to the presence of the two bodies can be computed as follows:

$$\vec{r}_{1s} = -G \frac{m_1 + m_s}{r_{1s}^3} \vec{r}_{1s} - G m_2 \left(\frac{\vec{r}_{2s}}{r_{2s}^3} - \frac{\vec{r}_{21}}{r_{21}^3} \right) \quad (3.63)$$

$$\vec{r}_{2s} = -G \frac{m_2 + m_s}{r_{2s}^3} \vec{r}_{2s} - Gm_1 \left(\frac{\vec{r}_{1s}}{r_{1s}^3} - \frac{\vec{r}_{12}}{r_{12}^3} \right) \quad (3.64)$$

Where, as we already know, the second term of both expressions can be split into two contributes:

- The first one represents the main acceleration experienced by m_s due to the presence of either m_1 or m_2 ;
- The second one can be assumed to be the perturbative acceleration that comes from the presence of m_2 in the first case and of m_1 in the second case.

A compact form can be written:

$$\vec{r}_{1s} = \vec{a}_{1s} + \vec{a}_{pert1} \quad (3.65)$$

$$\vec{r}_{2s} = \vec{a}_{2s} + \vec{a}_{pert2} \quad (3.66)$$

If we consider now m_1 as the principal body and m_2 as the perturbative body, the radius of m_1 's sphere of influence will be the value of r_{1s} that satisfies the following expression:

$$\frac{\|\vec{a}_{pert1}\|}{\|\vec{a}_{1s}\|} = \frac{\|\vec{a}_{pert2}\|}{\|\vec{a}_{2s}\|} \quad (3.67)$$

That can be approximated by means of Laplace's definition of sphere of influence. This states that the gravitational pull of a body m_1 perturbed by the presence of another body m_2 can be computed as follows:

$$R_{soi}(m_1, m_2) = r_{12} \left(\frac{m_1}{m_2} \right)^{2/5} \quad (3.68)$$

By means of this simple relation it is possible to calculate the radius of Earth's gravitational upon the perturbative effect of the Sun:

$$R_{soi}(Earth, Sun) = r_{Earth, Sun} \left(\frac{m_{Earth}}{m_{Sun}} \right)^{2/5} = 924600 \text{ km} \quad (3.69)$$

While, if we focus on the Moon under the perturbative presence of Earth itself:

$$R_{soi}(Moon, Earth) = r_{Moon, Earth} \left(\frac{m_{Moon}}{m_{Earth}} \right)^{2/5} = 66280 \text{ km} \quad (3.70)$$

3.7 Gravity Assist

As we already know, the gravitational attraction of a celestial body, for example a planet, can be exploited with the goal of increase or reduce a spacecraft's speed relative to the Sun. When the probe enters the planet's sphere of influence, a rotation of its velocity vector occurs, while its modulus remains unchanged with respect to the planet itself. This effect takes the name of *gravity assist* or *fly-by* and can be easily adapted to any pair of celestial bodies that can gravitationally interact.

Throughout this work, the two bodies of primary importance will be Earth and its natural satellite, the Moon, that orbits around the first on a path that is assumed to be circular. This Earth-relative motion can be exploited to boost the velocity of a spacecraft without requiring any propellant. In particular, when the spacecraft enters the Moon's sphere of influence, it follows a hyperbolic trajectory characterized by a hyperbolic excess of velocity that coincides with the probe's speed relative to the Moon itself.

By considering a reference frame with respect to which the Moon can be assumed stationary and by observing the phenomenon by an energetic point of view, it is possible to state that the spacecraft's kinetic energy increases until the periselenium, while its gravitational potential contribute decreases. After the point of closest approach to the Moon, during the outbound leg, the two contributes follows opposite trends during time. The probe eventually reaches the border of the Moon's sphere of influence with a velocity vector that possesses the same modulus it entered with, but with a different direction. An illustration of the maneuver is reported in Figure 3.10.

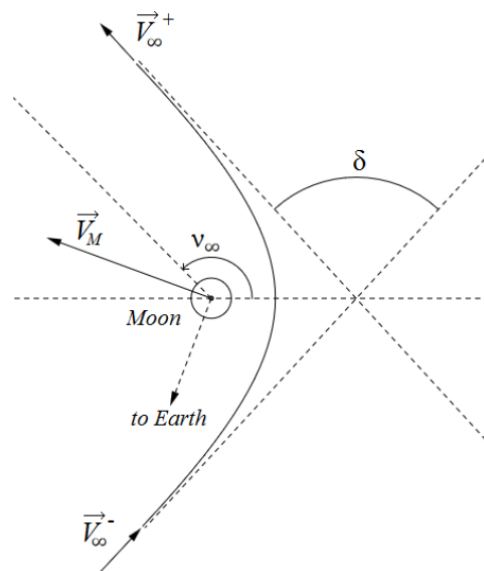


Figure 3.10: Geometry of a gravity assist

It is now useful to introduce two simplifying hypothesis:

- the Moon's sphere of influence is assumed dimensionless, so that the Moon-centered leg is neglected and the junction point between the two Earth-centered branches (before and after the gravity assist) coincides with the position of the Moon at the time of fly-by;
- the period of time necessary to complete the Moon-centered leg is neglected, so that the rotation of the relative velocity vector is assumed to occur instantaneously.

By means of these two assumptions, the gravity assist will be referred to as an impulsive variation of the absolute velocity vector of the spacecraft that occurs at a specific point in space and time.

3.7.1 Mathematical model of the Gravity Assist maneuver

This subsection is intended to lay down the mathematical foundations of the gravity assist, and particularly focusing on the LGA maneuver, which stands for Lunar Gravity Assist. In order to do this, two coordinate systems must be recalled:

- T_{GL} , the Geocentric Lunar reference frame;
- T_{ZEN} , centered in the position of the Moon at the time of fly-by, t_{fb} , that coincides with the position of the spacecraft at the same instant.

Furthermore, it will be useful to distinguish the pre fly-by orbit, that will be referred to as O^- , from the post fly-by path, identified by O^+ . The Moon is assumed to follow a circular path around Earth, so that its orbital velocity \vec{V}_M remains constant and perpendicular to the line joining the centers of Earth and Moon. For what concerns the spacecraft, its Earth-relative velocity vector before and after the gravity assist are, respectively, \vec{V}^- and \vec{V}^+ , while the same vectors can be written as \vec{V}_∞^- and \vec{V}_∞^+ , with respect to the Moon. Where the ∞ subscript is due to the fact that the Moon-relative velocity vectors can be seen as hyperbolic excess velocities.

As a consequence of what has just been reported, the following relation is valid:

$$\vec{V}_\infty^\pm = \vec{V}^\pm - \vec{V}_M \quad (3.71)$$

It is now convenient to adopt the ZEN reference frame to express the velocity components because, with respect to it, the fly-by event necessarily occurs in either the ascending or the descending node of the O^- and O^+ orbits. The components are:

$$(\vec{V}_M)_{ZEN} = \begin{bmatrix} 0 \\ v_M \\ 0 \end{bmatrix} \quad (\vec{V}^\pm)_{ZEN} = \begin{bmatrix} u^\pm \\ v^\pm \\ w^\pm \end{bmatrix} \quad (\vec{V}_\infty^\pm)_{ZEN} = \begin{bmatrix} u_\infty^\pm \\ v_\infty^\pm \\ w_\infty^\pm \end{bmatrix}$$

Where p , e , μ and i are, respectively, the semilatus rectum, eccentricity, true anomaly at fly-by and inclination of the two orbits O^- and O^+ .

By means of Equation 3.71, it simply follows that:

$$(\vec{V}_\infty^-)_{ZEN} = \begin{bmatrix} \sqrt{\frac{\mu}{p^-}} e^- \sin \nu_{fb}^- \\ \sqrt{\frac{\mu}{p^-}} (1 + e^- \cos \nu_{fb}^-) \cos i^- - v_M \\ \pm \sqrt{\frac{\mu}{p^-}} (1 + e^- \cos \nu_{fb}^-) \sin i^- \end{bmatrix}$$

$$(\vec{V}_\infty^+)_{ZEN} = \begin{bmatrix} \sqrt{\frac{\mu}{p^+}} e^+ \sin \nu_{fb}^+ \\ \sqrt{\frac{\mu}{p^+}} (1 + e^+ \cos \nu_{fb}^+) \cos i^+ - v_m \\ \pm \sqrt{\frac{\mu}{p^+}} (1 + e^+ \cos \nu_{fb}^+) \sin i^+ \end{bmatrix}$$

In the third component, the + subscript is used in case of a fly-by in the ascending node, while – implies that the maneuver is performed in the descending node.

3.7.2 Pump and crank angles

The geometry of the gravity assist can be determined by means of two characteristic angles: the *pump angle* P and the *crank angle* C , whose value depends on the mutual orientation of the two vectors \vec{V}_∞ and \vec{V}_M . The geometry is reported in Figure 3.12.

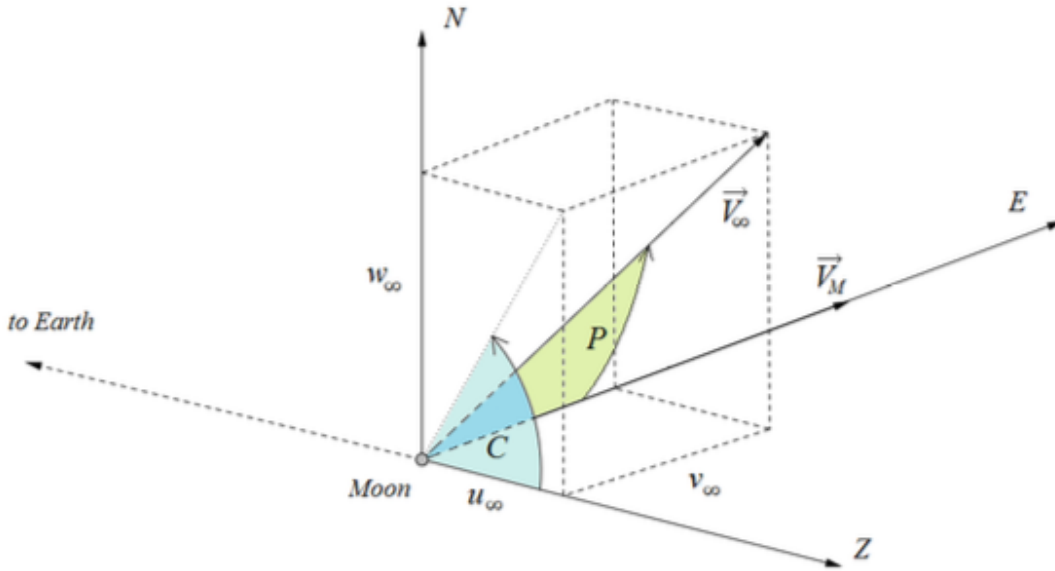


Figure 3.12: Pump and crank angles

The pump angle is defined as that between the two vectors \vec{V}_M and \vec{V}_∞ , while the crank

angle is identified as the inclination between these two vectors and the Moon's orbital plane. Their expressions are the following ones:

$$P = \arccos\left(\frac{\vec{V}_\infty \cdot \vec{V}_M}{\|\vec{V}_\infty\| \|\vec{V}_M\|}\right) \in [0; \pi] \quad (3.73)$$

And

$$C = \begin{cases} \arccos\left(\frac{u_\infty}{\sqrt{u_\infty^2 + w_\infty^2}}\right) & \text{if } w_\infty > 0 \\ \arccos\left(\frac{u_\infty}{\sqrt{u_\infty^2 + w_\infty^2}}\right) & \text{if } w_\infty < 0 \end{cases} \in [-\pi; +\pi] \quad (3.74)$$

However, these two quantities can be expressed in more compact forms, that are:

$$P = \arccos\left(\frac{v_\infty}{V_M}\right) \quad (3.75)$$

And

$$C = \arctan 2(w_\infty, u_\infty) \quad (3.76)$$

Due to the fact that the pump and crank angles can be defined for O^- and O^+ , it is possible to introduce their values: P^- , P^+ , C^- and C^+ . Furthermore, the gravity assist causes a variation of these four quantities and their delta is a key parameter of the phenomenon:

$$\Delta P = P^+ - P^-$$

$$\Delta C = C^+ - C^-$$

Where ΔP is related to the energy exchange that occurs during the fly-by event between the two bodies, and ΔC tells us information about the variation of inclination experienced by the spacecraft's orbit. As a consequence, a fly-by where $\Delta P \neq 0$ and $\Delta C = 0$ will be characterized only by a variation of the probe's energy, while the inclination remains unchanged and viceversa.

Furthermore, it must be noted that the spacecraft's energy is increased if $\Delta P < 0$; in other words, the energy increases if the pump angle is reduced by the gravity assist.

3.7.3 Turn angle

The turn angle is defined as that between the two vectors \vec{V}_∞^- and \vec{V}_∞^+ , in other words the angle between the asymptotes of the Moon-relative hyperbola. It can be expressed as follows:

$$\delta = \arccos\left(\frac{\vec{V}_\infty^+ \cdot \vec{V}_\infty^-}{\|\vec{V}_\infty^+\| \|\vec{V}_\infty^-\|}\right) \in [0; \pi] \quad (3.77)$$

Despite what Equation 3.77 states, δ is limited by the magnitude of V_∞ and by the radius of the major body, so that the actual range can be more precisely expressed by $[0, \delta_{max}]$, where $\delta_{max} = f(r, V_\infty)$.

An expression for δ_{max} can be computed by recalling the conic sections equation:

$$r = \frac{p}{1 + e \cos \nu} \quad \rightarrow \quad \nu = \arccos\left(\frac{p-r}{er}\right)$$

Where p and e are those of the hyperbolic trajectory followed by the spacecraft. By considering the true anomaly at infinite distance from the Moon, denoted as ν_∞ , one can write:

$$\nu_\infty = \lim_{r \rightarrow \infty} \nu = \arccos\left(-\frac{1}{e}\right)$$

Where, by operating simple geometric considerations on Figure 3.10, it is possible to state that $\nu_\infty = \delta/2 + \pi/2$, so that:

$$\sin\left(\frac{\delta}{2}\right) = \sin\left(\nu_\infty - \frac{\pi}{2}\right) = -\cos \nu_\infty = \frac{1}{e} \quad (3.78)$$

And, by means of the definitions of periapsis and hyperbolic excess of velocity, the following relation is valid:

$$r_p = \frac{\mu_M}{V_\infty^2}(e - 1) \quad (3.79)$$

Now, in order to avoid the impact with the surface of the Moon, r_p must necessarily be greater than the Moon's radius R_M . Hence:

$$\frac{\mu_M}{V_\infty^2}(e - 1) > R_M \quad (3.80)$$

So that:

$$e_{min} = 1 + R_M \frac{V_\infty^2}{\mu_M} \quad (3.81)$$

Now, by using of Equation 3.78 and Equation 3.81, it is possible to derive a relation for the maximum admissible turn angle:

$$\delta_{max} = 2 \arcsin\left(\frac{1}{1 + R_M \frac{V_\infty^2}{\mu_M}}\right) \quad (3.82)$$

The ΔV resulting from the gravity assist is strictly connected with the turn angle δ . By observing Figure 3.13, in which we assumed as coplanar the three velocity vectors \vec{V}_∞^- , \vec{V}_∞^+ and \vec{V}_M , it is possible to relate δ to ΔV , in fact:

$$\Delta V = 2V_\infty \sin\left(\frac{\delta}{2}\right) \quad (3.83)$$

This relation does not depend on the mutual orientation of the vectors previously mentioned. Furthermore, by using Equation 3.82, it is possible to evaluate the ΔV_{max} :

$$\Delta V_{max} = \frac{2V_{\infty}}{1 + R_M \frac{V_{\infty}^2}{\mu_M}} \quad (3.84)$$

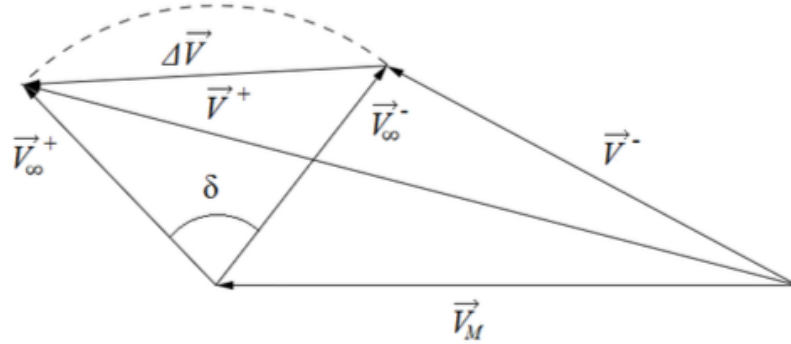


Figure 3.13: Turn angle and ΔV

3.8 Canonical Units

Nowadays, astronomers are still unable to calculate with sufficient approximation the masses and distances of objects in space. Such quantities, among which, for example, there are the mean Earth-Sun and Earth-Moon distances and these bodies' masses, are not precisely known yet, even though they are of primary importance in mission analysis. This issue can be avoided by simply normalizing all the mathematical quantities that appear in the equations with the unknown constants. For example, Earth's mass could be referred to as *1 mass unit*, while its distance from the Sun could take the name of *1 astronomical unit*. This normalized system of units is known in astronomy as *Canonical Units*.

Throughout this work, three main systems of units will be used, which are:

1. Standard Metric Units;
2. Solar Canonical Units;
3. Terrestrial Canonical Units.

3.8.1 Standard Metric Units

This set adopts the kilometer for the distance quantities and the second for the time quantities, so that the speed is evaluated in kilometers per second.

The parameters involved, which will be later used to define the Solar and Terrestrial Canonical Units, are: the mean Earth radius R_E , the mean Earth-Sun distance r_E , the Earth gravitational parameter μ_E and the Sun gravitational parameter μ_S . Their value is reported below:

$$R_E = 6378.1363 \text{ km}$$

$$r_E = 1.49597870691 \cdot 10^8 \text{ km}$$

$$\mu_E = 3.9860044150 \cdot 10^5 \text{ km}^3/\text{s}^2$$

$$\mu_S = 1.32712440018 \cdot 10^{11} \text{ km}^3/\text{s}^2$$

Where the gravitational parameter of a generic celestial body with mass M can be computed, as we already know, as:

$$\mu = GM$$

And G is the gravitational universal constant:

$$G = 6.67408 \cdot 10^{-11} \text{ m}^3/(\text{kg} \cdot \text{s}^2)$$

3.8.2 Solar Canonical Units

This metric system is based on two of the parameters introduced before: the gravitational parameter of the Sun and the Earth-Sun distance. In particular, the latter takes the name of *astronomical unit* and it has been defined as the distance unit, so that:

$$1DU_S = r_E$$

In Solar Canonical Units, the gravitational parameter of the Sun is defined to be unitary:

$$\mu_S = \frac{1DU_S^3}{1TU_S^2}$$

By means of the two previous expressions it is possible to derive a relation for the time unit:

$$1TU_S = \sqrt{\frac{r_E^3}{\mu_S}}$$

While the velocity unit can be computed by simply dividing the distance unit by the time unit:

$$1VU_S = \frac{1DU_S}{1TU_S}$$

It has to be noted that the velocity unit is defined so that it represents the circular velocity of a body orbiting the Sun at a distance equal to r_E . In fact:

$$1VU_S = \sqrt{\frac{r_E}{\frac{r_E^3}{\mu_S}}} = \sqrt{\frac{\mu_S}{r_E}} = v_c$$

By means of the previous expressions, the Solar Canonical Units can be evaluated and so the conversions with respect to the Standard Metric Units:

$$1DU_S = 1.49597870691 \cdot 10^8 \text{ km}$$

$$1TU_S = 5.0226 \cdot 10^6 \text{ s} \approx 58.13 \text{ days}$$

$$1VU_S = 29.7856 \text{ km/s}$$

3.8.3 Terrestrial Canonical Units

This metric system is based on the other two parameters introduced before: the gravitational parameter of Earth and its mean radius.

In this case, the distance unit coincides with the second one:

$$1DU_E = R_E$$

In Terrestrial Canonical Units, the gravitational parameter of Earth is defined to be unitary:

$$\mu_E = \frac{1DU_E^3}{1TU_E^2}$$

By means of the two previous expressions it is possible to derive a relation for the time unit:

$$1TU_E = \sqrt{\frac{R_E^3}{\mu_E}}$$

While the velocity unit can be computed by simply dividing the distance unit by the time unit:

$$1VU_E = \frac{1DU_E}{1TU_E}$$

It has to be noted that the velocity unit is defined so that it represents the circular velocity of a body orbiting Earth at a distance equal to R_E . In fact:

$$1VU_E = \sqrt{\frac{R_E}{\frac{R_E^3}{\mu_R}}} = \sqrt{\frac{\mu_R}{R_E}} = v_c$$

By means of the previous expressions, the Terrestrial Canonical Units can be evaluated and so the conversions with respect to the Standard Metric Units:

$$1DU_E = 6378.1363 \text{ km}$$

$$1TU_E = 806.78 \text{ s}$$

$$1VU_E = 7.9056 \text{ km/s}$$

Chapter 4

Analysis

This chapter is intended to present the feasible mission scenarios that, by exploiting one or more Lunar Gravity Assists, allow to reach the border of Earth's sphere of influence. As explained in the previous chapter, it is possible to perform trustworthy and relatively simple calculations in a small amount of time by means of the Patched Conic Approximation. This technique, adopted throughout this work, is based on the hypothesis of Keplerian motion.

4.1 Mission scenarios

As previously stated, the primary goal of this work is to carry out an optimization process of a spacecraft's escape trajectory that will eventually rendezvous with an asteroid in heliocentric orbit. Furthermore, due to the fact that the motion of the Moon around Earth affects the outcome of the gravity assist in terms of the O^+ orbital parameters, the launch date needs to be precisely programmed so that the payload mass that will eventually reach the asteroid results maximized.

The inputs of the analysis, that depends on the designed target asteroid, are:

- the time of escape t_{esc} , defined as the instant at which the spacecraft reaches the edge of Earth's sphere of influence;
- the hyperbolic excess of velocity V_{esc} of the probe, with respect to Earth, at t_{esc} .

Earth's path around the Sun implies that the trajectory the spacecraft will follow after t_{esc} , i.e. in the interplanetary space, will be characterized by a Sun-relative velocity $\vec{V}_{esc} + \vec{V}_E$, where V_E is Earth's orbital velocity around the Sun.

In order to introduce the feasible scenarios, it is convenient to split the escape trajectory into different legs by means of the Patched Conic Approximation, so that every single step of the mission can be subject to the optimization process. For the sake of simplicity, in this work the launch phase will not be analyzed; in fact, it will be supposed that the

spacecraft will depart for its mission from a Low Earth Orbit. Three fundamental steps can be identified: the *departure leg*, the *intermediate leg* and the *escape leg*.

The departure leg

This branch lies between the perigee of the low Earth parking orbit and the position of the Moon at the time of fly-by, due to the fact that in the introduction of *Chapter 3.7* we considered the gravity assist to take place instantaneously. It will be referred to as *P-L transfer*, because it starts from the P point of the parking orbit and it ends in the L point, which stands for lunar encounter.

The necessary ΔV to put the spacecraft onto this Earth-Moon transfer orbit is a key parameter of the analysis and it is strictly connected to the payload mass capability of the launch vehicle.

After the LGA, depending on the scenario of interest, the spacecraft could either re-encounter the Moon for another speed boost (intermediate leg) or proceed towards the edge of Earth's sphere of influence (escape leg).

The intermediate leg

The intermediate leg is an Earth-centered Moon to Moon transfer orbit that will be referred to as *L-L transfer*. Two different cases are possible:

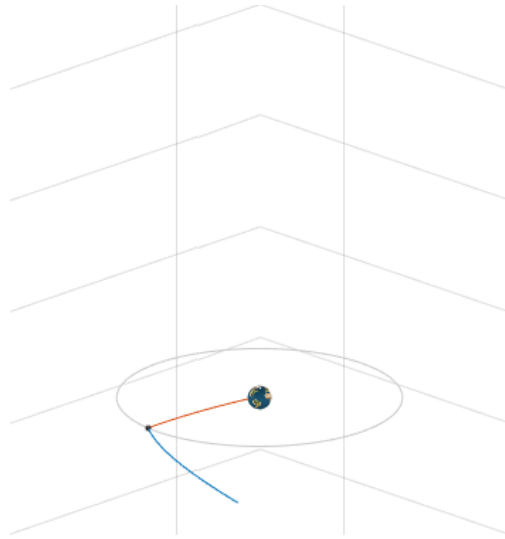
- *Resonant transfers*, in which the two fly-by events occur at the same point in space, meaning that these are closed orbits and that the interval of time between the two encounters is a multiple of the Moon's revolution period around Earth;
- *Non-resonant transfers*, characterized by the fact that the two gravity assists take place in different points of the Moon's orbit.

The escape leg

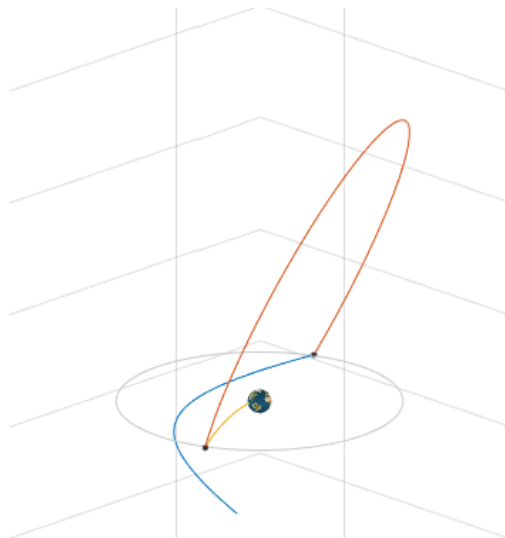
This path joins the point in which the last fly-by event occurs, designated by L, with the intersection point between the hyperbolic trajectory of the spacecraft and Earth's sphere of influence, defined as point E. It will be referred to as *L-E transfer* and it is such that the probe must reach E at t_{esc} with a velocity vector whose magnitude is V_{esc} .

Now that the mission phases have been described, it is possible to outline the different scenarios that will be taken into account during the optimization process. They are:

- **PLE scenario**, in which only one Lunar Gravity Assist is sufficient to provide the necessary ΔV to escape from Earth's gravitational attraction. This implies that the mission profile consists of only two phases: the departure leg and the escape leg.

Figure 4.1: **Example of a PLE scenario**

- **PLLE scenario**, that requires, in order to reach E, two gravity assist events, so that the total number of legs is three. At first, the departure leg takes the spacecraft from LEO to the Moon, where a close encounter puts the probe on an Earth-centered path that will reencounter the satellite in another point of its orbit. After the second LGA, a hyperbolic trajectory is followed until Earth's sphere of influence.

Figure 4.2: **Example of a PLLE scenario**

- **PLLEr scenario**, that is identical to the previous one, except for the fact that the first and the second fly-by occur at the same point in space, i.e. the L-L transfer is a closed orbit.

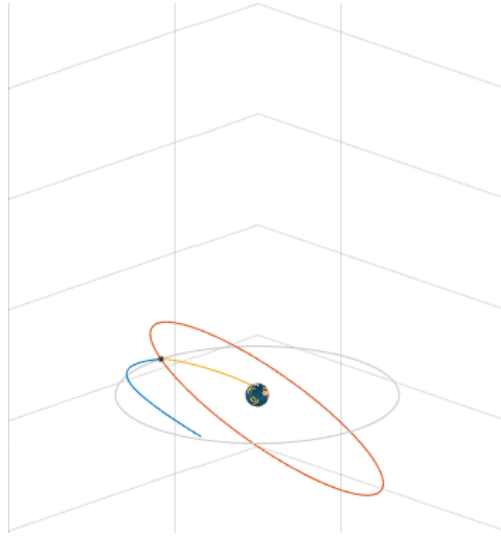


Figure 4.3: **Example of a resonant PLLE scenario**

4.2 Resolution method

The calculations are performed backwards in time, i.e the first branch to be evaluated will be the escape leg, due to the fact that the inputs relate to the spacecraft's motion at the end of the escape trajectory. Once the final section has been computed, depending on the scenario of interest, we will proceed with the P-L transfer (in the case of a PLE mission profile) or the L-L transfer (if two Moon encounters are needed).

Both for the P-L transfer and the L-L leg, a whole set of transfer orbits will be computed, but in order for these three branches to constitute a feasible trajectory, two geometrical hypothesis must necessarily be satisfied. The first one implies that the magnitude of the relative velocity vector cannot result changed by the fly-by event, so that:

$$|\vec{V}_{\infty}^{-}| = |\vec{V}_{\infty}^{+}| \quad (4.1)$$

The second one states that the turn angle δ must not exceed the maximum allowed value δ_{max} , as already defined in *Chapter 3.7.3*:

$$\delta < \delta_{max} \quad (4.2)$$

In the case of a multiple fly-by scenario, these two relations must obviously be satisfied both for the first and the second LGA.

4.3 Evaluation of the escape leg L-E

This section is intended to investigate the process that, departing from the inputs t_{esc} and V_{esc} , eventually allows to compute the values of the escape leg's orbital parameters,

that are: a_{le} , e_{le} , i_{le} , Ω_{le} , ω_{le} and $\nu_{fb,le}$. From now on, the "le" subscript will be neglected, but it will be implied that all the involved parameters are those of the escape leg L-E. All the calculations will be performed with respect to a Geocentric Lunar coordinate system $T_{GL}(X_{GL}, Y_{GL}, Z_{GL})$, but the results can be easily transformed into any other reference frame, such as the Geocentric Equatorial $T_{GE}(X_{GE}, Y_{GE}, Z_{GE})$.

4.3.1 Escape leg scenarios

As we already know since *Chapter 2*, the fundamental plane of T_{GL} coincides with the Moon's orbital plane, meaning that the last fly-by must necessarily occur in one of the nodes of the hyperbola.

This implies that the node at which the gravity assist maneuver occurs can be seen as the third input of the analysis, depending on which two different families of escape hyperbolas can be evaluated.

If we now introduce the unit vectors \hat{i}_{GL} , \hat{j}_{GL} and \hat{k}_{GL} in the direction of, respectively, X_{GL} , Y_{GL} and Z_{GL} , an additional distinction can be made: the Z_{GL} -component of V_{esc} , expressed by $\vec{V}_{esc} \cdot \hat{k}_{GL}$, can either be greater or smaller than zero.

These two possibilities, combined with the option of performing the fly-by in the ascending or descending node, allow to distinguish four different types of escape hyperbolas, defined as H_A^+ , H_A^- , H_D^+ and H_D^- and reported in Figure 4.4. For the sake of clarity, the subscript defines the node at which the fly-by occurs, while the superscript stands for the value of $\vec{V}_{esc} \cdot \hat{k}_{GL}$.

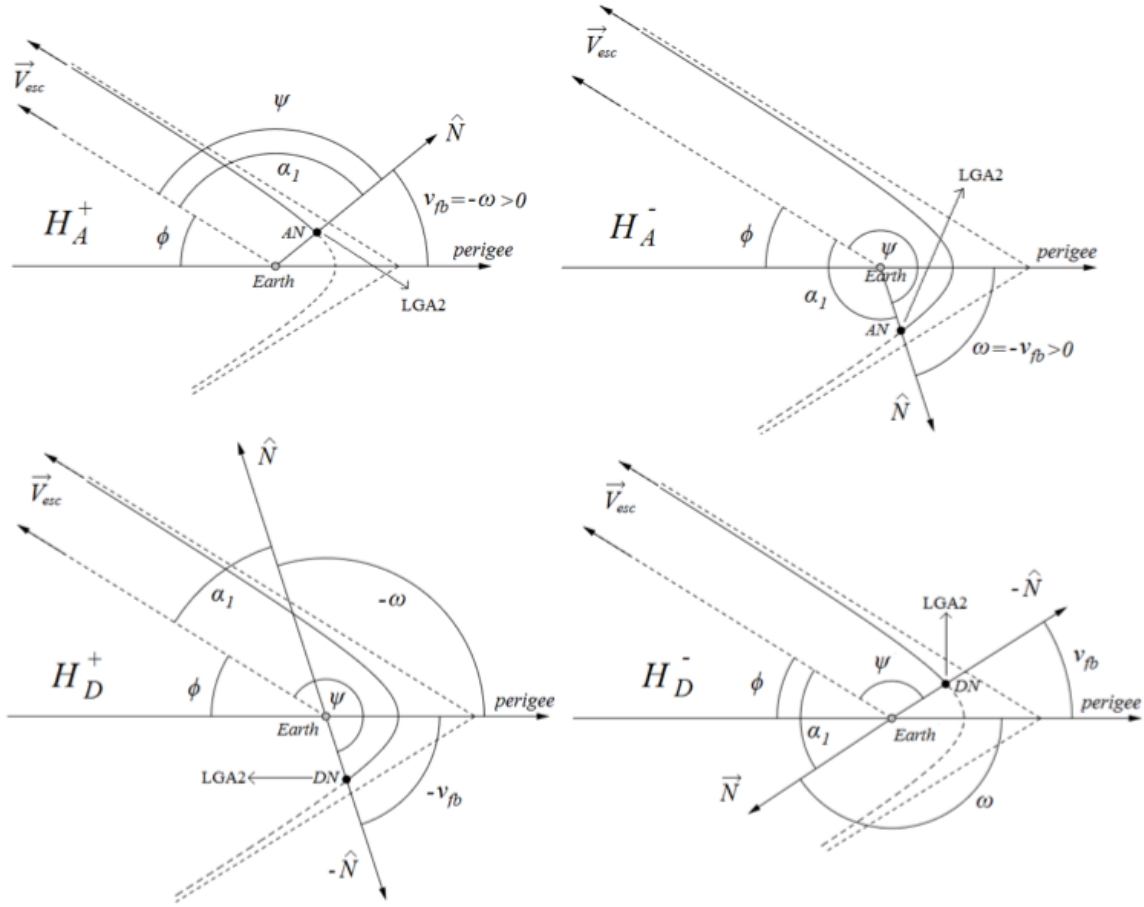


Figure 4.4: Different types of escape hyperbolas

In Figure 4.4, \hat{N} refers to the line of nodes and the angle between \hat{N} and \vec{V}_{esc} , identified as α_1 , can be expressed as follows:

$$\alpha_1 = \arccos\left(\frac{\vec{V}_{esc} \cdot \hat{N}}{\|\vec{V}_{esc}\| \|\hat{N}\|}\right) \in [0, \pi] \quad (4.3)$$

The line of nodes divides the orbital plane, on which the hyperbolic trajectory lies, into two regions: one that is above the fundamental plane (X_{GL}, Y_{GL}) and an other whose points are below it, so that they possess a component $Z_{GL} < 0$.

The angle ψ between $r(\nu_{fb})$ and $r(\nu_{\infty})$, where r is a vector joining the center of the Earth with the probe's position upon the hyperbolic trajectory, is swept by the spacecraft upon the escape leg and, in this case, ν_{fb} refers to the last fly-by event. Now, by simple geometrical considerations, it is easy to note that for H_A^+ and H_D^- , ψ must necessarily be smaller than π , while for H_A^- and H_D^+ , ψ needs to be larger than π , otherwise the constraints regarding the node at which the fly-by occurs and the sign of $\vec{V}_{esc} \cdot \hat{k}_{GL}$ would be violated. Table 4.1 summarises the properties of the four families.

Trajectory	Fly-by node	$\vec{V}_{esc} \cdot \hat{k}_{GL}$	ψ
\mathbf{H}_A^-	AN	<0	$>\pi$
\mathbf{H}_A^+	AN	>0	$<\pi$
\mathbf{H}_D^-	DN	<0	$<\pi$
\mathbf{H}_D^+	DN	>0	$>\pi$

Table 4.1: Overview of the feasible escape hyperbolas

4.3.2 Determination of the orbital parameters

In Figure 4.4, another characteristic angle, ϕ , is illustrated. It is defined as:

$$\phi = \pi - \nu_\infty = \arccos\left(\frac{1}{e}\right) \quad (4.4)$$

While the argument of periapsis can be expressed by the following relations:

$$\omega = \begin{cases} \phi + \alpha_1 - \pi & \text{if } \vec{V}_{esc} \cdot \hat{k}_{GL} < 0 \\ \phi - \alpha_1 + \pi & \text{if } \vec{V}_{esc} \cdot \hat{k}_{GL} > 0 \end{cases} \quad (4.5)$$

And the true anomaly at fly-by is:

$$\nu_{fb} = \begin{cases} -\omega & \text{if fb at AN} \\ -\omega + \pi & \text{if fb at DN} \end{cases} \quad (4.6)$$

Some more complicated calculations need to be performed in order to derive a value for the eccentricity e ; in fact, its value can be computed only if the angle α_1 is known, but it cannot be evaluated a priori. This means that an iterative process, whose principal steps will be briefly reported, needs to be carried out.

At first, as stated in Equation 4.3, it must be noted that α_1 is directly related to vector \hat{N} , expressible by means of the right ascension of the ascending node Ω . In fact:

$$\hat{N} = \begin{bmatrix} \cos \Omega \\ \sin \Omega \\ 0 \end{bmatrix} \quad (4.7)$$

This means that, in order for us to compute the eccentricity, a value for Ω , i.e. the position of the Moon at fly-by, needs to be found and this is the goal of the whole iterative process. The *RAAN* can be expressed as follows:

$$\Omega = \begin{cases} \alpha_M(t = t_{fb}) & \text{if fb at AN} \\ \alpha_M(t = t_{fb}) + \pi & \text{if fb at DN} \end{cases} \quad (4.8)$$

Where $\alpha_M(t = t_{fb})$ refers to the position of the Moon along its orbit at the time of the last fly-by, evaluated by means of a propagation algorithm based on ephemeris data.

However, t_{fb} is unknown because it depends on the time of flight of the escape leg tof_{le} . In fact:

$$t_{fb} = t_{esc} - tof_{le} \quad (4.9)$$

A first guess for the value of Ω must be chosen, so that the iterative process can start, and the best way to do it is to assume Ω_{start} as coincident with the angular position of the Moon at t_{esc} , so that:

$$\Omega_{start} = \begin{cases} \alpha_M(t_{esc}) & \text{if fb at AN} \\ \alpha_M(t_{esc}) + \pi & \text{if fb at DN} \end{cases} \quad (4.10)$$

This value allows us to calculate, by means of the previous expressions, in order: \hat{N} , α_1 , e , ϕ , ω and ν_{fb} . Once ν_{fb} is known, the time of flight on the escape hyperbola can be evaluated by means of Kepler's equation for hyperbolic orbits: an expression that puts into relation the time of flight with the semimajor axis a , the eccentricity e and the two values for the true anomaly ν_{fb} and ν_∞ :

$$tof_{le} = \sqrt{-a^3}[(e \sinh F_\infty - F_\infty) - (e \sinh F_{fb} - F_{fb})] \quad (4.11)$$

Where F_∞ and F_{fb} are, respectively, the hyperbolic eccentric anomalies relative to the true anomalies ν_∞ and ν_{fb} , defined as:

$$F = 2 \operatorname{arctanh}\left(\sqrt{\frac{e-1}{e+1}} \tan \frac{\nu}{2}\right) \quad (4.12)$$

It is now possible to determine t_{fb} and the position of the Moon at that instant of time $\alpha_M(t_{fb})$. For the following iteration, we need to assign a new value to Ω , hence:

$$\Omega_{new} = \begin{cases} \alpha_M(t_{fb}) & \text{if fb at AN} \\ \alpha_M(t_{fb}) + \pi & \text{if fb at DN} \end{cases} \quad (4.13)$$

While the error of each iteration can be computed as follows:

$$err = |\Omega_{new} - \Omega_{start}| \quad (4.14)$$

Where Ω_{start} is set equal to Ω_{new} at the end of each iteration. The whole process stops when err goes under a predetermined tolerance tol .

4.4 Evaluation of the intermediate leg L-L

This section is dedicated to an overview of the Moon-Moon transfer, that will eventually outline its orbital parameters: a_{ll} , e_{ll} , i_{ll} , Ω_{ll} , ω_{ll} , $\nu_{fb1,ll}$ and $\nu_{fb2,ll}$, due to the fact that this scenario involves two LGAs. From now on, the "ll" subscript will be neglected, but it will be implied that all the involved parameters are those of the intermediate leg L-L.

Also in this case, as we already did for the escape leg, the calculations will be made with respect to a Geocentric Lunar coordinate system $T_{GL}(X_{GL}, Y_{GL}, Z_{GL})$, but simple transformation matrices allow to obtain the same results in another frame of reference, for example the Geocentric Equatorial one $T_{GE}(X_{GE}, Y_{GE}, Z_{GE})$.

4.4.1 Resonant transfers

An L-L transfer orbit is considered to be resonant if the two fly-by events occur at the same point in space, in other words if the following relation is satisfied:

$$MT_u = NT_M \quad (4.15)$$

Where $T_u = tof_u$ and T_M are, respectively, the orbital periods of the intermediate leg and of the Moon's orbit around Earth and M, N two integers. This means that if the spacecraft is intended to follow a resonant transfer, it will complete M revolutions around Earth in the same amount of time required by the Moon to cover N of them.

By applying the definition of orbital period to Equation 4.15, it is easy to obtain:

$$M2\pi\sqrt{\frac{a^3}{1}} = N2\pi\sqrt{\frac{a_M^3}{1}} \quad (4.16)$$

Hence:

$$a = a_M\left(\frac{N}{M}\right)^{2/3} \quad (4.17)$$

Where Earth's gravitational parameter has been set as unitary because we are using the Terrestrial Canonical Units and a and a_M are the semimajor axes of, respectively, the L-L transfer and the Moon's orbit.

If we now introduce the angles α_{M1} and α_{M2} , representing the position of the Moon at the time of the two fly-bys then, necessarily:

$$\alpha_{M1} = \alpha_{M2} \quad (4.18)$$

4.4.2 Non resonant coplanar prograde transfers

This subsection is dedicated to the investigation of those transfers for which the spacecraft's angular momentum is parallel and concordant to that of the Moon, i.e. for which the orbit's inclination with respect to the fundamental plane (X_{GL}, Y_{GL}) is null.

A simplified representation of the involved geometry is reported in Figure 4.5.

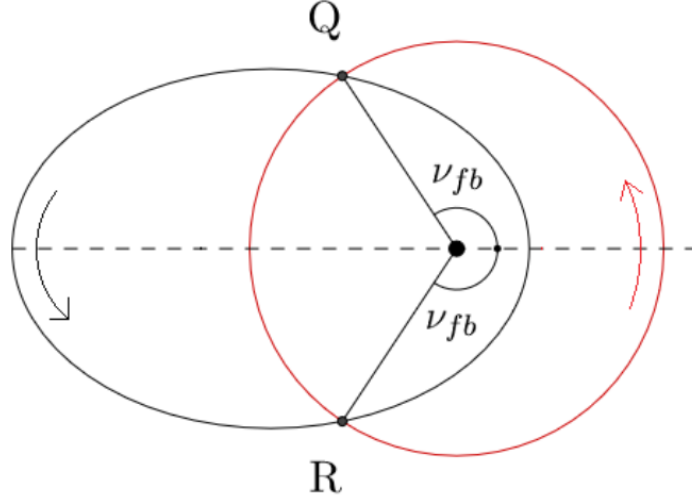


Figure 4.5: **Geometry of coplanar prograde transfers**

In Figure 4.5, the red circle represents the Moon's orbit, the black ellipse stands for the L-L transfer and their intersection points are defined as Q and R, that can be distinguished by introducing the *flight path angle* γ . This particular angle, defined as that between the local horizontal plane and the direction of the velocity, can be expressed as:

$$\gamma = \frac{\pi}{2} - \arccos\left(\frac{\vec{r} \cdot \vec{V}}{\|\vec{r}\| \|\vec{V}\|}\right) \in \left[-\frac{\pi}{2}, \frac{\pi}{2}\right] \quad (4.19)$$

We now assume to consider, due to limitations to the overall mission time, only those trajectory in which both the spacecraft and the Moon, between the two fly-by events, sweep angles that do not exceed 4π , or 720° .

Under this assumption, combined with the fact that the perturbation of the Sun is neglected, i.e. we consider only Keplerian orbits, just a few feasible trajectories can be outlined.

In particular, the transfer can either start at point R or Q, but the angles swept by both the Moon and the spacecraft can be greater or smaller than 2π : this means that only 8 possible combinations can be made. However, when it comes to reality, only four of them are actually feasible.

For example, the transfer that joins R to Q in which both the spacecraft and the Moon sweep an angle smaller than 2π is not physically possible. In fact, during this kind of intermediate leg, the Earth-Moon distance is always smaller than the Earth-spacecraft distance, so that the spacecraft's mean angular velocity would be greater than the Moon's, meaning that two consecutive encounters would be impossible.

The four feasible trajectories are described below and summarized in Table 4.2.

- **QR1 transfer**, in which the first fly-by occurs in point Q and the second in point R, while the angles swept by the spacecraft and the Moon are, respectively, smaller

than 2π and greater than 2π ;

- **QR2 transfer**, in which the first fly-by occurs in point Q and the second in point R, while the angles swept by the spacecraft and the Moon are both greater than 2π ;
- **RQ1 transfer**, in which the first fly-by occurs in point R and the second in point Q, while the angles swept by the spacecraft and the Moon are, respectively, greater than 2π and smaller than 2π ;
- **RQ2 transfer**, in which the first fly-by occurs in point R and the second in point Q, while the angles swept by the spacecraft and the Moon are both greater than 2π .

Transfer	LGA1	LGA2	Spacecraft angle	Moon angle
QR1	Q	R	$< 2\pi$	$> 2\pi$
QR2	Q	R	$> 2\pi$	$> 2\pi$
RQ1	R	Q	$> 2\pi$	$< 2\pi$
RQ2	R	Q	$> 2\pi$	$> 2\pi$

Table 4.2: Non resonant coplanar prograde intermediate transfers

4.4.3 Non resonant coplanar retrograde transfers

When the magnitude of the relative velocity vector at fly-by V_∞ is quite large and only direct transfers are taken into account, it is possible that no feasible trajectories can be found. In this particular case, coplanar retrograde transfers can be quite useful.

A simplified overview is reported in Figure 4.6, where the red circle represents the Moon's orbit around Earth, while the black ellipse stands for the spacecraft's trajectory. The intersection points are the same of the previous subsection, but in this case the spacecraft's angular momentum is parallel and discordant with respect to the Moon's.

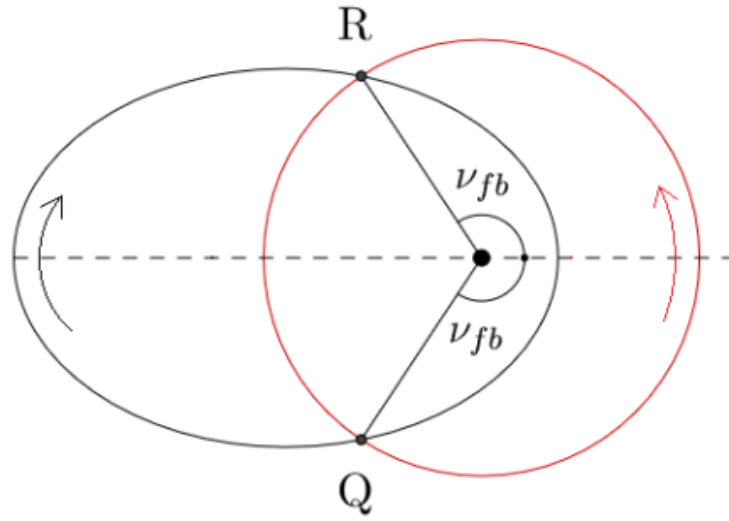


Figure 4.6: **Geometry of coplanar retrograde transfers**

We assume, also in this case, that the angles swept by both the spacecraft and the Moon are smaller than 4π , meaning that the time of flight upon the intermediate leg tof_u does not exceed $2T_M = 56$ days.

By means of this assumption, combined with the fact that the perturbation of the Sun is neglected, i.e. we consider only Keplerian orbits, just six feasible trajectories can be outlined. They are reported below.

- **QR1 transfers**, in which the first fly-by occurs in point Q and the second in point R, while the angles swept by the spacecraft and the Moon are both smaller than 2π ;
- **QR2 transfers**, in which the first fly-by occurs in point Q and the second in point R, while the angles swept by the spacecraft and the Moon are, respectively, smaller than 2π and greater than 2π ;
- **QR3 transfers**, in which the first fly-by occurs in point Q and the second in point R, while the angles swept by the spacecraft and the Moon are, respectively, greater than 2π and smaller than 2π ;
- **QR4 transfers**, in which the first fly-by occurs in point Q and the second in point R, while the angles swept by the spacecraft and the Moon are both greater than 2π ;
- **RQ1 transfers**, in which the first fly-by occurs in point R and the second in point Q, while the angles swept by the spacecraft and the Moon are both smaller than 2π ;

- **RQ2 transfers**, in which the first fly-by occurs in point R and the second in point Q, while the angles swept by the spacecraft and the Moon are both greater than 2π

The properties of every retrograde coplanar transfer are summarized in Table 4.4.

Transfer	LGA1	LGA2	Spacecraft angle	Moon angle
QR1	Q	R	$< 2\pi$	$< 2\pi$
QR2	Q	R	$< 2\pi$	$> 2\pi$
QR3	Q	R	$> 2\pi$	$< 2\pi$
QR4	Q	R	$> 2\pi$	$> 2\pi$
RQ1	R	Q	$< 2\pi$	$< 2\pi$
RQ2	R	Q	$> 2\pi$	$> 2\pi$

Table 4.3: Non resonant coplanar retrograde intermediate transfers

4.4.4 Non resonant non coplanar transfers

By making some simple geometrical considerations, it is possible to state that the semi-latus rectum p of this family of transfers must necessarily coincide with the radius of the Moon's orbit r_M and that the true anomalies at the fly-by events, $\nu_{fb1,2} = \pm \frac{\pi}{2}$. This is due to the fact that the intersection points between the L-L leg and the Moon's orbit lie on a straight line that crosses the center of the Earth. This configuration is reported in Figure 4.7.

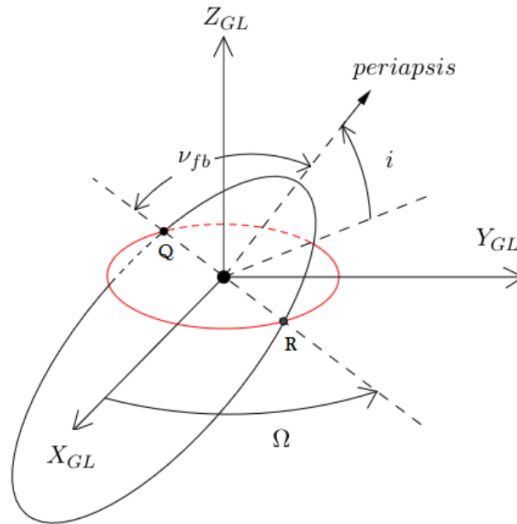


Figure 4.7: Geometry of non coplanar transfers

Also in this case we assume that, during the intermediate leg, both the spacecraft and the Moon sweep angles that do not exceed the value of 4π . This assumption, in combination

with the hypothesis of Keplerian motion, allows to identify a finite number of feasible trajectories: three, that are reported below.

- **QR transfer**, in which the first fly-by occurs in point Q and the second in point R, while the angles swept by the spacecraft and the Moon are, respectively, smaller than 2π and greater than 2π ;
- **RQ transfer**, in which the first fly-by occurs in point R and the second in point Q, while the angles swept by the spacecraft and the Moon are both greater than 2π ;
- **C transfer**, that is a circular orbit, identical to that of the Moon, but with a non zero inclination.

Transfer	LGA1	LGA2	Spacecraft angle	Moon angle
QR	Q	R	$< 2\pi$	$> 2\pi$
RQ	Q	R	$> 2\pi$	$> 2\pi$
C	-	-	$< 2\pi$	$< 2\pi$

Table 4.4: **Non resonant non coplanar intermediate transfers**

It has to be noted that for the *C transfer*, the Q and R points are equivalent since the flight path angle $\gamma = 0^\circ$ in any point of the orbit. Furthermore, the tof_u of the C transfer is equal to that of the Moon, due to the fact that they are both circular.

If we now consider all the prograde, retrograde and non coplanar L-L transfers, we come up with a total of thirteen different scenarios that can be exploited to escape Earth's gravitational attraction.

After the evaluation of the L-L transfer, the next step requires the optimization of the departure leg, to which the following section is dedicated.

4.5 Evaluation of the departure leg P-L

As stated in *Chapter 4.1*, the departure leg lies between the perigee of the parking orbit around Earth and the position of the Moon at the first Lunar encounter, i.e. between points P and L.

The optimization process takes into account a whole family of feasible departure trajectories, in order to find that particular P-L transfer that maximizes the payload mass at destination. Its orbital parameters are a_{pl} , e_{pl} , i_{pl} , Ω_{pl} , ω_{pl} and ν_{pl} , but throughout this section the "pl" subscript will be neglected and it will be implied that all the involved parameters are those of the departure leg.

The calculations will be performed with respect to a Geocentric Lunar coordinate system

$T_{GL}(X_{GL}, Y_{GL}, Z_{GL})$, but by means of simple transformation matrices, the results can be obtained also in another frame of reference, for example the Geocentric Equatorial $T_{GE}(X_{GE}, Y_{GE}, Z_{GE})$.

In order for the spacecraft to be put onto the P-L transfer, the propulsive system needs to provide a certain ΔV , that deeply affects the payload mass and that can be evaluated as follows:

$$\Delta \vec{V} = \vec{V}_p - \vec{V}_c \quad (4.20)$$

Where V_p is the magnitude of the spacecraft's velocity vector at the perigee of the P-L transfer, while V_c is the magnitude of the parking orbit's circular velocity.

Once r_p is known, V_p can be expressed by means of the eccentricity e :

$$V_p = v_\theta(\nu = 0) = \sqrt{\frac{1}{p}}(1 + e) = \sqrt{\frac{1 + e}{r_p}} \quad (4.21)$$

Where both e and V_p can be related to the inclination i and to the magnitude of the relative velocity vector at fly-by V_∞ : $e = f(i, V_\infty)$ and $V_p = f(i, V_\infty)$.

But once the inputs t_{esc} and V_{esc} are set and the node at which the fly-by occurs is fixed, the value for V_∞ can be also univokely identified.

4.6 Mass evaluation

As will be explained in *Chapter 5.1*, the best trajectories will be chosen by means of the maximum value of the destination mass, or m_{fin} , defined as the one that eventually reaches the target asteroid. During the interplanetary leg, i.e. after exiting Earth's sphere of influence, the spacecraft will exploit Solar Electric Propulsion, meaning that it will consume some additional propellant, thus resulting in $m_{fin} < m_{esc}$.

4.6.1 Mass at escape

The departure maneuver is supposed to be performed at the perigee of the parking orbit around Earth and, as stated in the previous section, the magnitude of the impulse can be expressed as:

$$\Delta V = V_p - V_c$$

Where $V_c = \sqrt{\frac{1}{r_p}}$ due to the fact that, by using the Terrestrial Canonical Units, Earth's gravitational parameter μ_E is assumed unitary. That, by using Equation 4.21, leads to:

$$\Delta V = \sqrt{\frac{1 + e_{pl}}{r_p}} - \sqrt{\frac{1}{r_p}} \quad (4.22)$$

The propulsive system of the spacecraft, in order to provide the necessary ΔV , must burn a certain mass of propellant that can be evaluated by means of the so-called *rocket equation*, also known as *Tsiolkovsky equation*. Its expression is:

$$\frac{m_f}{m_0} = e^{-\frac{\Delta V}{c}} \quad (4.23)$$

Where m_0 and m_f are, respectively, the probe's mass before and after the impulsive maneuver and c is the effective exhaust velocity of the propulsive system. By recombining the terms it is possible to evaluate the propellant mass:

$$m_p = m_0 - m_f = m_0[1 - e^{-\frac{\Delta V}{c}}] \quad (4.24)$$

However, the ΔV and, by direct consequence, the propellant mass and the payload mass, can also be related to the so-called launch azimuth angle Az , defined as that between the spacecraft's velocity vector at perigee and the North direction. Due to the fact that Earth revolves from West to East, launching eastward (so that $Az = 90^\circ$) will result in a minor propellant mass needed to put the spacecraft into orbit.

The launch vehicle is capable of putting into a Low Earth Orbit a total mass that can be written as:

$$m_{LEO} = m_{u,LEO} + m_{dry} \quad (4.25)$$

Where $m_{u,LEO}$ is the payload mass and m_{dry} takes into account the dry mass of the launch vehicle's upper stage. The first contribute can be expressed as a function of the azimuth angle by means of the following relation:

$$m_{u,LEO} = m_{u,LEO,Az=90^\circ} - k[Az - 90^\circ]^2 \quad (4.26)$$

This expression, in which $m_{u,LEO,Az=90^\circ}$ and k depend on the launch vehicle, states that any deviation from the East direction at launch causes an increase in the ΔV necessary to reach the same orbit, resulting in a smaller payload mass.

The LEO payload mass can be seen as the sum of three contributes:

$$m_{u,LEO} = m_p + m_{esc} + m_{paf} \quad (4.27)$$

Where m_p is the propellant mass, m_{esc} is the spacecraft's mass at the end of the escape leg and m_{paf} is the so-called *payload attach fitting mass*, i.e. the structural element that joins the payload with the launch vehicle.

If we now consider the departing maneuver, the spacecraft's mass before and after the burn can be expressed as, respectively:

$$\begin{aligned} m_0 &= m_{LEO} \\ m_f &= m_{LEO} - m_p = m_{esc} + m_{dry} + m_{paf} \end{aligned}$$

Therefore, by applying the rocket equation, it is possible to obtain:

$$m_{esc} + m_{dry} + m_{paf} = m_{LEO} e^{-\frac{\Delta V}{c}} \quad (4.28)$$

It is now useful to take into account an additional 5% of ΔV for off-design eventualities, so that we introduce in the equation $\Delta V^* = 1.05\Delta V$. By solving for m_{esc} and substituting Equation 4.26 it follows that:

$$m_{esc} = [m_{u,LEO,Az=90^\circ} - k(Az - 90)^2 + m_{dry}] e^{-\frac{\Delta V^*}{c}} - m_{dry} - m_{paf} \quad (4.29)$$

This relation, once chosen the launch vehicle, allows to compute the escape mass of the spacecraft. In this work, the reference launcher will be the *Delta IV Heavy*, whose characteristic masses are:

$$\begin{aligned} m_{u,LEO,Az=90^\circ} &= 26045 \text{ kg} \\ m_{paf} &= 250 \text{ kg} \\ m_{dry} &= 3550 \text{ kg} \end{aligned}$$

Where $m_{u,LEO,Az=90^\circ}$ is related to a circular parking orbit at an altitude of 300 km from Earth's surface.

The k coefficient can be evaluated by means of an interpolation of the following data:

$$m_{u,LEO,Az=90^\circ} = 26045 \text{ kg} \quad \text{and} \quad m_{u,LEO,Az=0^\circ} = 20780 \text{ kg}$$

and by means of the following expression:

$$k = \frac{m_{u,LEO,Az=90^\circ} - m_{u,LEO,Az=0^\circ}}{90^2}$$

Hence:

$$k = 0.65$$

4.6.2 Mass at destination

Once m_{esc} has been evaluated, m_{fin} can be computed by means of t_{esc} . In fact, once the time of escape is known, it is possible to obtain the relative position of the spacecraft and the target asteroid and to calculate the amount of propellant needed for the interplanetary journey, m_{SEP} . This quantity is given assuming that the spacecraft escapes with a mass of 10^4 kg, meaning that m_{fin} can be computed as follows:

$$m_{fin} = m_{esc} - m_{SEP} \frac{m_{esc}}{10^4} = m_{esc} \left[1 - \frac{m_{SEP}}{10^4} \right] \quad (4.30)$$

The relative position of the two bodies of interest varies over time and m_{SEP} by direct consequence; this implies that the maximum m_{esc} could not coincide with the best m_{fin} .

Chapter 5

Results

This chapter is intended to present the results of the performed analysis, with particular attention upon in plane and out of plane escape trajectories and their V_{esc} module.

At first, in plane trajectories with $V_{esc} \approx 1$ km/s will be proposed and the best scenarios, defined as those with the higher mass at destination, will be analyzed and plotted. Then, due to the fact that out of plane trajectories require a larger turn angle to rotate the velocity vector, a comparison between those two families will be carried out.

In particular, it will be shown and demonstrated that, in the case of an out of plane V_{esc} , the multiple fly-by scenario is the only feasible way to escape Earth's gravitational influence, because the turn angle required by the single fly-by trajectory would be too high.

In the last section of the chapter we will dedicate our attention on finding the limit value of V_{esc} for which the single fly-by scenario results inconvenient from the destination mass' point of view.

Apart from the value of m_{fin} , there are a few more parameters that are useful to evaluate the performance of a particular escape scenario. They are:

- *velocity at the end of the departure maneuver* V_P , that must be provided by the propulsive system and that is directly connected to the launchable mass;
- *total time of flight TOF*, defined as the summation of the legs' times of flight;
- *Azimuth angle at launch* Az_{launch} , that affects the payload mass, as explained in *Section 4.6.1*.

It should be noted that the choice of assuming $V_{esc} \approx 1$ km/s is justified by the fact that these particular values of the escape velocity modulus are the best ones required to reach some of the most interesting NEAs, like those presented in *Chapter 1.3.2*.

5.1 In plane escape trajectories with small V_{esc}

For this family of escape trajectories, the asteroid of reference is assumed to be *2000SG344*, whose orbital plane is inclined of 0.1114° with respect to the heliocentric ecliptic plane. This orbital feature makes it the best candidate to analyze the in plane escape.

This input provided feasible solutions for single, multiple and resonant fly-by scenarios, whose detailed results will be presented in the following subsections.

5.1.1 Single fly-by scenario

The output data of the analysis conducted on this type of scenario can be plotted, in order to evaluate the best scenario in terms of escape mass as a function of the escape data. As can be observed in Figure 5.1, the best scenario is the one that escapes on the 21st of June 2022, or 141.19.

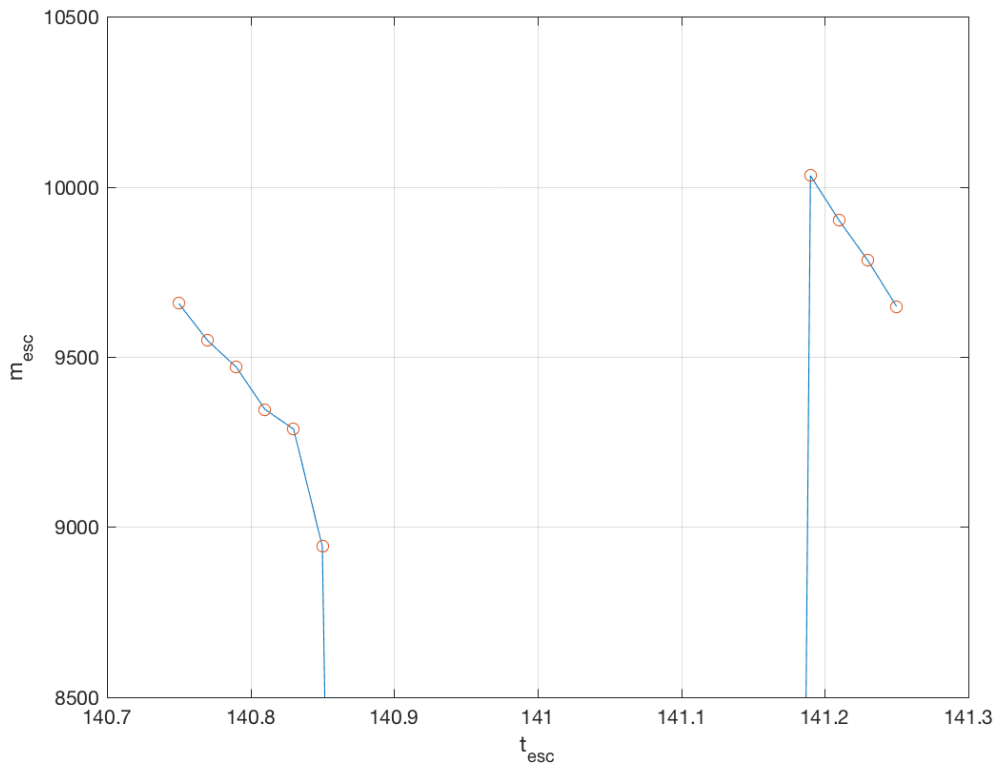


Figure 5.1: **Escape mass as a function of the escape data, single fly-by**

The absence of solutions for the central part of the time interval means that, for those inputs, the software could not evaluate any feasible trajectory. This is probably due to the unfavorable position of the Earth and the Moon, resulting in an excessive turn angle required by the fly-by event.

Due to the fact that the range of t_{esc} given as an input is equivalent to the Moon's period,

i.e. approximately 28 days, it is possible to note some sort of cyclicity with the solutions. This means that, in the case of a t_{esc} range from 141.1 to 141.6 the $m_{esc}-t_{esc}$ relation would be represent by a broken line between, approximately, 141.15 and 141.35, pretty similar to the one in Figure 5.4.

Asteroid	2000SG344
Escape	21 st June 2022
Departure	11 th June 2022
u_{∞}	$5.701 \cdot 10^{-3} VU_S$
v_{∞}	$3.988 \cdot 10^{-2} VU_S$
w_{∞}	$1.128 \cdot 10^{-4} VU_S$
r_{Earth}	1.016 DU_S
α_{Earth}	4.712°
δ_{Earth}	$4.840 \cdot 10^{-5}$ °
V_{esc}	1.2 km/s

Table 5.1: Overview of the single fly-by scenario inputs

By means of these inputs, a whole series of feasible scenarios is evaluated, but our attention must be focused on m_{esc} and m_{fin} . Their best values are, respectively:

m_{esc}	10032.55 kg
m_{fin}	9089.87 kg

Table 5.2: Escape and destination mass for the single fly-by scenario

Once the maximum value for the destination mass has been found, the trajectory that satisfies it must be plotted and analyzed.

a_{PL}	34.063 DU_E	a_{LE}	-97.222 DU_E
e_{PL}	0.969	e_{LE}	1.475
i_{PL}	15°	i_{LE}	4.715°
Ω_{PL}	263.722°	Ω_{LE}	263.722°
ω_{PL}	-175.207°	ω_{LE}	-52.515°
tof_{PL}	3.531 d	tof_{LE}	6.739 d

Table 5.3: Orbital parameters for the single fly-by scenario

In this case, a single fly-by is sufficient to acquire enough speed, so that the number of legs will be equal to two: the PL one and the LE one. The orbital parameters reported in Table 5.3 will be useful to plot the trajectories on Matlab. Other useful parameters are listed in Table 5.4.

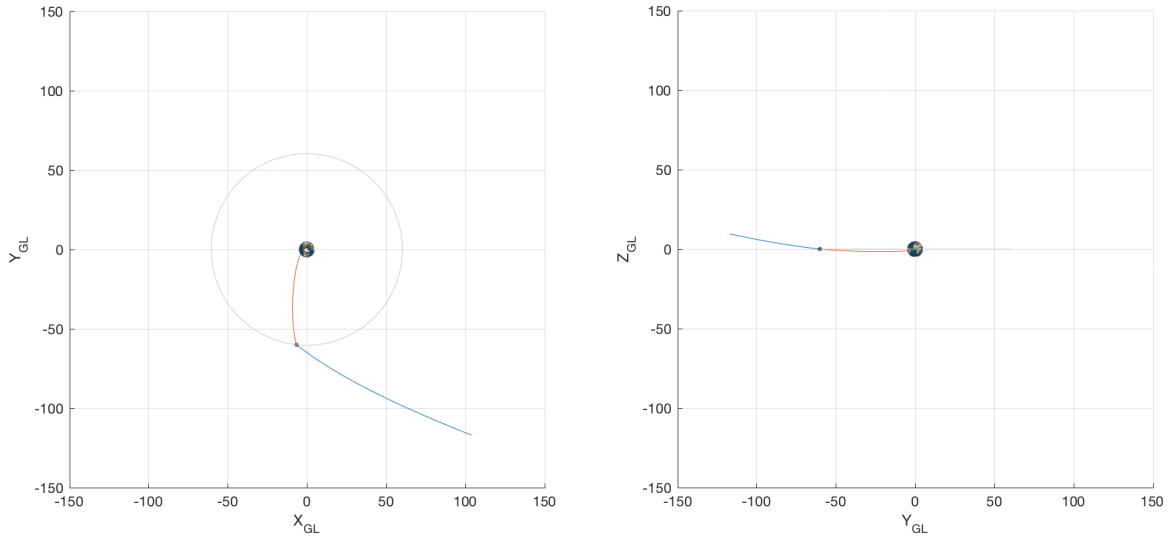
V_P	10.931 km/s	FB node	AN
ΔV	3.287 km/s	$V_{\infty, ZEN}$	0.951 km/s
Az_{launch}	83.884°	$r_{p, moon}$	2204.2 km
δ_{max}	97.512°	ΔP	1.456°
δ	90.561°	ΔC	66.481°

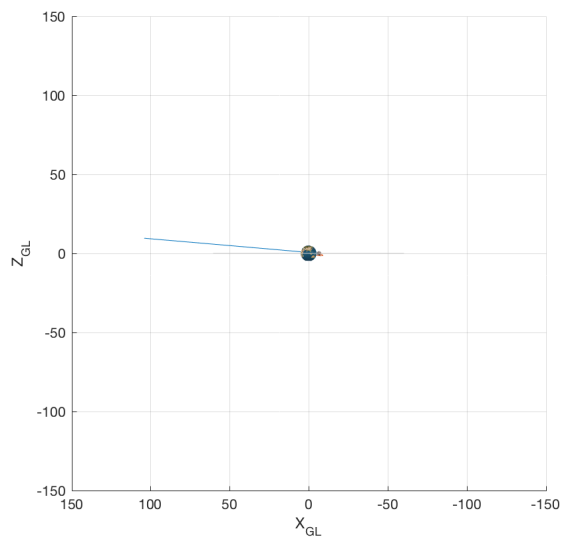
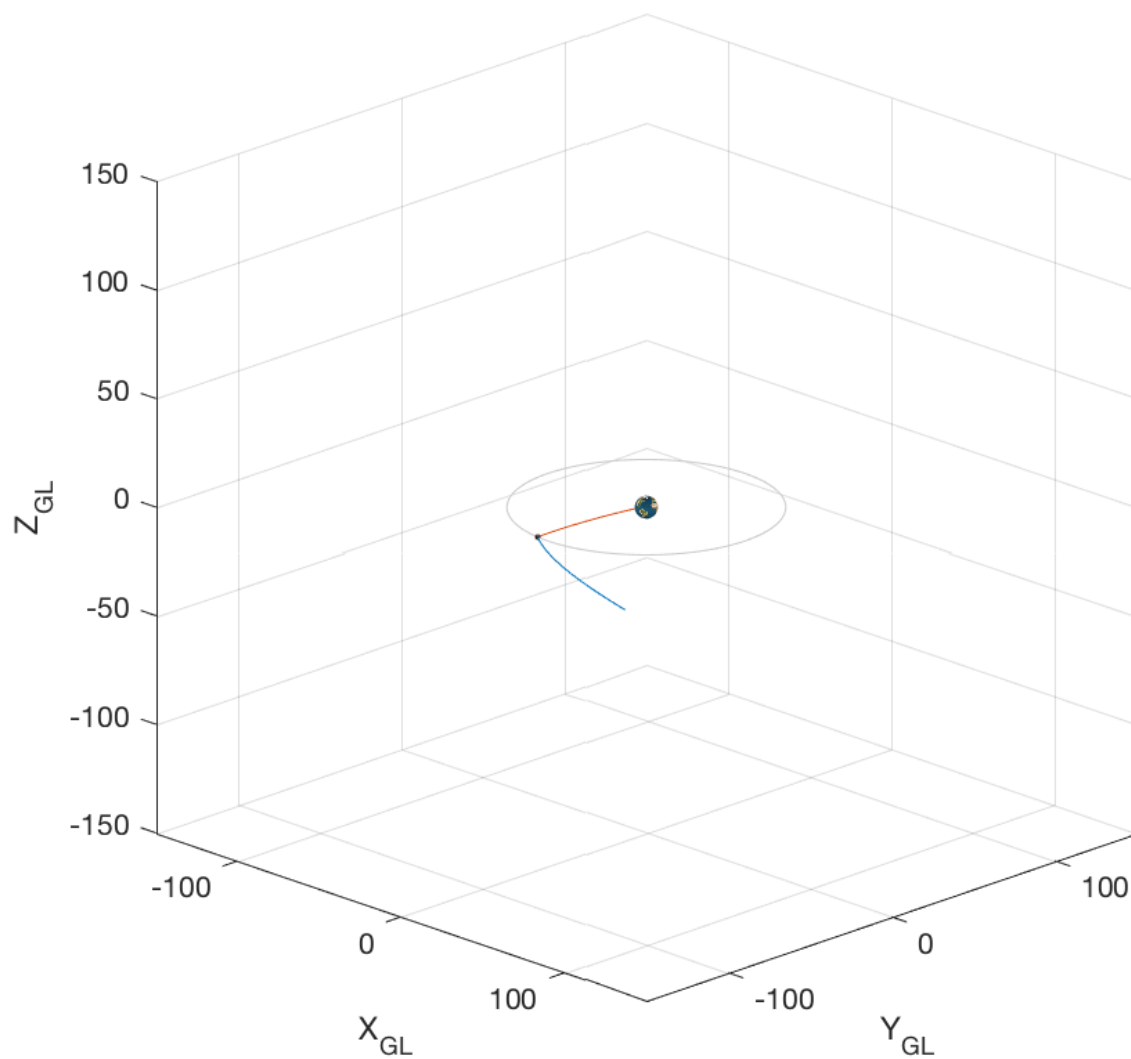
Table 5.4: Useful parameters for the single fly-by scenario

Where $V_{\infty, ZEN}$ is the magnitude of the Moon-relative velocity vector at fly-by and $r_{p, moon}$ is the periselenium radius, i.e. the minimum distance between the center of the Moon and the spacecraft during the fly-by event. The angles ΔP and ΔC , instead, are respectively the variations of Pump and Crank angles due to the LGA, as defined in *Section 3.7.2*.

As can be seen, the value for the Azimuth angle is higher than 80°, meaning that the launch will be directed towards East, in order to exploit Earth's motion around its axis. By assuming the radius of the Moon to be equal to 1737 km, one can easily compute that the fly-by event occurs on the 14th of June at an altitude of 467 km from the surface.

The following plots report three views of the trajectory and an overview of the whole path. In the $Z_{GL} - Y_{GL}$ view, it can be observed that the fly-by occurs in the ascending node of the spacecraft's trajectory with respect to the Moon's orbital plane.



Figure 5.2: **XY, YZ, XZ views of the single fly-by scenario**Figure 5.3: **Overview of the single fly-by scenario**

5.1.2 Multiple fly-by scenario

As we already did for the single fly-by scenario, the NEA of interest is, due to the small inclination of its heliocentric orbit with respect to the ecliptic plane, the one named 2000SG344.

By operating as in the single fly-by scenario, the data that guarantees the maximum escape mass can be evaluated and is the one that escapes on the 14th of June 2022, or 141.07.

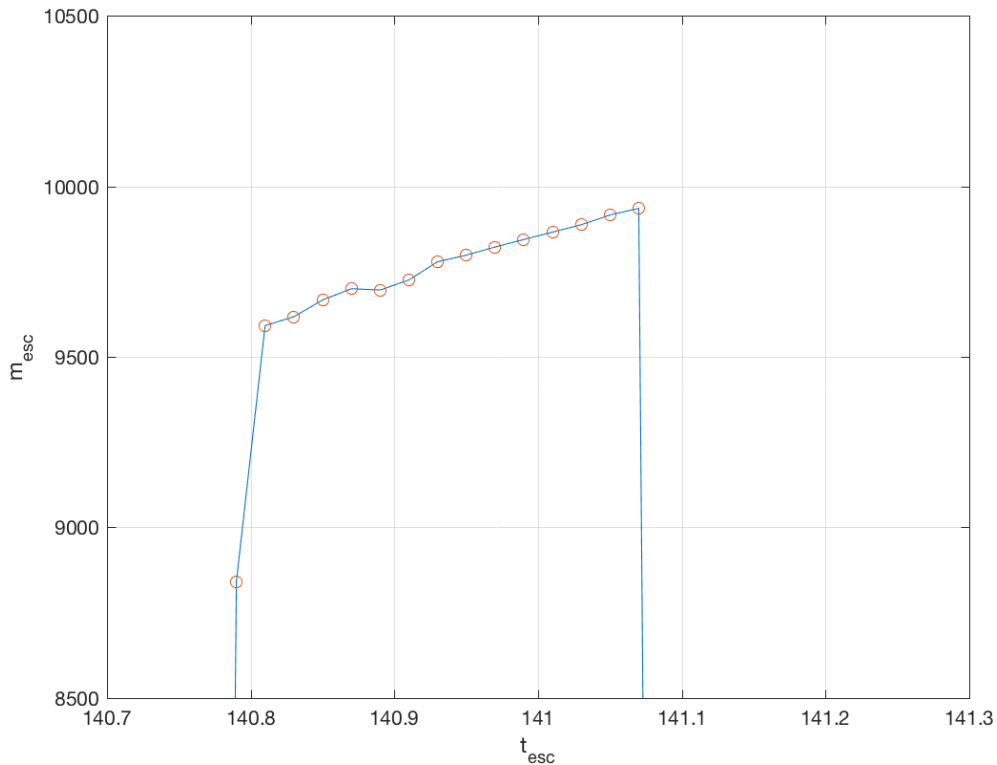


Figure 5.4: **Escape mass as a function of the escape data, multiple fly-by**

Differently from the trend shown in Figure 5.1, in the multiple fly-by scenario the value for m_{esc} increases with t_{esc} ; such behavior is attributable to the fact that here the second fly-by occurs in the descending node.

The absence of solutions for the central part of the time interval means that, for those inputs, the software could not evaluate any feasible trajectory. This is probably due to the unfavorable position of the Earth and the Moon, resulting in an excessive turn angle required by the fly-by event. The escape inputs of the best trajectory are summarized in Table 5.5, while its performances in terms of escape and destination mass are reported in Table 5.6.

Asteroid	2000SG344
Escape	14 th June 2022
Departure	19 th April 2022
u_{∞}	$6.322 \cdot 10^{-3} VU_S$
v_{∞}	$3.978 \cdot 10^{-2} VU_S$
w_{∞}	$2.693 \cdot 10^{-4} VU_S$
r_{Earth}	1.015 DU_S
α_{Earth}	4.596°
δ_{Earth}	$4.848 \cdot 10^{-5}$ °
V_{esc}	1.2 km/s

Table 5.5: Overview of the multiple fly-by scenario inputs

m_{esc}	9935.25 kg
m_{fin}	9007.61 kg

Table 5.6: Escape and destination mass for the multiple fly-by scenario

By means of further analysis of the output data for the multiple fly-by scenario, it is possible to recognize two different scenarios that both share the same m_{esc} and m_{fin} , because they also share the same t_{esc} .

The orbital parameters of the LE, LL and PL legs of the two possible scenario are listed in Table 5.7 and Table 5.9, while Table 5.8 and Table 5.10 contain some other useful parameters, such as the ΔV required to put the spacecraft onto the PL leg, the turn angles of the two LGAs, the Moon-relative velocity vector of the spacecraft at fly-by and the periselenium radii of the two events.

a_{PL}	54.551 DU_E	a_{LL}	90.365 DU_E	a_{LE}	-97.222 DU_E
e_{PL}	0.981	e_{LL}	0.566	e_{LE}	1.312
i_{PL}	4°	i_{LL}	66.114°	i_{LE}	7.587°
Ω_{PL}	293.142°	Ω_{LL}	113.142°	Ω_{LE}	293.142°
ω_{PL}	-170.186°	ω_{LL}	90°	ω_{LE}	-96.318°
tof_{PL}	2.731 d	tof_{LL}	42.343 d	tof_{LE}	11.036 d

Table 5.7: Orbital parameters for the multiple fly-by scenario, case 1

V_P	10.957 km/s	FB node	DN
ΔV	3.320 km/s	Az_{launch}	86.188°
δ_{max}	79.731°	$V_{\infty, ZEN}$	1.24 km/s
δ_{fb1}	48.829°	$r_{p,moon,fb1}$	4525.5 km
δ_{fb2}	73.798°	$r_{p,moon,fb2}$	2122.1 km

Table 5.8: Useful parameters for the multiple fly-by scenario, case 1

By means of these data, it is easy to derive that the first fly-by occurs on the 22nd of April at an altitude of 2788 km, while the second Lunar encounter is predicted for the 8th of June at a distance of 385 km from the surface of the Moon.

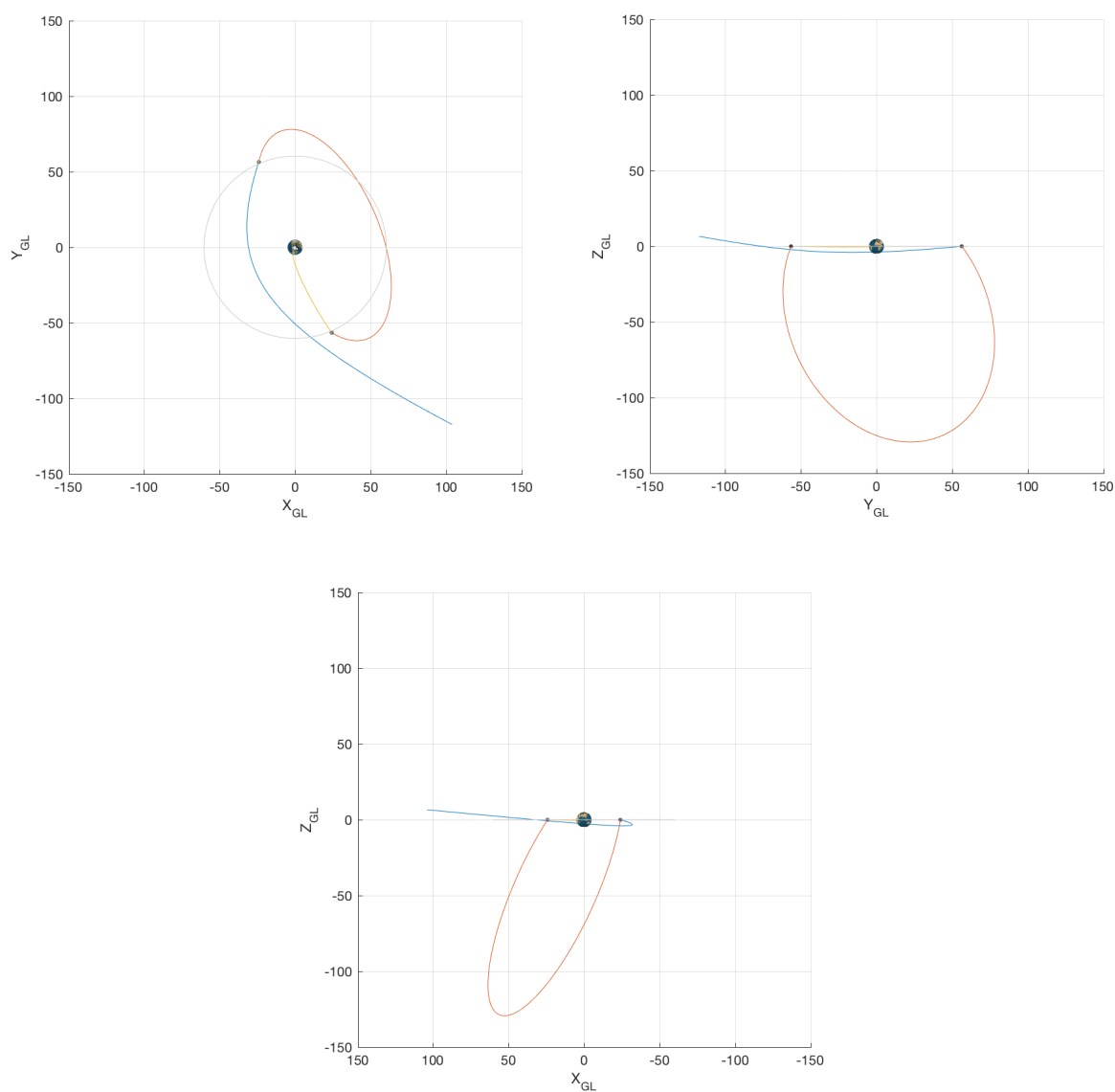


Figure 5.5: XY, YZ, XZ views of the multiple fly-by scenario, case 1

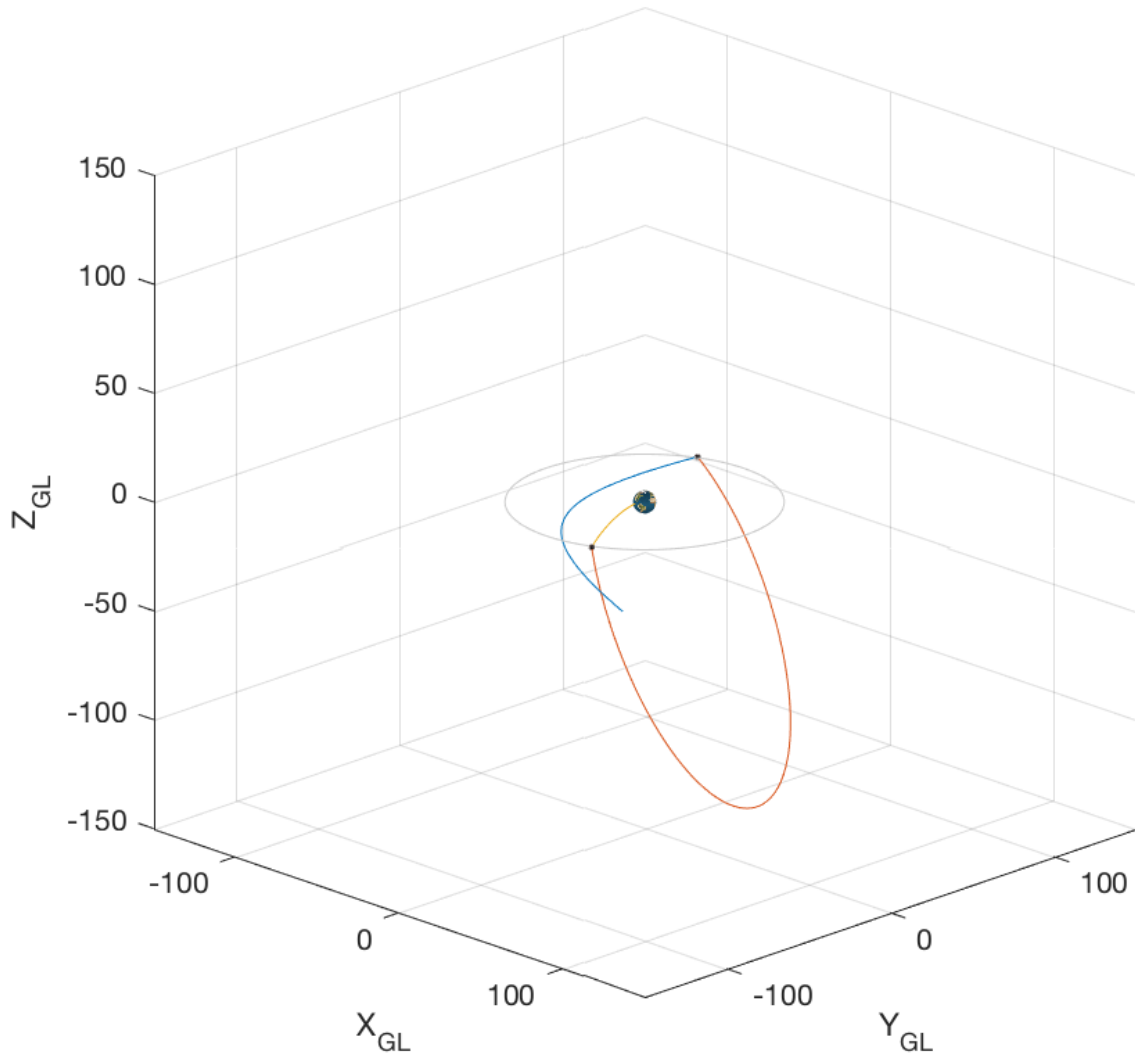


Figure 5.6: Overview of the multiple fly-by scenario, case 1

a_{PL}	54.551 DU_E	a_{LL}	90.365 DU_E	a_{LE}	-97.222 DU_E
e_{PL}	0.981	e_{LL}	0.566	e_{LE}	1.312
i_{PL}	4°	i_{LL}	66.114°	i_{LE}	7.587°
Ω_{PL}	-66.857°	Ω_{LL}	-66.857°	Ω_{LE}	293.142°
ω_{PL}	-170.186°	ω_{LL}	-90°	ω_{LE}	-96.318°
TOF_{PL}	2.731 d	TOF_{LL}	42.343 d	TOF_{LE}	11.036 d

Table 5.9: Orbital parameters for the multiple fly-by scenario, case 2

V_P	10.957 km/s	FB node	DN
ΔV	3.320 km/s	Az_{launch}	86.188°
δ_{max}	79.731°	$V_{\infty, ZEN}$	1.24 km/s
δ_{fb1}	47.647°	$r_{p,moon,fb1}$	4705.4 km
δ_{fb2}	62.900°	$r_{p,moon,fb2}$	2122.1 km

Table 5.10: Useful parameters for the multiple fly-by scenario, case 2

As already stated before, the two fly-by events occur on the 22nd of April and on the 8th of June at a distance of, respectively, 2974 km and 385 km from the surface of the Moon.

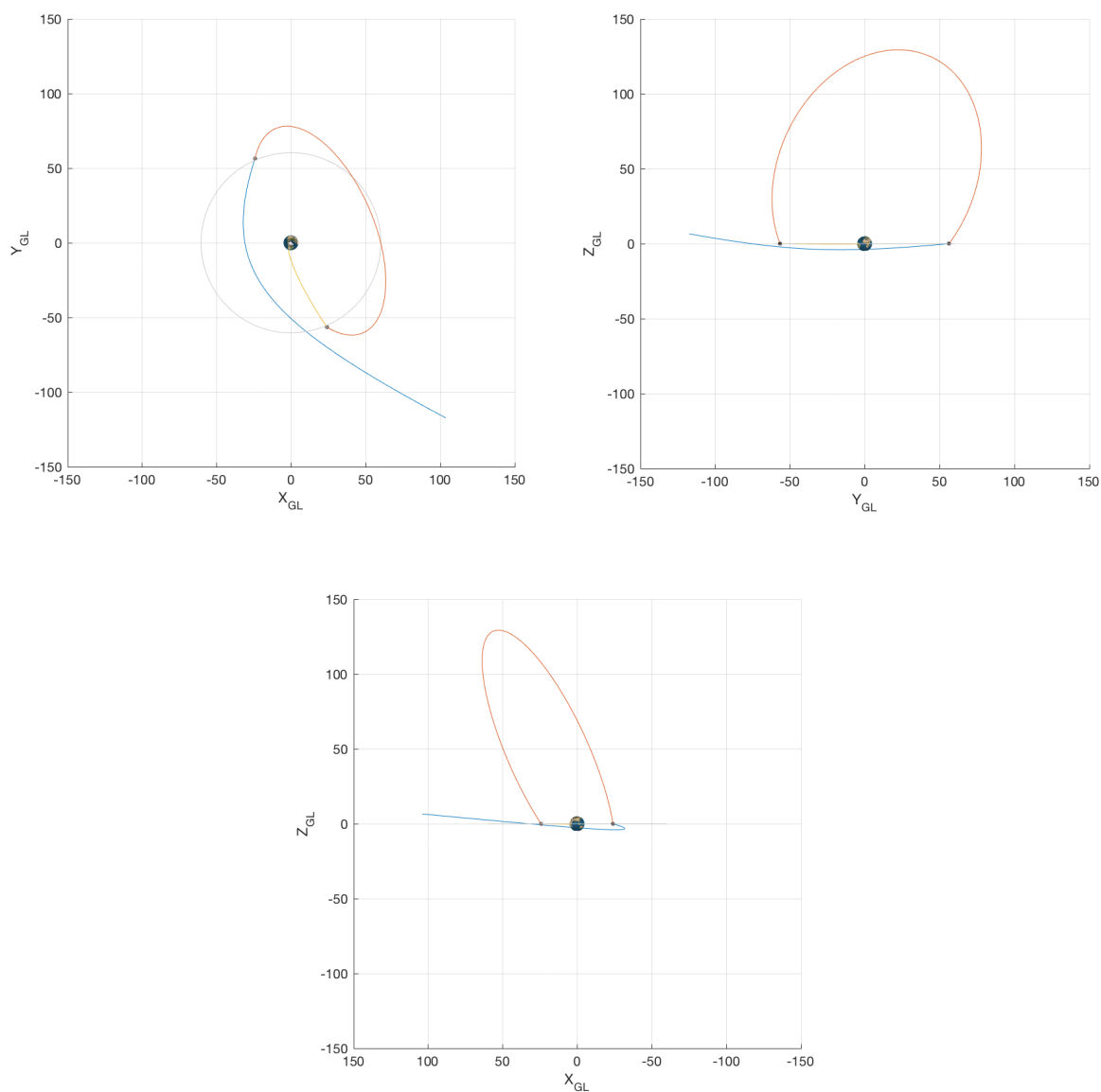


Figure 5.7: XY, YZ, XZ views of the multiple fly-by scenario, case 2

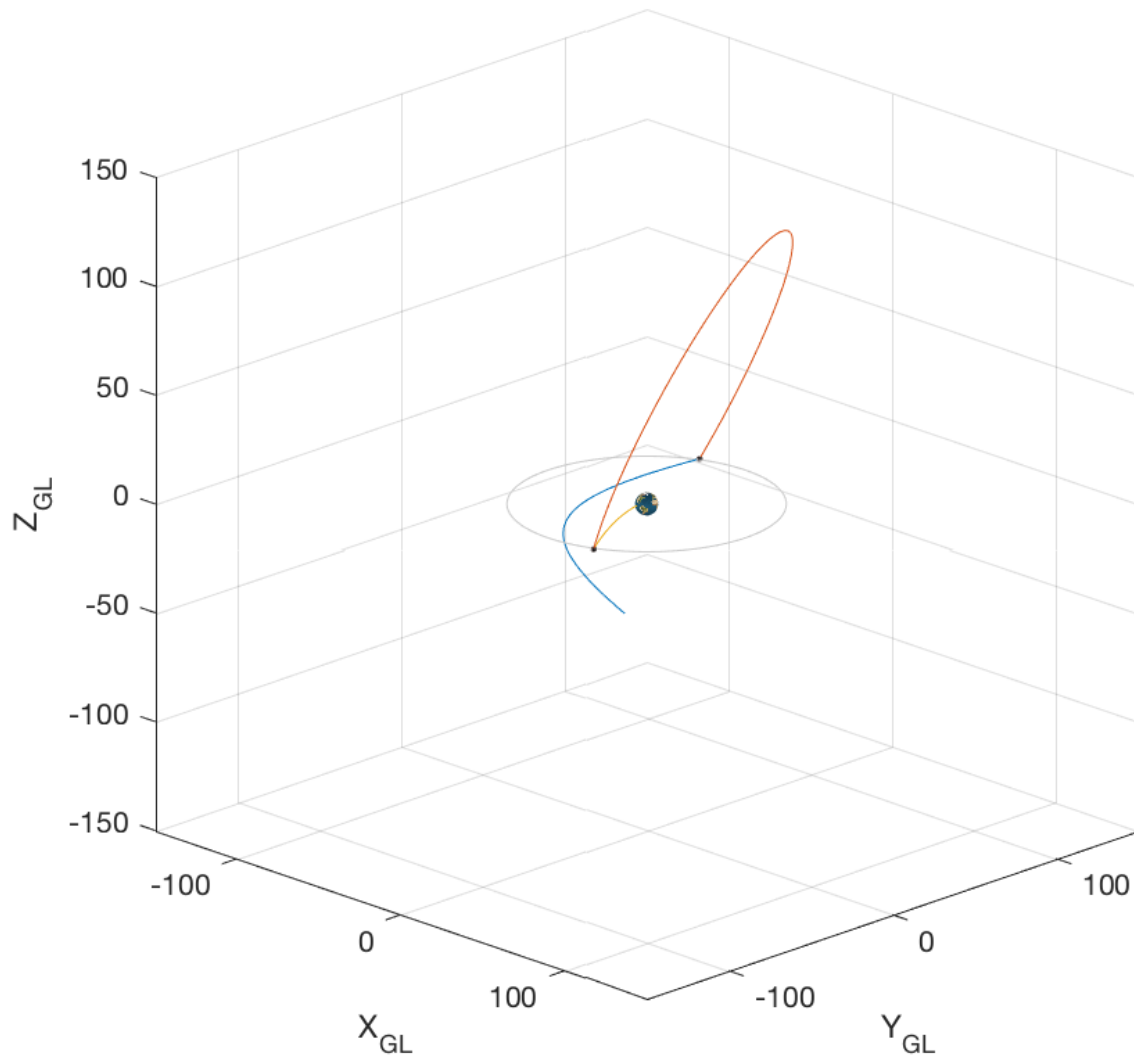


Figure 5.8: **Overview of the multiple fly-by scenario, case 2**

By looking at Figures 5.6 and 5.8, one easily understands how these two trajectories can deliver the same amount of payload. The LE and PL legs of the two scenarios are, in fact, exactly the same, while the LL trajectories are simply symmetric with respect to the fundamental plane of the T_{GL} coordinate system.

5.1.3 Resonant fly-by scenario

The analysis regarding this kind of scenario has been performed by operating a variation not only of the V_{esc} module, but also of the two integers' N and M values, whose meaning has been explained in *Chapter 4.4.1*.

The best scenarios are characterized, as will be presented throughout this subsection, by the following values for N and M :

$$\begin{array}{lll} N = 1 & M = 1 & \text{for the first case} \\ N = 3 & M = 2 & \text{for the second case} \end{array}$$

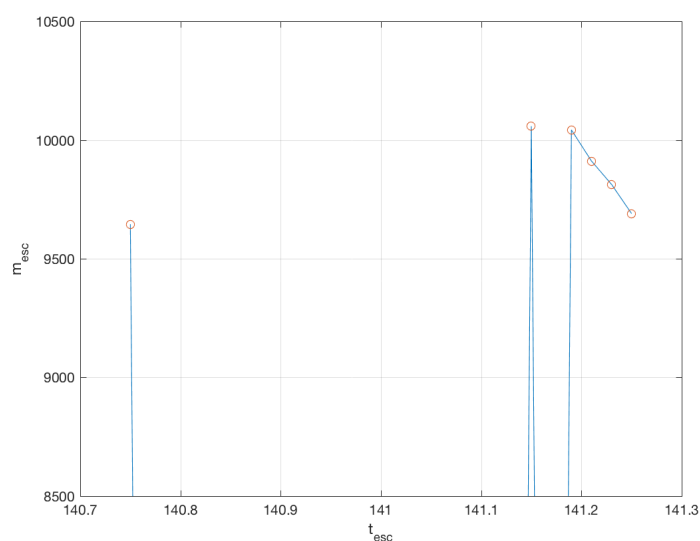


Figure 5.9: **Escape mass as a function of the escape data, resonant 11 fly-by**

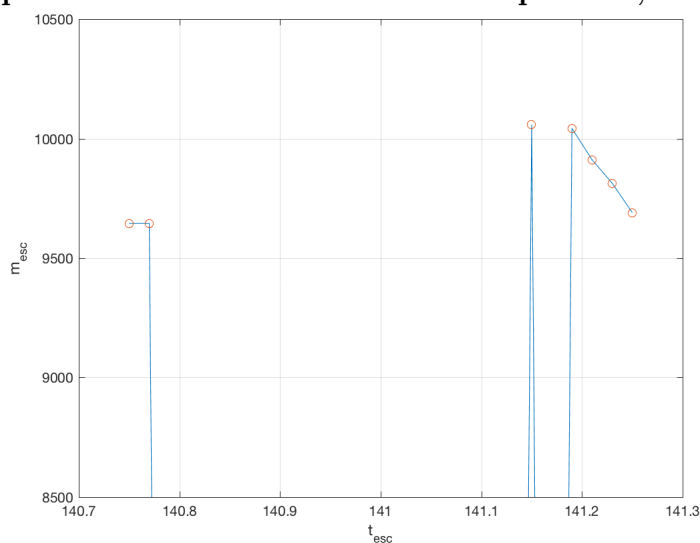


Figure 5.10: **Escape mass as a function of the escape data, resonant 32 fly-by**

In both cases, the best escape data is on the 19th of June 2022, or 141.15, but the departure date is not the same, due to the different length of the Moon to Moon transfer orbit.

Asteroid	2000SG344
Escape	19 th June 2022
Departure case 1	8 th May 2022
Departure case 2	24 th April 2022
u_∞	$5.919 \cdot 10^{-3} VU_S$
v_∞	$3.985 \cdot 10^{-2} VU_S$
w_∞	$1.673 \cdot 10^{-4} VU_S$
r_{Earth}	1.016 DU_S
α_{Earth}	4.673°
δ_{Earth}	$4.850 \cdot 10^{-5} \circ$
V_{esc}	1.2 km/s

Table 5.11: Overview of the resonant fly-by scenario inputs

The two scenarios, whose primary difference lies in the values for N and M, share the same escape and destination masses, as stated in Table 5.12.

m_{esc}	10058.21 kg
m_{fin}	9114.92 kg

Table 5.12: Escape and destination mass for the resonant fly-by scenario

Further analysis of the scenario for which N=1 and M=1, led to find out that there are 95 LL trajectories capable of the same performances. In such cases, the choice falls on the trajectory characterized by the smaller turn angles δ_{fb1} and δ_{fb2} , i.e. the farthest one from the Moon's surface.

The orbital parameters of its three legs are presented in Table 5.13, while some other useful parameters are reported in Table 5.14.

a_{PL}	31.507 DU_E	a_{LL}	60.531 DU_E	a_{LE}	-97.222 DU_E
e_{PL}	0.967	e_{LL}	0.376	e_{LE}	1.56
i_{PL}	2°	i_{LL}	46°	i_{LE}	16.719°
Ω_{PL}	357.648°	Ω_{LL}	177.648°	Ω_{LE}	177.648°
ω_{PL}	2.308°	ω_{LL}	247.863°	ω_{LE}	213.123°
TOF_{PL}	4.189 d	TOF_{LL}	27.631 d	TOF_{LE}	10.33 d

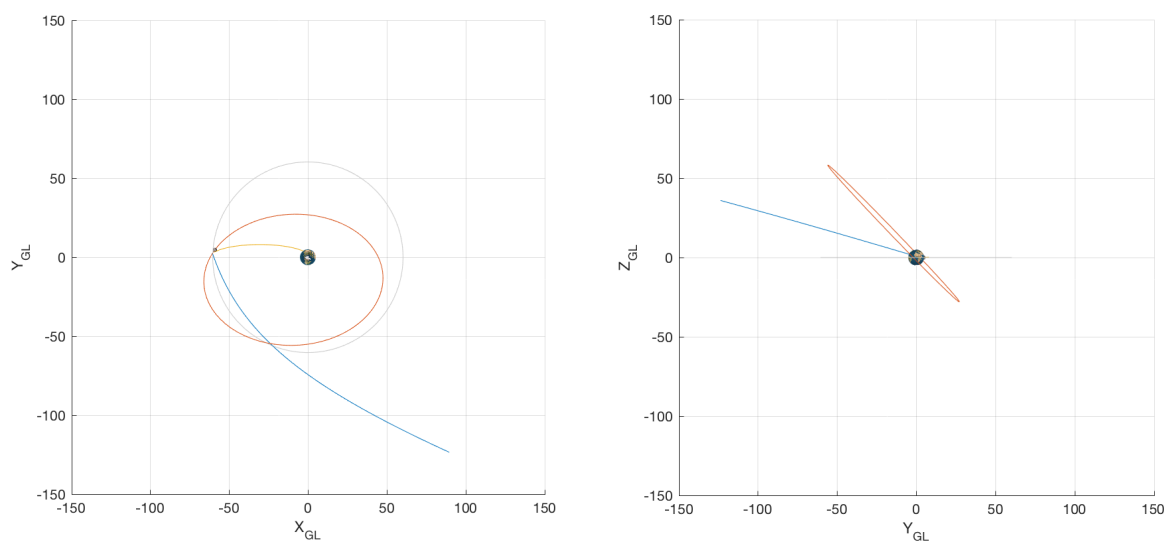
Table 5.13: Orbital parameters for the resonant fly-by scenario, case 1

In Table 5.14 are reported some other useful parameters. One of them, the turn angle for the first fly-by δ_{fb1} , has been chosen so that the stresses acting on the spacecraft resulted minimized, by transiting farthest from the Moon's surface.

V_P	10.924 km/s	FB node	AN
ΔV	3.280 km/s	Az_{launch}	84.681°
δ_{max}	104.098°	$V_{\infty, ZEN}$	0.858 km/s
δ_{fb1}	58.993°	$r_{p,moon,fb1}$	6865.6 km
δ_{fb2}	102.704°	$r_{p,moon,fb2}$	1867.3 km

Table 5.14: Useful parameters for the resonant fly-by scenario, case 1

By means of these data, it is easy to compute that the first LGA occurs on the 12th of May at a distance of 5119 km, while the second one happens on the 9th of June at an altitude of 130 km.



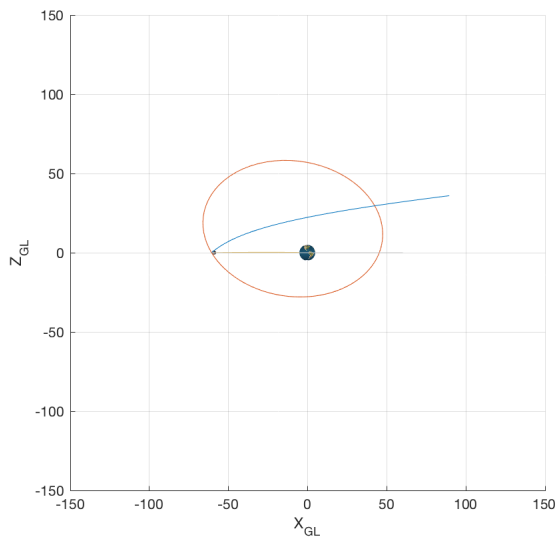


Figure 5.11: XY, YZ, XZ views of the resonant fly-by scenario, case 1

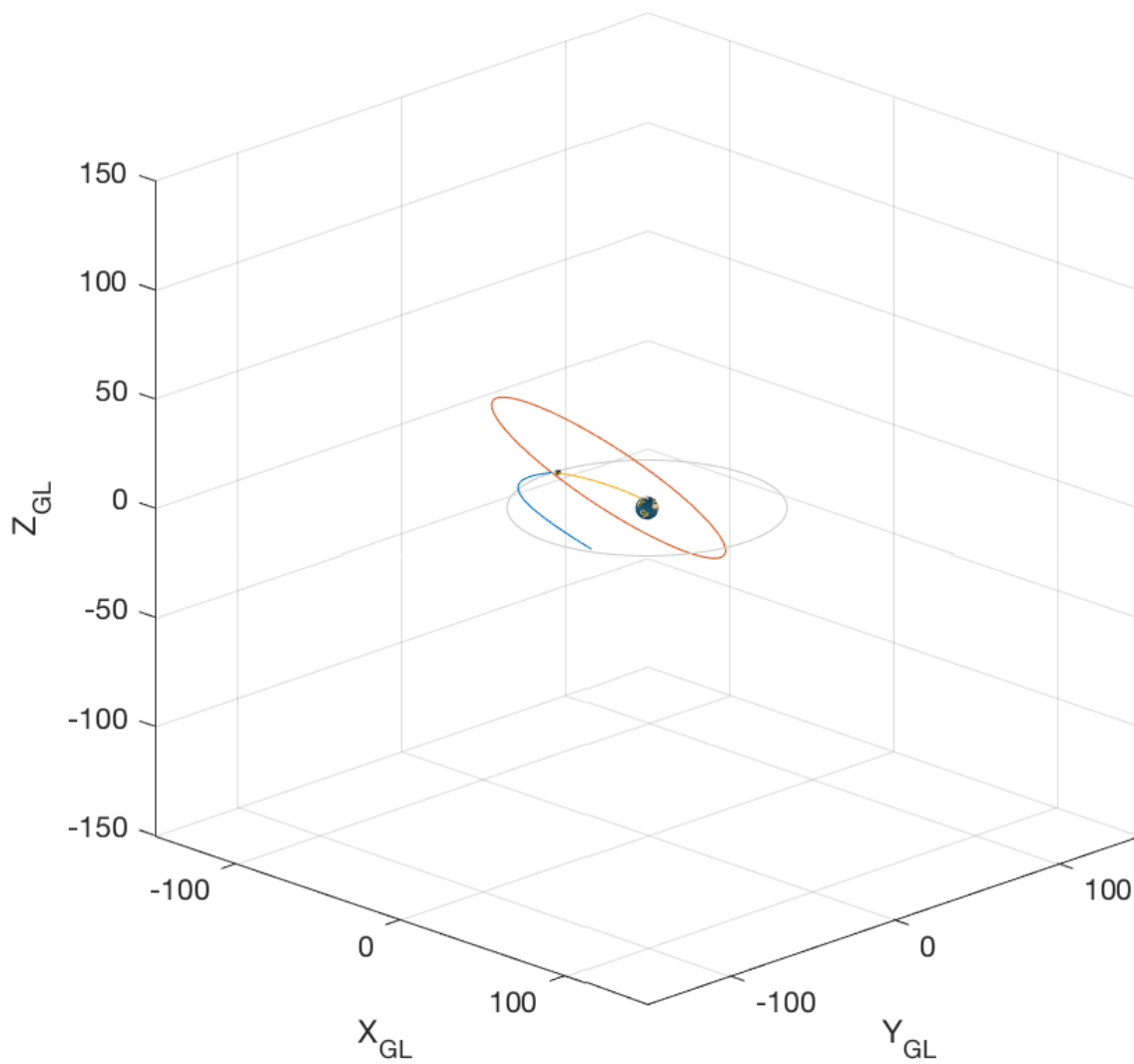


Figure 5.12: Overview of the resonant fly-by scenario, case 1

In the case of $N = 3$ and $M = 2$, meaning that the Moon to Moon orbit takes one Lunar period and a half to be completed, there are 93 possible LL trajectories that are capable of delivering the same amount of payload at t_{esc} . Also in this case, the choice must be done by considering the δ_{fb1} and δ_{fb2} values. The trajectory of interest possesses the following orbital parameters:

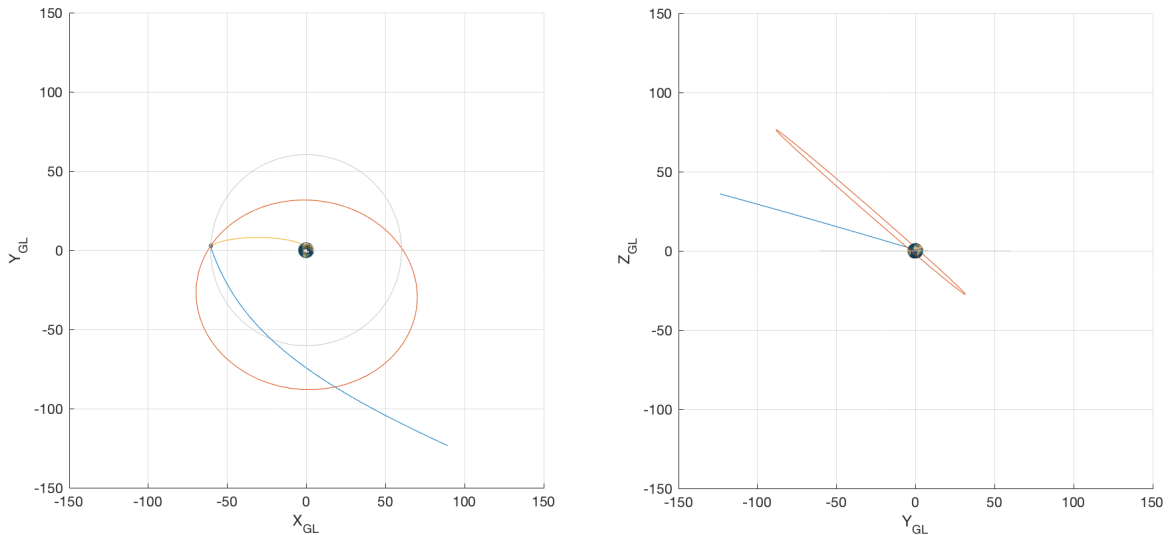
a_{PL}	31.507 DU_E	a_{LL}	79.319 DU_E	a_{LE}	-97.222 DU_E
e_{PL}	0.967	e_{LL}	0.471	e_{LE}	1.56
i_{PL}	2°	i_{LL}	41°	i_{LE}	16.719°
Ω_{PL}	357.648°	Ω_{LL}	177.648°	Ω_{LE}	177.648°
ω_{PL}	2.308°	ω_{LL}	272.321°	ω_{LE}	213.123°
TOF_{PL}	4.189 d	TOF_{LL}	41.446 d	TOF_{LE}	10.33 d

Table 5.15: **Orbital parameters for the resonant fly-by scenario, case 2**

As previously stated, in the following table are listed other of important parameters.

V_P	10.924 km/s	FB node	AN
ΔV	3.280 km/s	Az_{launch}	84.681°
δ_{max}	104.098°	$V_{\infty, ZEN}$	0.858 km/s
δ_{fb1}	66.028°	$r_{p,moon,fb1}$	5563.2 km
δ_{fb2}	102.570°	$r_{p,moon,fb2}$	1875.3 km

Table 5.16: **Useful parameters for the resonant fly-by scenario, case 2**



By means of these data, it is easy to compute that the first LGA occurs on the 28th of April at a distance of 3826 km, while the second one happens on the 9th of June at an altitude of 138 km.

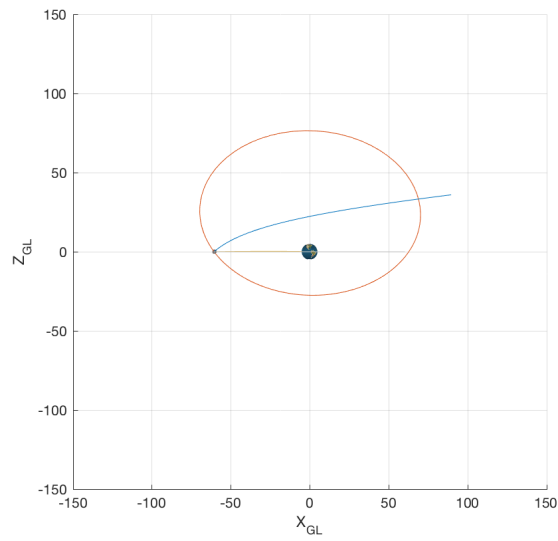


Figure 5.13: XY, YZ, XZ views of the resonant fly-by scenario, case 2

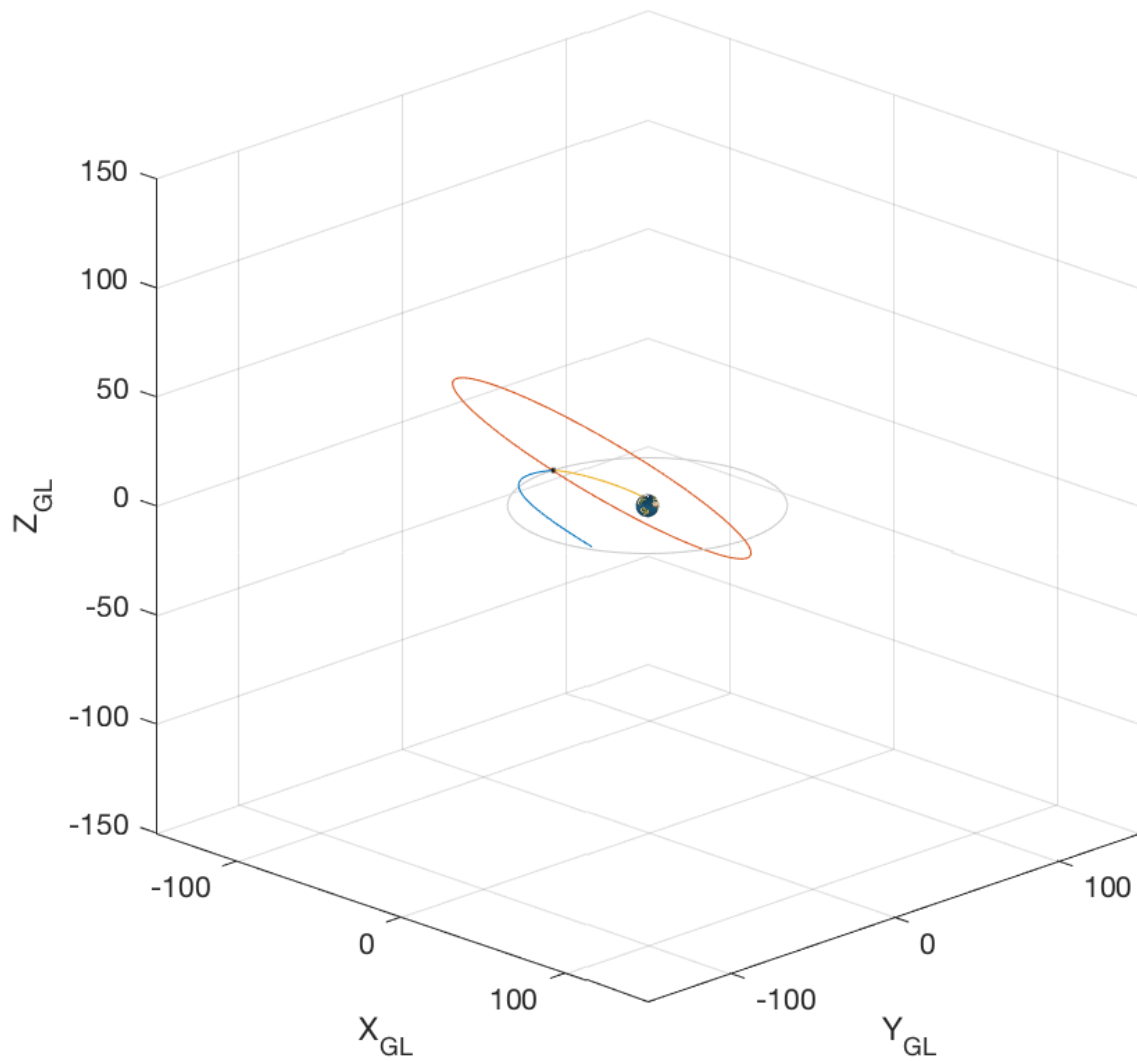


Figure 5.14: Overview of the resonant fly-by scenario, case 2

5.1.4 Considerations

Now that all the results of the in plane analysis have been presented, some considerations can be made. As stated in *Chapter 5.1.1*, apart from the m_{fin} value, there are some other important parameters that can be used for comparison.

One of them is the total time of flight, a quantity defined as the duration of the entire escape trajectory, between the departure maneuver and t_{esc} .

The following table is a summary of the performances.

Scenario	m_{fin}	TOF	ΔV
PLE	9089.87 kg	10.27 d	3.287 km/s
PLLE1	9007.61 kg	56.11 d	3.320 km/s
PLLE2	9007.61 kg	56.11 d	3.320 km/s
PLLEr1	9114.92 kg	42.15 d	3.280 km/s
PLLEr2	9114.92 kg	55.96 d	3.280 km/s

Table 5.17: Overview of the in plane scenarios performances

By looking at the data of Table 5.17, the following considerations can be made:

1. By adopting a payload point of view, the two resonant scenarios are the best; this mission architecture could be chosen for a cargo mission, in order to send a wide range of instrument at destination, before the arrival of the human mission;
2. By adopting a time of flight point of view, the best choice would be the single fly-by scenario; by exploiting this kind of architecture for a manned mission, in fact, the mission could result less dangerous for the astronauts, in terms of radiations absorbed by their bodies. However, these results need to be coupled with the length of the interplanetary leg;
3. By adopting a propulsive point of view, the resonant scenarios are the best, even if the the different mission architectures are quite similar in this regard.

To conclude, the best scenarios are the single fly-by and the resonant fly-by ones. By adopting the first one, it is possible to restrict the total time of flight by reducing the payload mass, a philosophy that could be adopted in the case of a manned mission. The second opportunity, instead, could be exploited for a cargo mission, due to its optimum value related to the payload mass.

5.2 Out of plane escape trajectories with small V_{esc}

This section of the chapter is dedicated to the optimization of the escape trajectories that, due to the relative position of Earth and the target asteroid, require an out of plane escape. The NEA of interest is, in this case, an Atens' asteroid named *2008EV5*, whose capabilities as a target have already been described in *Chapter 1.3.2*.

The results here presented are those reported in the paper *Design of Lunar-Gravity-Assisted escape maneuvers* by Lorenzo Casalino and Gregory Lantoine.

The authors focused their attention upon a double LGA mission, with the goal of optimizing its trajectory, a process they followed by means of two different approaches:

1. The first one pre-calculates the value of C3 as a function of its value before the fly-by event and of the date and eventually couples these results with the data regarding the interplanetary leg of the mission;
2. The second one is an analytical approximate method and operates by means of indirect methods that analyze the mission backwards, i.e. the escape leg first, then the LL branch and eventually the departure phase. These data are evaluated for different values of t_{esc} and V_{esc} .

It must be noted that the second approach is the best one to analyze short trajectories, for which the Sun's perturbative action can be neglected, but when it comes to optimize those trajectories whose LL leg takes months to be completed, the choice must fall on the pre-computed C3 method, due to its skill to take into account the Sun's perturbation. This is due to the fact that the path the spacecraft follows is not a conic anymore, i.e the first method is useless.

This approach relies on a group of pre-computed Moon to Moon trajectories, which consist of twelve families of orbits, as can be seen in Figure 5.15. Their name helps the user to understand their characteristics, by means of the following rules:

1. the position occupied in the alphabet by the uppercase letter corresponds to the number of months that lies between the two fly-by events;
2. the two lowercase letters indicate the direction, inbound or outbound, at which the two fly-bys occur with respect to Earth.

As can be seen in the E and F families of Figure 5.15, the longer the period of time between the two lunar encounters, the greater becomes the influence of the Sun's gravitational pull.

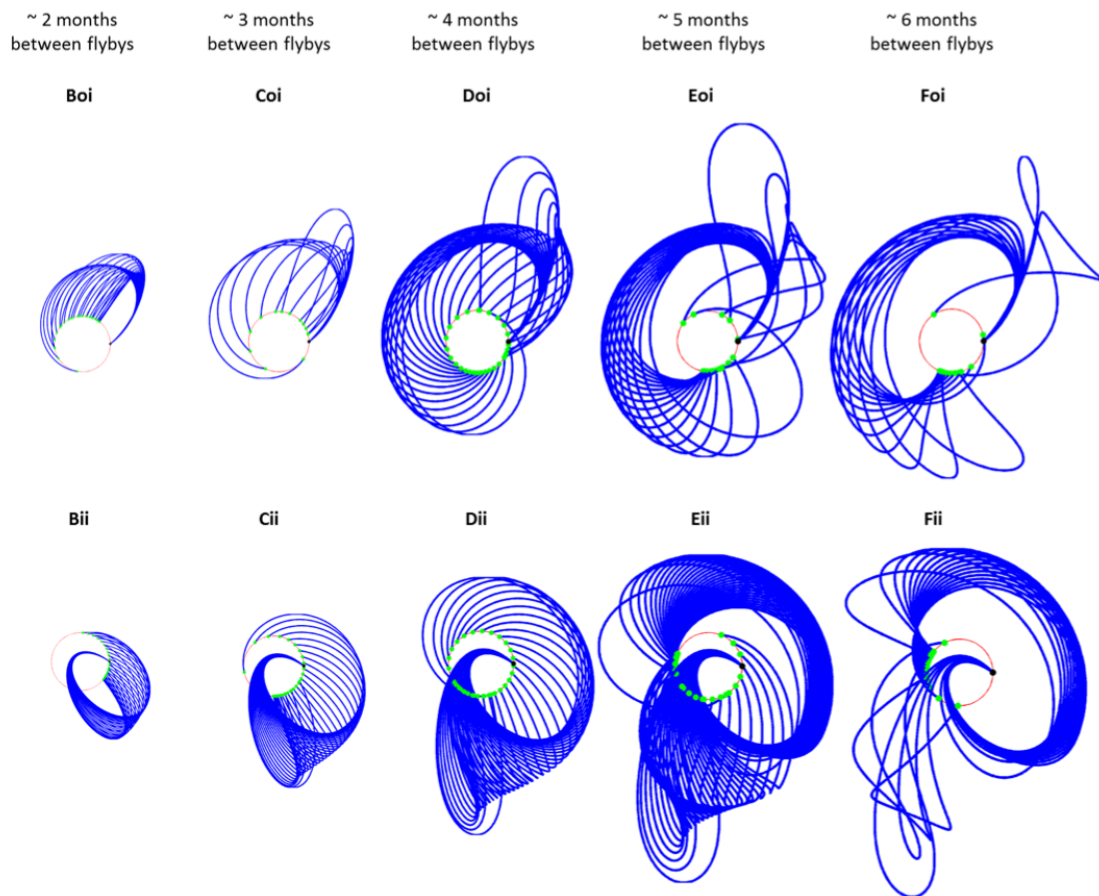


Figure 5.15: Families of pre-computed Moon to Moon trajectories

In the case of an out of plane escape, the fly-by event must provide a turn angle capable of both boost the energy of the spacecraft and change the plane of the trajectory, meaning that the out of plane scenarios cannot reach the values of $C3$ that the in plane ones do. The authors of the paper were able to derive a relation between the declination of the escape, i.e. its inclination with respect to the Earth's ecliptic plane, and the maximum achievable $C3$. This relation is plotted in Figure 5.16.

As the plot states, the maximum $C3$ achievable by means of two fly-bys is $2.5 \text{ km}^2/\text{s}^2$, equal to an escape velocity of 1.58 km/s , and as the declination increases, the allowed $C3$ needs to decrease. In the end, one can evaluate that even with a declination of about 85° , the guaranteed $C3$ will always be greater than $1.5 \text{ km}^2/\text{s}^2$.

This curve can be seen, to use the words of the authors, as "a lunar assisted launch vehicle curve".

Now that all the elements have been presented, it is possible to apply them to the optimization of an Asteroid Redirect Mission trajectory, that should rendez-vous with the

object of interest, 2008EV5.

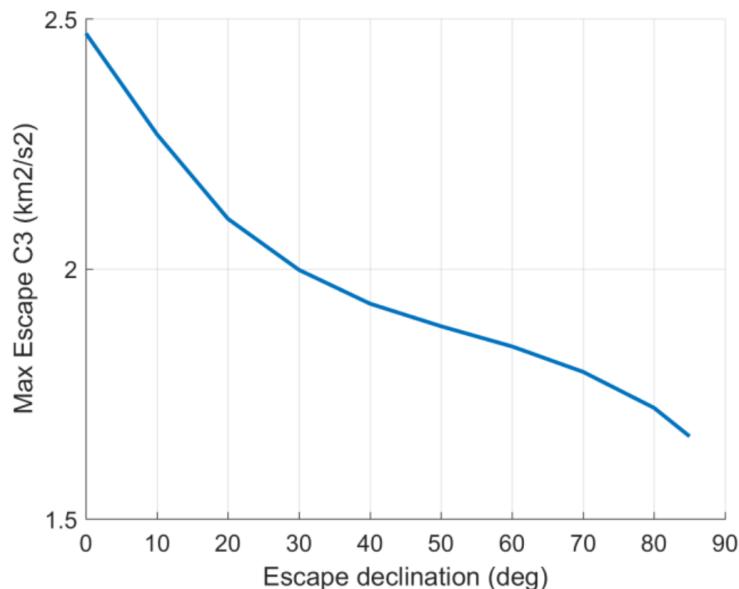


Figure 5.16: Achievable C3 as a function of the escape declination

5.2.1 ARRM Example - Analytical approach

For what concerns the short escape trajectories, the analysis conducted revealed that the single fly-by scenario cannot be exploited, so a PLLE scenario must be used: the authors chose a 28-day window of escape dates with 1-day steps centered in the 18th of June 2022. The values for V_{esc} are in the 1.3-1.4 km/s range, while the optimal value for escape leg inclination is approximately 68°.

The LL leg is, due to its better performance with respect to the backflip one, an elliptic orbit with the second fly-by occurring in the descending node.

The two fly-by events occur on the 4th of May and on the 14th of June 2022, at an altitude of, respectively, 670 km and 109 km. It can be easily derived that the two LGA are separated by an interval equal to one and a half lunar periods. The Moon relative velocity vector at fly-by is 1.66 km/s for both the encounters.

The best solution appears to be for an escape on the 21st of June 2022, with an escape velocity of 1.4 km/s. By means of this input, the escape mass value is 9674 kg, but xenon and hydrazine consumption must be taken into account, thus decreasing the escape mass to 9650 kg.

After the escape trajectory is completed, the probe must face the interplanetary leg of its voyage and eventually reach the target on the 21st of August 2023. The final mass,

also considering another 75 kg of xenon and hydrazine, now stands at 8272 kg. Summarizing:

Asteroid	2008EV5
Escape	21 st June 2022
Departure	2 nd May 2022
Destination	21 st August 2023
V_{esc}	1.4 km/s
Escape declination	68°
m_{esc}	9650 kg
m_{fin}	8272 kg

Table 5.18: Analytical approach - summary

While, for what regards the two lunar encounters:

LGA1	4 th May 2022	LGA2	14 th June 2022
Altitude	670 km	Altitude	109 km
$V_{\infty,ZEN}$	1.66 km/s	$V_{\infty,ZEN}$	1.66 km/s

Table 5.19: Analytical approach - fly-bys

In Figure 5.17 are reported two views of the trajectory, one in plane and one out of plane, so that its geometry and 3D shape can be visualized.

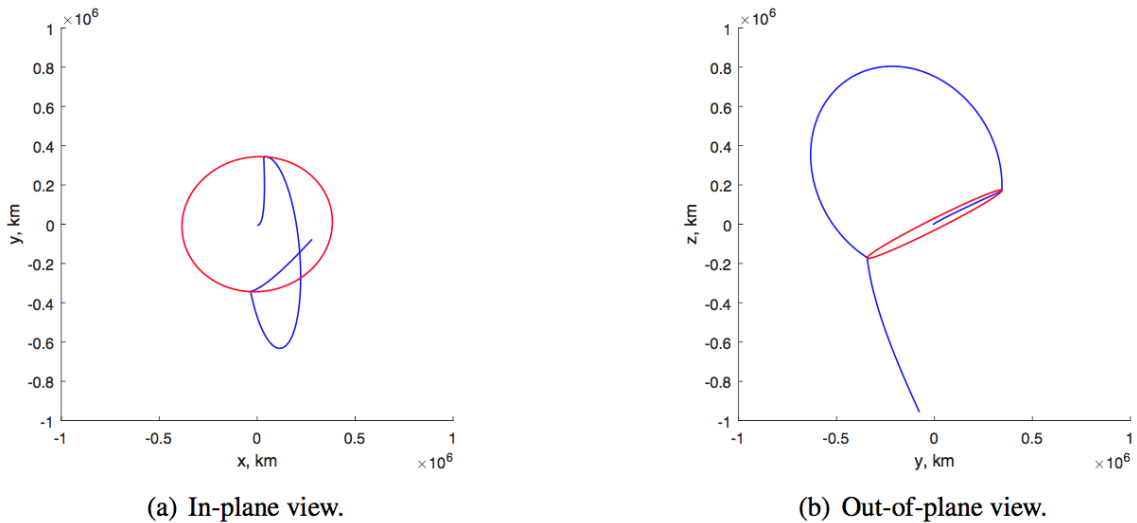


Figure 5.17: Overview of the trajectory from the analytical approach

5.2.2 ARRM Example - Precomputed trajectories approach

For the Solar perturbed escape trajectory, the process started by using MALTO, Mission Analysis Low Thrust Optimizer, a software tool for preliminary design of low-thrust trajectories. By means of this, it has been evaluated that an escape in June 2022 with an inclination of -65° should be the optimal choice.

Now that these inputs are known, the characteristics of the different families of orbits reported in Figure 5.15 can be consulted. The authors chose a Moon to Moon transfer orbit of the *Doi* family.

By means of further optimization steps, it has been derived that the two fly-bys occur on the 21st of February and on the 9th of June 2022 at an altitude of, respectively, 5119 km and 55 km, and with a Moon-relative velocity vector of 1.05 km/s in the first case and 2.15 km/s for the second case.

The precise value for the escape declination has been derived to be -67.6° .

If we take into account the necessary amount of xenon and hydrazine, the value for the escape mass is 9821.9 kg, while the arrival at the target is scheduled for the 25th of August 2023, with a mass of 8432.8 kg. The improvement with respect to the other approach is about 160 kg. Summarizing:

Asteroid	2008EV5
Escape	June 2022
Departure	February 2022
Destination	25 st August 2023
V_{esc}	1.319 km/s
Escape declination	-67.6°
m_{esc}	9821 kg
m_{fin}	8432 kg

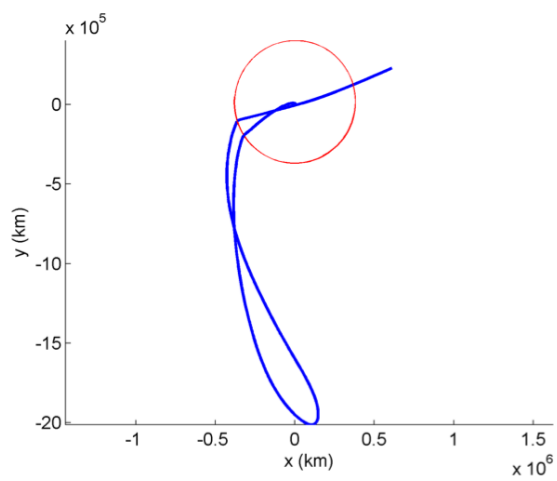
Table 5.20: Solar perturbed approach - summary

In this case, a Moon to Moon orbit of the *Doi* family has been used, meaning that approximately four months lie between the two fly-by events, as reported in Table 5.21. Other useful parameters regarding the two LGAs are listed in the following table.

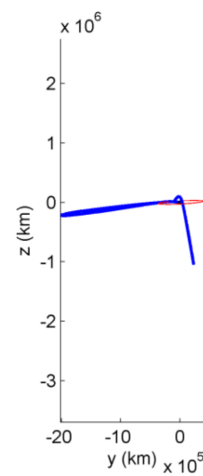
LGA1	21 st February 2022	LGA2	9 th June 2022
Altitude	5119 km	Altitude	55 km
$V_{\infty,ZEN}$	1.05 km/s	$V_{\infty,ZEN}$	2.15 km/s

Table 5.21: Solar perturbed approach - flybys

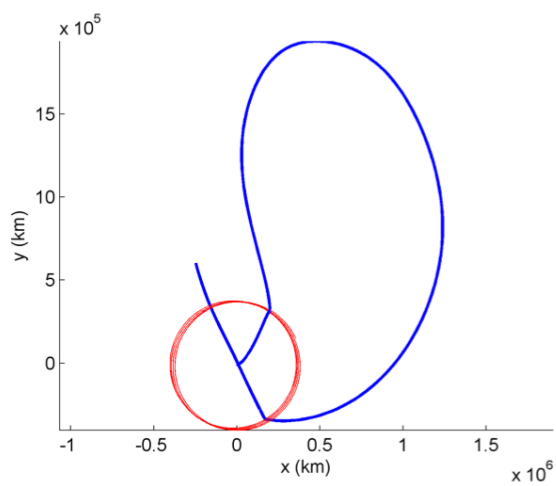
In Figure 5.18 are reported some views of the escape trajectory.



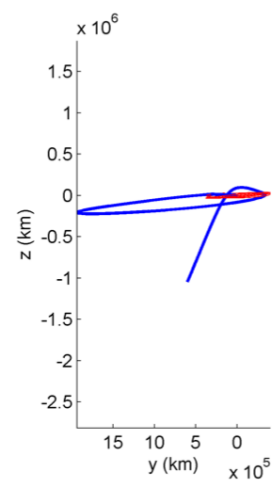
(a) In-plane view.



(b) Out-of-plane view.



(a) In-plane view.



(b) Out-of-plane view.

Figure 5.18: Overview of the trajectory from the precomputed approach

5.3 In plane escape trajectories with large V_{esc}

In plane and out of plane escape trajectories have already been discussed in the previous sections, where it has been demonstrated that the escape mass in the case of an out of plane destination is smaller than the one achievable with an in plane one.

We are now interested in investigating the same scenarios reported in *Chapter 5.1.1*, but in the eventuality that a greater escape velocity V_{esc} is needed.

Since a greater V_{esc} presupposes a higher ΔV at the perigee of the Earth parking orbit, we expect m_{esc} to experience a degrowth if the escape velocity rises.

This will be, for the sake of clarity, just a qualitative analysis, since the inputs used to evaluate the performances of the different scenarios are the same of *Chapter 5.1.1*, except for the V_{esc} components, that have been multiplied by a factor k .

If we wanted to improve the precision of the work, it would be necessary to choose another target characterized by the need of an out of plane escape trajectory; this could be an inspiration for further development of this work.

What follows is an investigation of the trajectories' feasibility and performances, in terms of payload mass, under increasing values of the multiplication factors. In addition, the reason some scenarios will not be feasible anymore will be subject of study.

Before proceeding with the results, it must be noted that by varying the inputs, also the date for which the best scenario occurs, i.e. t_{esc} , can be subject to modifications. The reason for this is that both the Moon and the Earth need to possess, at launch, the optimum alignment so that the performances of the trajectory can be reached.

5.3.1 Single fly-by scenario

By means of the original inputs, as reported in *Chapter 5.1.1*, this scenario was capable of bringing 10032.55 kg to the escape with a hyperbolic excess of velocity of 1.2 km/s. It is now object of our interest to evaluate the maximum escape mass of the single LGA scenario as a function of the multiplication factor k applied to the V_{esc} components. The results are presented in Table 5.22 and plotted in Figure 5.19.

k	m_{esc}	t_{esc}
1	10032.55 kg	141.19
1.1	9975.71 kg	141.19
1.2	9921.10 kg	141.19
1.3	9844.14 kg	141.19
1.4	9924.80 kg	141.17
1.5	9838.59 kg	141.17

Table 5.22: Escape mass as a function of k , single fly-by scenario

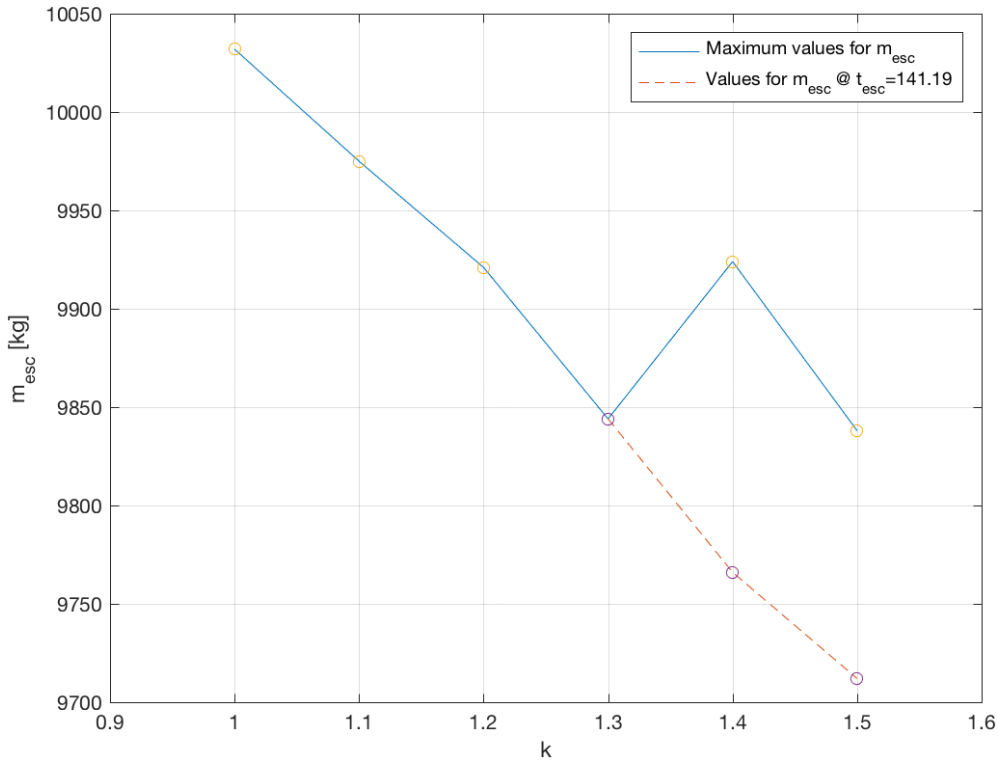


Figure 5.19: Escape mass as a function of k , single fly-by scenario

As reported in Table 5.22, by changing the value for k , also the t_{esc} for which the best scenario occurs is subject to variations. This implies that, in order to maximize the

payload mass, if k rises it is necessary to anticipate the escape date. However, it must be taken into account the fact that every t_{esc} possesses one limit value for k below which the fly-by cannot be executed, due to the excessive turn angle required by the maneuver. For example, at $t_{esc}=141.17$, the minimum value for which some feasible solutions can be found is $k_{limit}=1.4$.

The peculiar relation between $m_{esc} - t_{esc} - k$ is reported by the orange dashed line in Figure 5.19, that underlines how the escape mass simply decreases if we consider fixed the value for t_{esc} , in this case 141.19.

By means of this, it is possible to state that the relation $m_{esc} - k$ is always decreasing if the value for t_{esc} is fixed. However, if we assume the latter as a free parameter, we obtain a series of curves where, fixed k , m_{esc} increases if t_{esc} anticipates.

Now that the trend of m_{esc} has been presented, our attention can be focused upon the evolution of the turn angle as a function of the multiplication factor.

Before presenting the details, it must be noted that the single fly-by scenario is always feasible, if the time of departure from the perigee of the Earth parking orbit is precisely evaluated. In fact, if the V_{esc} module rises, the turn angle decreases and the periselenium radius increases until the trajectory ceases to be definable as "gravity assisted" and turns out to be a simple hyperbolic escape, for which $\delta = 0^\circ$. This implies that, in the case of a single fly-by scenario, it is not possible to evaluate a value for k after which this trajectory architecture cannot be exploited anymore.

The same analysis already conducted on the escape mass can now be repeated for the turn angle δ as a function of k . The results are presented in Table 5.23 and in Figure 5.20.

k	δ_{fb1}	δ_{max}	t_{esc}
1	90.56°	97.51°	141.19
1.1	66.24°	86.08°	141.19
1.2	53.78°	76.60°	141.19
1.3	45.71°	68.68°	141.19
1.4	75.10°	78.01°	141.17
1.5	65.41°	69.96°	141.17

Table 5.23: Turn angles as a function of k , single fly-by scenario

Figure 5.20 reports the values for δ and δ_{max} relative to the cases of Table 5.22.

If we now focus on the range $k=[1, 1.3]$, for which t_{esc} is constant and equal to 141.19, it is possible to observe that the minimum difference between δ_{max} and δ stands for the smaller value of the interval. The same effect can be observed for $k=1.4$ and $k=1.5$, for which $t_{esc}=141.17$.

Such a behavior is coherent with what stated before in regards to the evolution of the trajectory with the multiplication factor value; in fact, when k rises, the periselenium radius increases and the turn angle decreases.

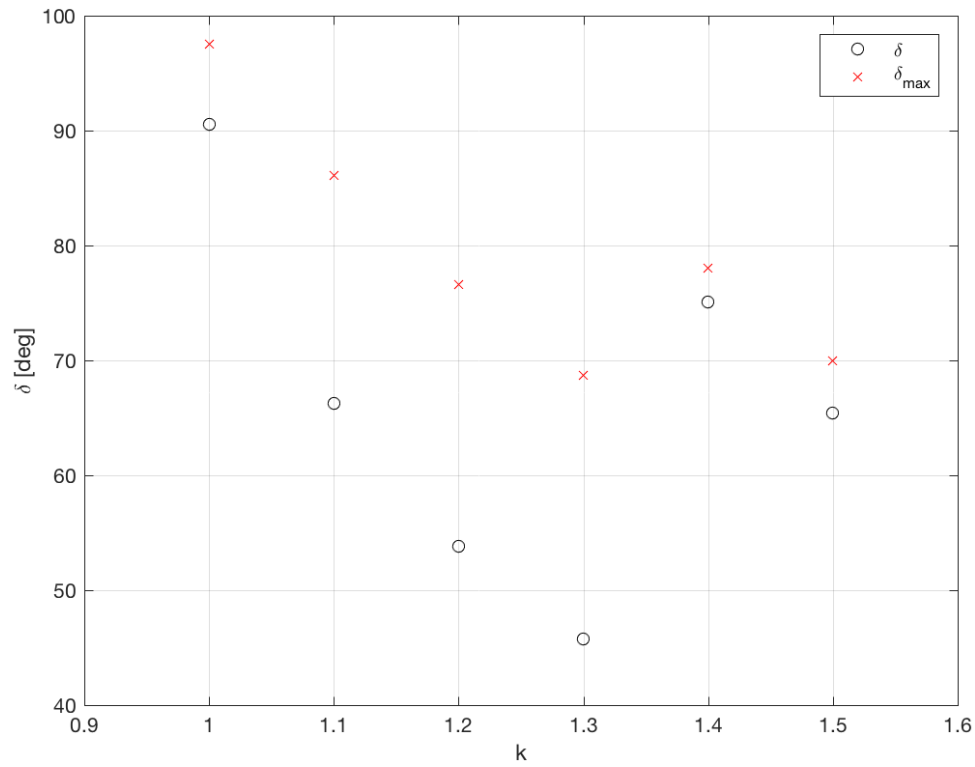


Figure 5.20: Turn angles as a function of k , single fly-by scenario

Now that the trends for both the escape mass and the turn angle have been described and analyzed, it is useful to visualize how the trajectory architecture evolves with k .

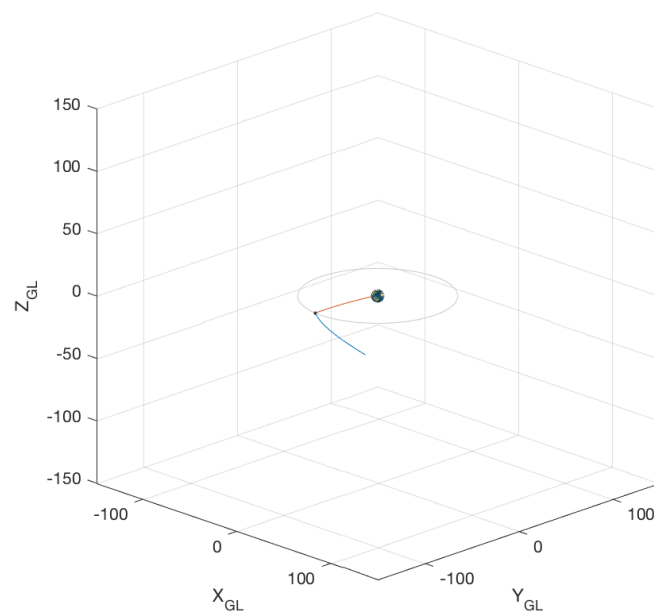


Figure 5.21: Trajectory architecture for $k=1$, single fly-by scenario

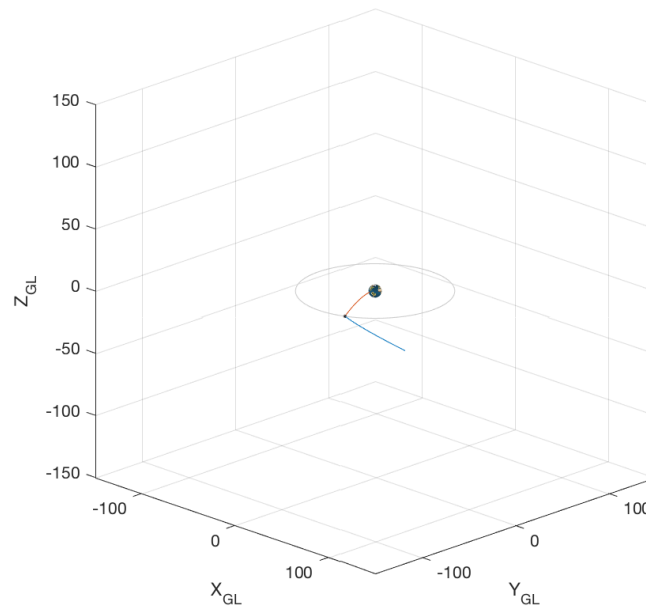


Figure 5.22: **Trajectory architecture for $k=1.3$, single fly-by scenario**

Figure 5.21 represents the trajectory architecture for $k=1$, while Figure 5.22 is relative to $k = 1.3$; these two cases were chosen due to the big difference in their respective turn angles, although the t_{esc} value is constant and equal to 141.19.

As can be seen, in the case of a greater value for the multiplication factor, the required turn angle results reduced and the intensity of the fly-by event is damped.

5.3.2 Multiple fly-by scenario

This scenario, by means of the original inputs, as reported in *Chapter 5.1.2*, was capable of bringing 9935.25 kg to the edge of Earth's sphere of gravitational influence with a hyperbolic excess of velocity of 1.2 km/s.

Just like in the single fly-by scenario, we are now interested in evaluating how the escape mass and the turn angle behave by varying the multiplication factor k we apply to the V_{esc} components. The results are presented in Table 5.24 and plotted in Figure 5.23.

k	m_{esc}	t_{esc}
1	9935.25 kg	141.07
1.1	9921.05 kg	141.11
1.2	9882.03 kg	141.09
1.3	9792.92 kg	141.09
1.4	no solutions	-

Table 5.24: Escape mass as a function of k , multiple fly-by scenario

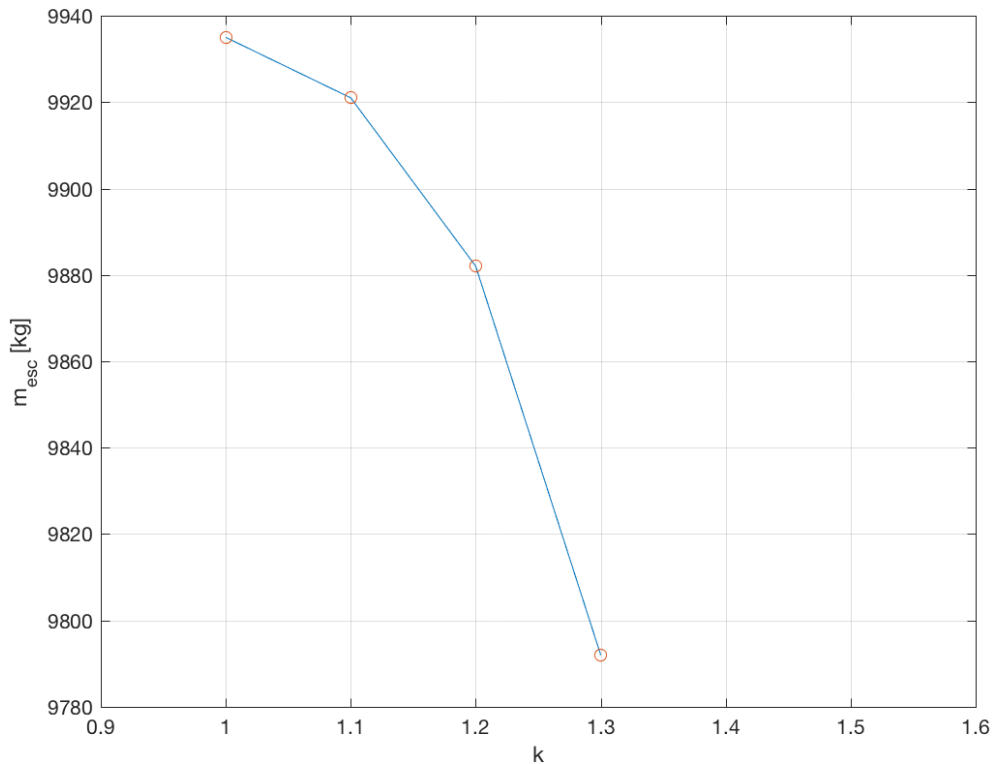


Figure 5.23: Escape mass as a function of k , multiple fly-by scenario

As already reported in the single LGA scenario, also in this case it is possible to observe a variation of the time of escape for which the best escape mass occurs. This implies

that, in order to maximize the payload mass, the time of departure (from which the time of escape depends) must be accurately evaluated.

However, differently from the previous case, the trend of Figure 5.23 is always decreasing, even if an adjustment in the escape date needs to be made.

Furthermore, it exists a value for the multiplication factor for which no more feasible solutions can be found, in this case $k=1.4$. The reason for this will be explained later by means of the $\delta - \delta_{max} - k$ behavior.

Now that the escape mass as a function of k has been analyzed, we can focus our attention upon the evolution of the turn angle and its maximum allowable value. The results are presented in Table 5.25 and plotted in Figure 5.24.

k	δ_{fb1}	δ_{fb2}	δ_{max}	t_{esc}
1	47.64°	62.90°	79.73°	141.07
1.1	47.75°	49.67°	77.29°	141.11
1.2	47.63°	59.71°	72.19°	141.09
1.3	51.28°	53.38°	61.31°	141.09

Table 5.25: Turn angles as a function of k , multiple fly-by scenario

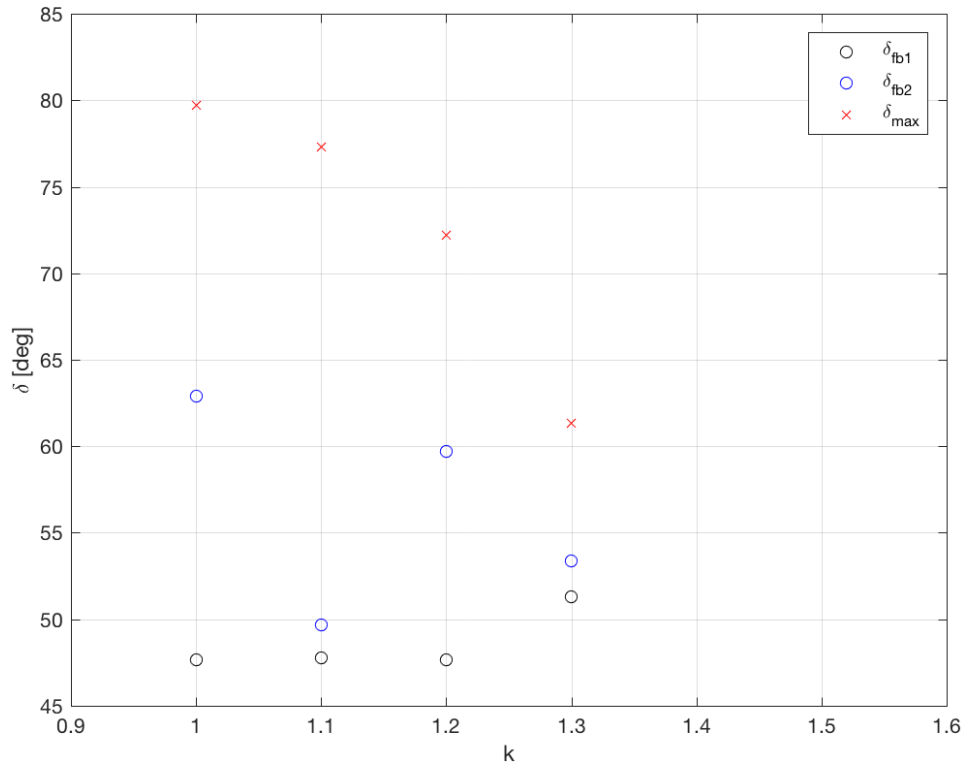


Figure 5.24: Turn angles as a function of k , multiple fly-by scenario

As can be seen in Figure 5.24, the value for δ_{max} decreases if the multiplication factor rises. This trend is justified by the fact that, as described in *Chapter 3.7.3*, the maximum allowable turn angle δ_{max} is inversely proportional to the value of the Moon relative velocity vector, that turns out to be related to the escape velocity module.

Furthermore, δ_{fb2} , between $k=1.2$ and 1.3 , decreases of approximately 6° , but the maximum allowable δ_{max} experiences a degrowth of 11° . This eventually leads to $\delta_{fb2} > \delta_{max}$ for $k \geq 1.4$.

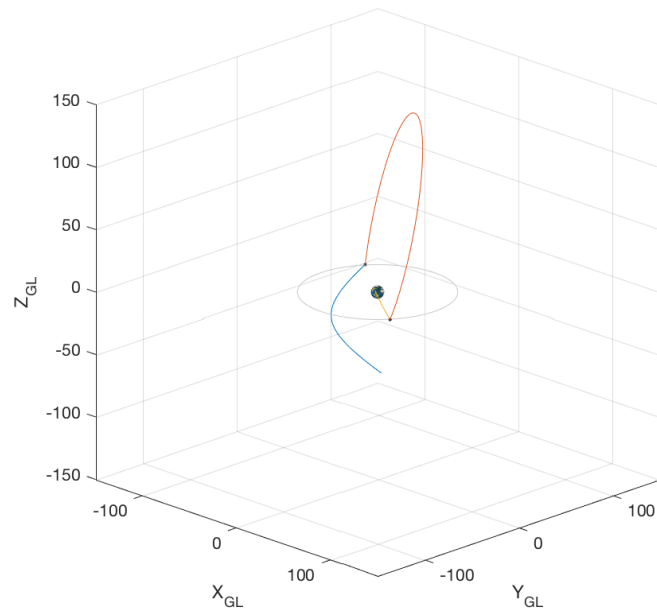
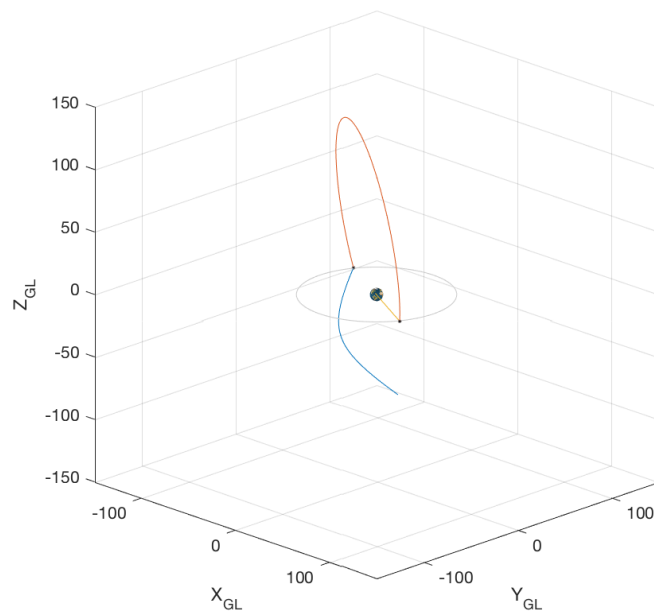
The value of δ_{fb1} , instead, needs to grow with k because the spacecraft needs to be put onto a more inclined Moon to Moon transfer orbit by the first Lunar encounter.

Now, in order for us to understand the reason why for $k=1.4$ and beyond no more feasible solutions can be found, it is useful to visualize how the trajectory architecture evolves with k . To do that, we consider the best multiple fly-by scenarios for $k = 1.2$ and $k = 1.3$.

Figure 5.25 represents the trajectory architecture for $k=1.2$, for which the inclination of the Moon to Moon transfer is equal to 77° . Figure 5.26, instead, is relative to a multiplication factor of 1.3 and the inclination of the LL leg is now equal to 97° .

These orbital features can be appreciated by the lateral views reported in Figure 5.27.

These two plots can explain the reason why, for $k=1.4$ and beyond, no feasible solutions can be found in the case of a planar escape. In fact, as the multiplication factor increases, also the inclination of the Moon to Moon transfer orbit experiences a growth. This implies that, in order for the second Moon encounter to ensure a low inclination LE leg, δ_{fb2} needs to be larger than before, eventually exceeding the maximum allowable value for $k=1.4$.

Figure 5.25: Trajectory architecture for $k=1.2$, multiple fly-by scenarioFigure 5.26: Trajectory architecture for $k=1.3$, multiple fly-by scenario

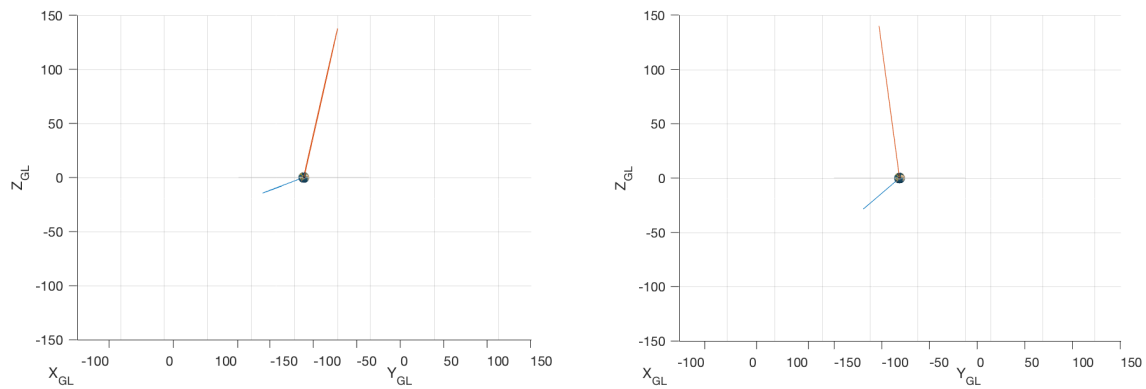


Figure 5.27: **Lateral views for $k=1.2$ (left) and $k=1.3$ (right)**

As a matter of fact, the backflip scenario, i.e. the one with an approximately 90° degrees inclined Moon to Moon transfer orbit, is quite convenient in the case of an out of plane escape. The reason for this resides in the fact that the rotation of the velocity vector can be split into the two Lunar encounters, thus avoiding to exceed the maximum allowable turn angle.

Instead, if a planar escape is needed, this kind of LL leg is unfavorable due to the fact that the second LGA must provide a great turn angle in order to ensure a zero inclination trajectory.

5.3.3 Resonant fly-by scenario

This scenario, by means of the original inputs and as reported in *Chapter 5.1.3*, was capable of bringing 10058.21 kg to the escape with a hyperbolic excess of velocity equal to 1.2 km/s. Such a performance was demonstrated to be valid both for the N=1 M=1 and the N=3 M=2 cases.

It is now object of our interest to analyze how the escape mass and the turn angle behave by varying the value of the multiplication factor k . The results in the case of N=1 and M=1 are presented in Table 5.26 and plotted in Figure 5.28.

k	m_{esc}	t_{esc}
1	10058.21 kg	141.15
1.1	10064.79 kg	141.15
1.2	10062.17 kg	141.15
1.3	10009.52 kg	141.13
1.4	9934.94 kg	141.17
1.5	no solutions	-

Table 5.26: Escape mass as a function of k , resonant fly-by scenario 11

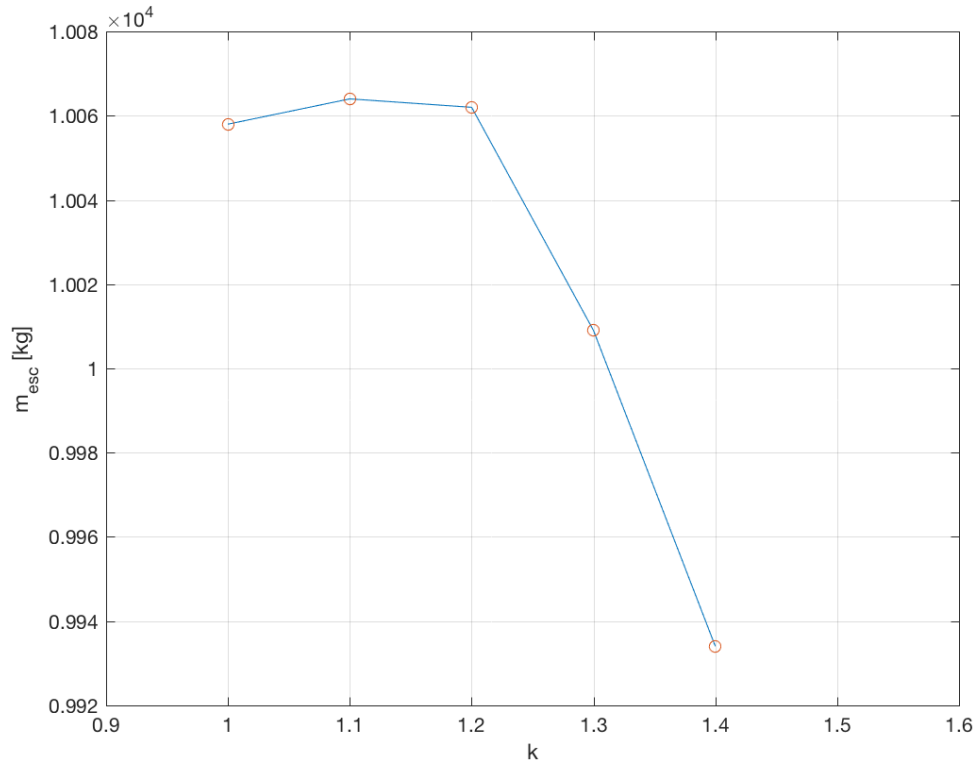


Figure 5.28: Escape mass as a function of k , resonant fly-by scenario 11

As reported in the previous plot, the value for m_{esc} at $k=1$ does not represent an absolute maximum from which the escape mass starts to decrease with k . In fact, the trend appears to be initially increasing until $k=1.1$, after which an always decreasing behavior is assumed. Such a trend was already known from the analysis whose results have been presented in *Chapter 5.1.3*, but the maximum value for $k=1.1$ was not taken into account as the best resonant fly-by scenario due to the lower destination mass it was capable of delivering. The reason for this probably resides in the unfavorable relative position of both the Earth and the target asteroid.

However, apart from this little consideration, Figure 5.28 exactly reports what we expected to: a decreasing escape mass as the V_{esc} module rises.

Also in the resonant fly-by scenario, as already observed in the single and multiple fly-by cases, the escape date is subject to variations; the reason for this is related to the optimum relative position of Moon and Earth that guarantees the feasibility and performances of the trajectory.

Now that the escape mass as a function of k has been analyzed, it is possible to focus our attention upon the $\delta - k$ and $\delta_{max} - k$ trends. The results are presented in Table 5.27 and plotted in Figure 5.29.

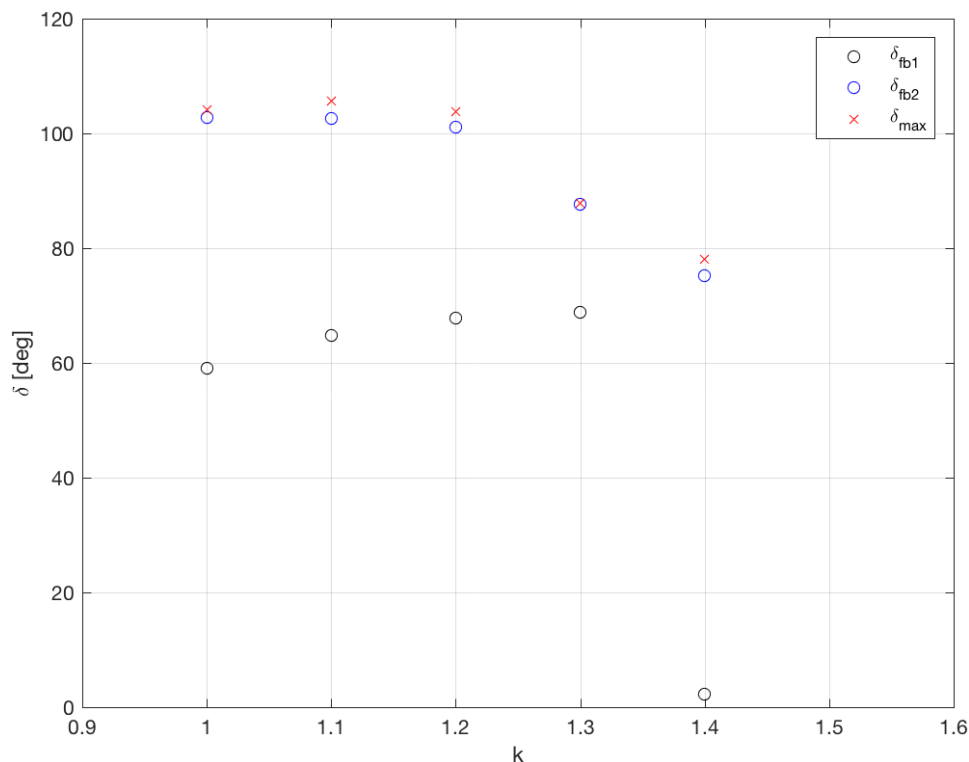
k	δ_{fb1}	δ_{fb2}	δ_{max}	t_{esc}
1	58.99°	102.79°	104.09°	141.15
1.1	64.86°	102.60°	105.66°	141.15
1.2	67.86°	101.09°	103.86°	141.15
1.3	68.88°	87.65°	87.76°	141.13
1.4	2.31°	75.19°	78.01°	141.17

Table 5.27: **Turn angles as a function of k, resonant fly-by scenario 11**

As already stated before, the maximum allowable value for the turn angle experiences a degrowth if the multiplication factor rises; the same can be said for the second LGA turn angle, that eventually exceeds δ_{max} for $k \geq 1.5$.

In Figure 5.29 it is well depicted how the values for δ and δ_{max} approach when the multiplication factor rises, almost coincide for $k=1.3$ and eventually making impossible the completion of the maneuver for $k \geq 1.5$.

As a matter of fact, it must be noted that within the range $k=[1, 1.2]$, for which t_{esc} is constant and equal to 141.15, the inclination of the intermediate leg assumes a value of 46° for $k=1$, 48° if $k=1.1$ and ends up at 50° for $k=1.2$. This is coherent with what stated regarding the multiple fly-by scenario.

Figure 5.29: Turn angles as a function of k , resonant fly-by scenario 11

As already reported in *Chapter 5.1.3*, the resonant fly-by scenario succeeded to find feasible solutions both in the $N=1$ $M=1$ and in the $N=3$ $M=2$ cases. The results regarding the latter scenario are presented in Table 5.28 and plotted in Figure 5.30.

k	m_{esc}	t_{esc}
1	10058.21 kg	141.15
1.1	10064.79 kg	141.15
1.2	10062.17 kg	141.15
1.3	10052.65 kg	141.15
1.4	9934.94 kg	141.17
1.5	9867.21 kg	141.17
1.6	no solutions	-

Table 5.28: Escape mass as a function of k , resonant fly-by scenario 32

The trend is very similar to that of Figure 5.28, apart from the fact that this scenario appears to be feasible also with a value 1.5 for the multiplication factor, while the 11 scenario found solutions only until $k=1.4$.

The reason for this probably resides in the different intermediate leg architecture, that allows greater V_{esc} module without exceeding the value for δ_{max} . In fact, the time of flight

upon the intermediate leg was equal to a Lunar period in the $N=1$ $M=1$ case, while, if $N=3$ $M=2$, it takes one and a half Lunar periods to complete the Moon to Moon transfer.

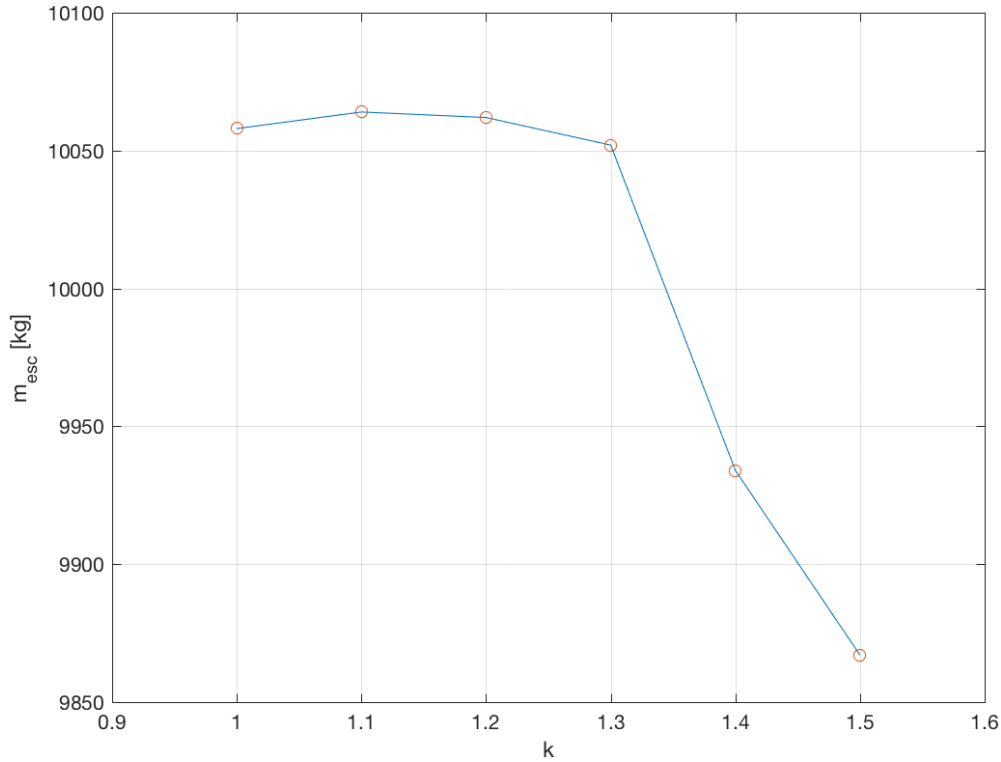


Figure 5.30: **Escape mass as a function of k, resonant fly-by scenario 32**

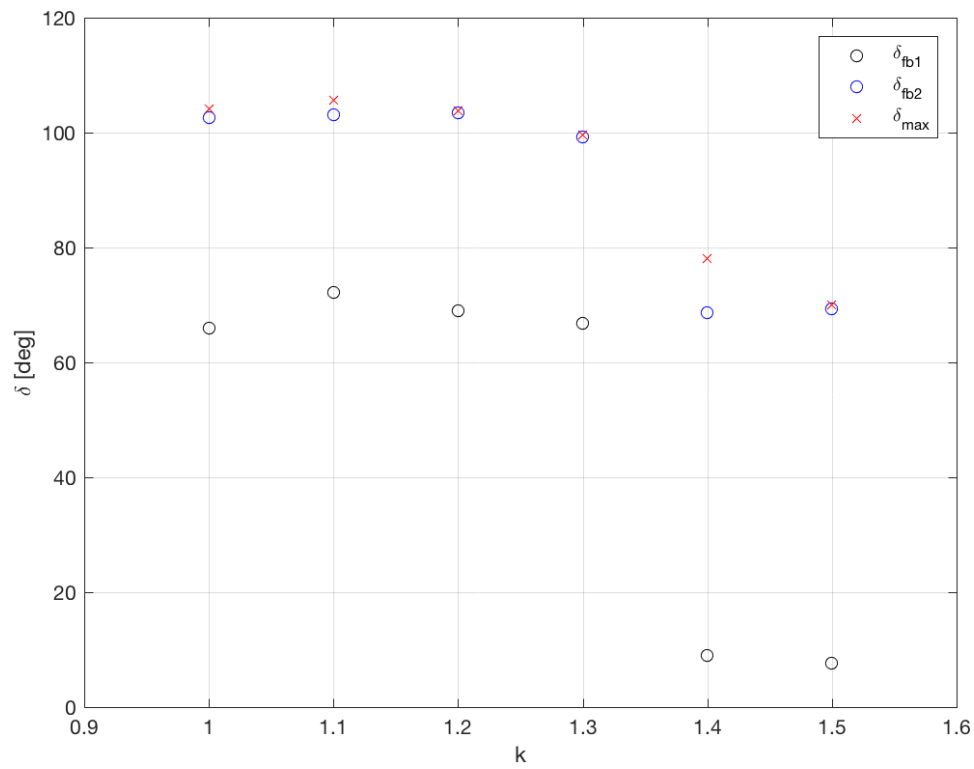
As usual, the following step regards the analysis of the $\delta - \delta_{max} - k$ behavior. The results are reported in Table 5.29 and plotted in Figure 5.31.

k	δ_{fb1}	δ_{fb2}	δ_{max}	t_{esc}
1	66.02°	102.57°	104.09°	141.15
1.1	72.17°	103.15°	105.66°	141.15
1.2	69.01°	103.46°	103.86°	141.15
1.3	66.81°	99.27°	99.67°	141.15
1.4	8.97°	68.84°	78.01°	141.17
1.5	7.66°	69.28°	69.96°	141.17

Table 5.29: **Turn angles as a function of k, resonant fly-by scenario 32**

The trends are pretty identical to those of the 11 scenario: δ_{max} experiences a degrowth if k rises, eventually falling below the value for δ_{fb2} if $k \geq 1.6$.

Also in this case, the inclination of the intermediate leg within the interval $k=[1, 1.3]$, for which t_{esc} is constant and equal to 141.15, experiences a growth from 41° to 50°.

Figure 5.31: Turn angles as a function of k , resonant fly-by scenario 32

5.3.4 Considerations

Now that the evolution of all of possible scenarios has been analyzed with respect to the V_{esc} input value, it is possible to present some considerations regarding the different architectures, as already done in *Chapter 5.1.4* with the original inputs.

- **Single fly-by scenario**, for which the trajectory is always feasible. However, for a certain value of the multiplication factor, this scenario ceases to be definable as "gravity assisted".
- **Multiple fly-by scenario**, for which the trajectory is feasible until $V_{esc} \approx 1.6$ km/s.
- **Resonant fly-by scenario**, for which the trajectory is feasible until $V_{esc} \approx 1.7$ km/s if we adopt a 11 scenario and until $V_{esc} \approx 1.8$ km/s if we adopt a 32 scenario.

Both in the case of a multiple fly-by scenario and in the eventuality of a resonant architecture, the trajectory becomes unfeasible due to the excessive turn angle required by the second Lunar encounter. The reason for this resides in the fact that if the spacecraft's path between the two fly-by events is highly inclined with respect to the T_{GL} fundamental plane, the second LGA must provide a big rotation to the velocity vector, in order to obtain a low inclination escape leg.

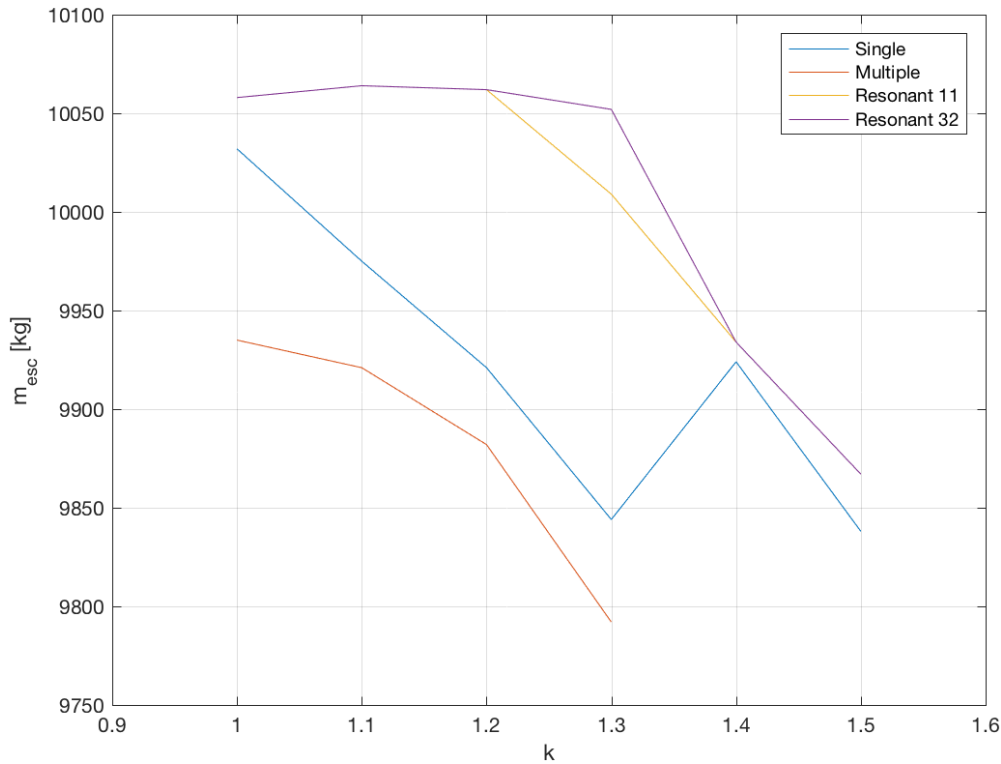


Figure 5.32: Comparison of the different scenarios' performances

It is now useful to visualize in a single plot how the performances of the different scenarios evolve with respect to k . By means of Figure 5.32, it is possible to observe that the best choice from the payload mass point of view is the resonant fly-by architecture.

More precisely, this scenario is characterized by an almost constant behavior of m_{esc} for small values of k , combined with the possibility of feasible solutions for greater values of the multiplication factor.

Such a variety of use could be pretty appreciated in the mission design phase.

As already stated before, this part of the work has been carried out by simply multiplying the V_{esc} components, without modifying the orbital parameters of the target asteroid. This is, in fact, a purely qualitative analysis that could eventually be refined by means of more accurate inputs. These could come, for example, by considering other target asteroids, the ones that need a greater hyperbolic excess of velocity with respect to 2000SG344.

5.4 Conclusions

By means of this work, I managed to develop and test a methodology that allows to design and optimize Lunar gravity assisted escape maneuvers towards Near Earth Asteroids. These particular trajectories can be exploited to improve the payload capability of the mission, due to the fact that the fly-by events result in an additional ΔV without the need of additional propellant.

This trajectory architecture, already exploited in a few past missions, could be adopted for future missions to explore both the origin and the chemical composition of small asteroids belonging to the Main Belt.

Another interesting possibility, never carried out before, regards the possibility for the payload of using one or more Lunar gravity assists to reach a Geostationary or Geosynchronous orbit.

Another field of interest could be that of asteroid mining, as already explained in *Chapter 1.3*, and it's been some time since the discovery that the vast majority of asteroids contain enormous quantities of valuable metals. Furthermore, the revolution space travel is now experiencing by means of the reusability of rockets, could allow to reach these Solar System's bodies with unthinkably low prices if compared to those of just two decades ago.

In conclusion, my work could be used as a starting point for the design of a mission to the inner Solar System. Such a mission could either possess a purely scientific purpose, even with the possibility of a crew, or an economical one.

Bibliography

- [1] NEO basics
<https://cneos.jpl.nasa.gov/about/basics.html>
- [2] NEO groups
https://cneos.jpl.nasa.gov/about/neo_groups.html
- [3] Deep Space Industries
<http://deepspaceindustries.com/mining/>
- [4] NASA Mission OSIRIS-REx
<https://www.nasa.gov/osiris-rex>
- [5] NASA's Asteroid Sample Return Mission
<https://www.nasa.gov/content/goddard/bennus-journey>
- [6] STEREO Trajectory and Maneuver Design
<http://www.jhuapl.edu/techdigest/TD/td2802/Dunham.pdf>
- [7] R. V. Ramanan, V. Adimurthy, "*Precise Lunar Gravity Assist Transfer to Geostationary Orbits*", in Journal Of Guidance, Control and Dynamics, Vol. 29, No. 2, March-April 2006
- [8] NASA Mission ISEE-3/ICE
<https://heasarc.gsfc.nasa.gov/docs/heasarc/missions/isee3.html>
- [9] American Mathematical Society, Slingshots and Space Shots
<http://www.ams.org/publicoutreach/feature-column/fcarc-slingshot>
- [10] J. A. Van Allen, "*Gravitational Assist in Celestial Mechanics*", in American Journal of Physics, Vol. 71, No. 5, May 2003
- [11] R. C. Johnson, "*The Slingshot Effect*"
<http://maths.dur.ac.uk/~dma0rcj/Psling/sling.pdf>
- [12] R. R. Bate, D. D. Mueller, J. E. White, "*Fundamentals of Astrodynamics*", Dover Publications, New York, 1971

- [13] United Launch Alliance, "*Delta IV Launch Services User's Guide*", June 2013
- [14] L. Casalino, G. Lantoine, "*Design of Lunar-Gravity-Assisted Escape Maneuvers*", in 2017 AAS/AIAA Astrodynamics Specialist Conference, AAS 17-749